NASA-CR-201894

93017

WORKSHOP ON EVOLUTION OF MARTIAN VOLATILES

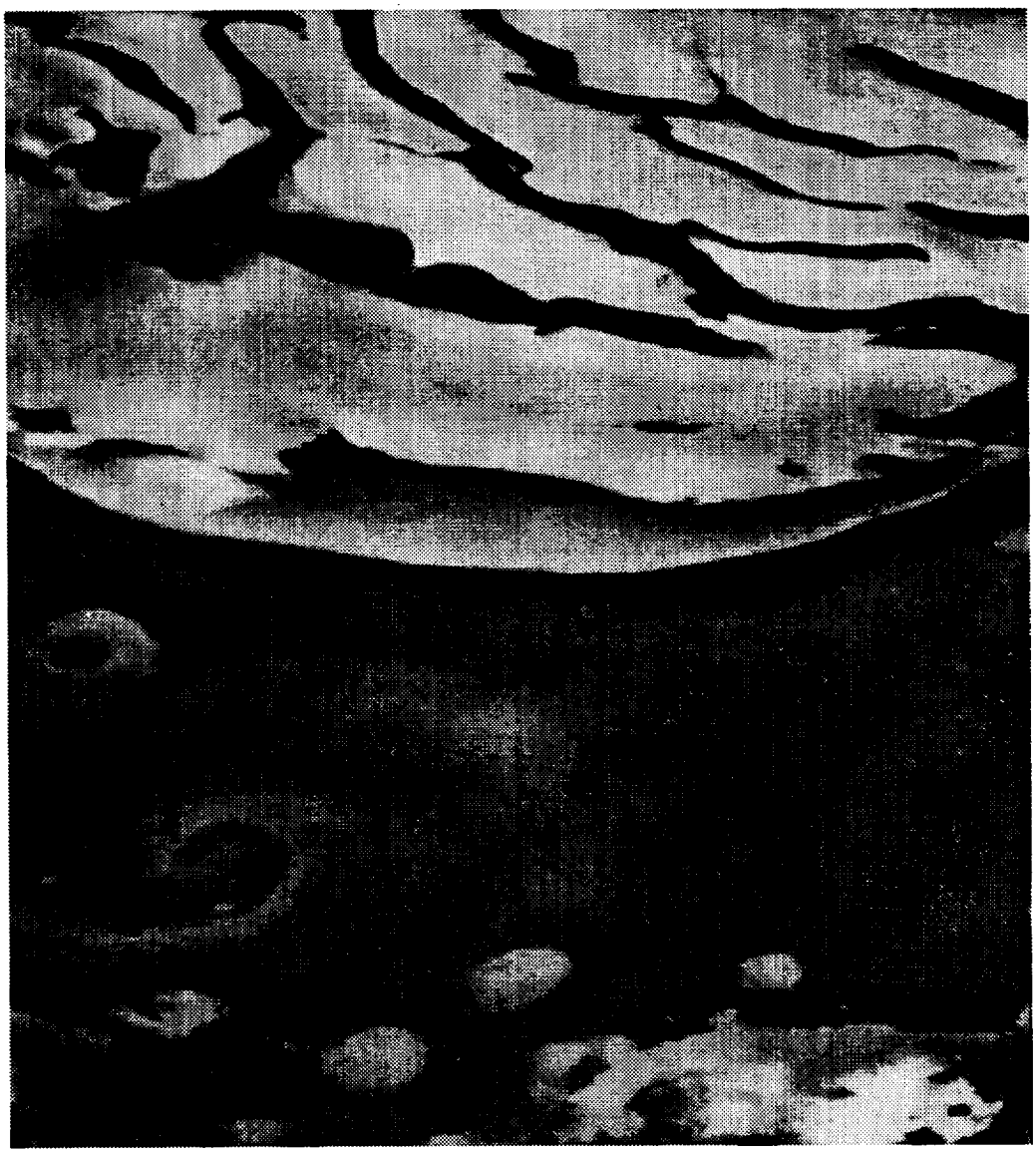

LPI Technical Report Number 96-01, Part 1

Lunar and Planetary Institute 3600 Bay Area Boulevard Houston TX 77058-1113

LPI/TR--96-01, Part 1

WORKSHOP ON

EVOLUTION OF MARTIAN VOLATILES

Edited by

B. Jakosky and A. Treiman

Held at
Houston, Texas

February 12–14, 1996

Sponsored by
Lunar and Planetary Institute

Lunar and Planetary Institute 3600 Bay Area Boulevard Houston TX 77058-1113

LPI Technical Report Number 96-01, Part 1
LPI/TR--96-01, Part 1

Compiled in 1996 by
LUNAR AND PLANETARY INSTITUTE

The Institute is operated by the Universities Space Research Association under Contract No. NASW-4574 with the National Aeronautics and Space Administration.

Material in this volume may be copied without restraint for library, abstract service, education, or personal research purposes; however, republication of any paper or portion thereof requires the written permission of the authors as well as the appropriate acknowledgment of this publication.

This report may be cited as

Jakosky B. and Treiman A., eds. (1996) *Workshop on Evolution of Martian Volatiles*. LPI Tech. Rpt. 96-01, Part 1, Lunar and Planetary Institute, Houston. 48 pp.

This report is distributed by

ORDER DEPARTMENT
Lunar and Planetary Institute
3600 Bay Area Boulevard
Houston TX 77058-1113

Mail order requestors will be invoiced for the cost of shipping and handling.

Cover: Volatiles on Mars: Water and carbon dioxide ices in the north polar icecap (top), and water vapor in cyclonic and convection clouds. *Viking Orbiter image 738A28.*

Contents

What Will Returned Samples Tell Us About Martian Volatiles?
C. C. Allen 1

Evolution of the Solar EUV Radiation and Its Impact on Martian Exospheric Constituents Over Time
T. R. Ayres 2

Acidic Volatiles and the Mars Soil
A. Banin, F. X. Han, I. Kan, and A. Cicelsky 2

Implications of Subsurface Volatile Distribution from Martian Impact Crater Morphology
N. G. Barlow 4

The Ancient Mars Thermosphere
S. W. Bougher and J. L. Fox 5

Primitive Methane Atmospheres on Earth and Mars
L. L. Brown and J. F. Kasting 6

Quantitative Analysis of the 3-μm Water of Hydration Absorption Feature in the Eastern Valles Marineris
W. M. Calvin 7

Formation of the Martian Drainage System: Redistribution of Groundwater in Response to Global Topography and Cold Climates
M. H. Carr 7

Atmospheric Dust-Water Ice Interactions: Do They Play Important Roles in the Current Mars Climate?
R. T. Clancy 9

Hydraulic and Thermal Constraints on the Development of the Martian Valley Networks
S. M. Clifford 9

Is Mars Water Rich? Hydrologic, Topographic, and Latitudinal Considerations in the Search for Subpermafrost Groundwater
S. M. Clifford 11

The Evolution of Martian Water
T. M. Donahue 12

The Role of SO_2 for the Climate History of Mars
G. Dreibus and H. Wänke 12

Volatiles and Volcanos: Very Late Amazonian Ash Deposits and Explosive Activity Along the Western Flanks of the Tharsis Montes, Mars
K. S. Edgett, B. J. Butler, J. R. Zimbelman, and V. E. Hamilton 13

The Contribution of Volatiles to the Surface and Atmosphere of Mars by the Accretion of Interplanetary Dust Particles
G. J. Flynn 14

The Ancient Mars Ionosphere
J. L. Fox and S. W. Bougher 15

A Geochemical Model for Volatile Storage Via Hydrothermal Systems on Mars
L. L. Griffith and E. L. Shock 15

The Martian Climate System at High Obliquity: Simulations with the NASA Ames Mars General Circulation Model
R. M. Haberle 16

Some Constraints on the Amount of CO_2 Stored in the Polar Regions of Mars
R. M. Haberle and D. Tyler 17

Geology of the Polar Layered Deposits on Mars
K. E. Herkenhoff and J. J. Plaut 17

Modeling the Martian Water Cycle
H. Houben, R. M. Haberle, R. E. Young, and A. Zent 18

Evolution of Martian Atmospheric Argon and Neon
K. S. Hutchins and B. M. Jakosky 19

Mars Volatile Evolution from Stable Isotope Abundances
B. M. Jakosky and J. H. Jones 20

Martian Dust Storms: Hubble Space Telescope Observations
P. B. James, J. Bell, R. T. Clancy, S. W. Lee, L. J. Martin, and M. Wolff 20

Sputtering of the Atmosphere of Mars
R. E. Johnson, D. Schnellenberger, and M. Liu 21

Martian Volatiles: Insights from the SNC Meteorites
J. H. Jones 21

Isotopic Composition of Carbonates in Some SNC Meteorites
A. J. T. Jull, S. Cloudt, and C. J. Eastoe 22

Deposition and Badlands Erosion of Martian Chemical and Clastic Lacustrine Rocks
J. S. Kargel 23

Mineralogy of the Martian Surface Analyzed *In Situ* by Mössbauer Spectroscopy, and Implications for Volatile Evolution on Mars
G. Klingelhöfer, B. Fegley Jr., R. V. Morris, E. Kankeleit, E. Evlanov, O. Priloutskii, J. M. Knudsen, and M. B. Madsen 25

SPICAM Solar Occultation Experiment
O. Korablev, M. Ackerman, E. Neefs, C. Muller, H. Deceuninck, D. Moreau, C. Hermans, W. Peertermans, P. C. Simon, S. Shadeck, E. Van Ransbeek, V. Moroz, A. Rodin, A. Stepanov, D. Perepelkin, V. Jegoulev, A. Krysko, and V. Troshin 26

Lightweight Solar Occultation Spectrometer Experiment
O. I. Korablev, V. I. Moroz, M. Ackerman, E. Van Ransbeek, P. C. Simon, and J.-L. Bertaux 27

Photochemical Weathering of Martian Carbonates and Sulfates
A. P. Koscheev, L. M. Mukhin, Yu. P. Dikov, J. Huth, and H. Wänke 28

Hubble Space Telescope Observations of Time-Variable Regional Albedo Features on Mars
S. W. Lee, M. J. Wolff, P. B. James, L. J. Martin, R. T. Clancy, and J. F. Bell 29

CO_2 Ice: Rheological Properties and Impact Cratering
J. Leliwa-Kopystynski 30

Hydrogen Isotope Geochemistry of SNC (Martian) Meteorites and the History of Water on Mars
L. A. Leshin, S. Epstein, and E. M. Stolper 30

The Martian Noble Gas Isotope Paradox
L. K. Levsky 31

Trace-Element Geochemistry of Martian Weathering Products in Lafayette
D. J. Lindstrom, A. H. Treiman, and R. R. Martinez 31

Role of the Martian Magnetic Field History in Loss of Volatiles to Space
J. G. Luhmann 32

Water Ice in the Martian Atmosphere as Derived from Phobos/KRFM Data
W. J. Markiewicz, H. U. Keller, E. Petrova, N. Thomas, and M. W. Wuttke 32

NASA's Mars Surveyor Program: Focus on Volatiles
D. J. McCleese 33

Limits on the CO_2 Content of the Martian Polar Deposits
M. T. Mellon 34

Iron, Sulfur, and Chlorine Phases on Mars
R. V. Morris, D. C. Golden, D. W. Ming, and J. F. Bell III 35

Observational Tests for the Identification of Shore Morphology on Mars
T. J. Parker 36

The Rich Geomorphic Legacy of the Argyre Basin: A Martian Hydrologic Saga
T. J. Parker 36

Are the Martian Valley Networks Really Sapping Channels?
J. W. Rice Jr. 37

Condensation-driven Vertical Profile of Water in Mars Troposphere: Phobos Revisited
A. V. Rodin, O. I. Korablev, and V. I. Moroz 38

Oxygen Isotopes in Martian SNC Meteorites
C. S. Romanek, E. K. Gibson Jr., R. A. Socki, and E. C. Perry 39

Iron Formations on Mars?
M. W. Schaefer 40

Spectroscopic Measurements of Martian Atmospheric Water Vapor
A. L. Sprague, D. M. Hunten, and R. E. Hill 41

Diurnal Variability of the Atmospheric Water Content on Mars:
Observations and Desorption Model
D. V. Titov 45

An Early Warm, Wet Mars? Little Support from the Martian Meteorite ALH 84001
A. H. Treiman 45

Thermal Evolution Models of Mars: Implications for Release of Volatiles
A. Weizman, D. Prialnik, and M. Podolak 46

Has Martian Atmospheric CO_2 Become Depleted in ^{13}C with Time?
I. P. Wright, M. M. Grady, and C. T. Pillinger 47

New Estimates of the Adsorption of H_2O on Martian Surface Materials
A. P. Zent 47

Preface

This volume contains papers that were accepted for presentation at the Evolution for Martian Volatiles Workshop, February 12–14, 1996, in Houston, Texas. Members of the Program Committee were B. Jakosky *(University of Colorado)* and A. Treiman *(Lunar and Planetary Institute)*, co-conveners; J. Jones *(NASA Johnson Space Center)*; and S. Clifford *(Lunar and Planetary Institute)*. Other members of the Scientific Organizing Committee included J. Bell III *(Cornell University)*, R. Haberle *(NASA Ames Research Center)*, J. Kargel *(U.S. Geological Survey)*, J. Kasting *(Pennsylvania State University)*, L. Leshin *(University of California, Los Angeles)*, and J. Luhmann *(University of California, Berkeley)*.

Logistics and administrative and publications support were provided by the Publications and Program Services Department staff at the Lunar and Planetary Institute.

Abstracts

WHAT WILL RETURNED SAMPLES TELL US ABOUT MARTIAN VOLATILES? C. C. Allen, Lockheed-Martin Engineering and Sciences Company, Houston TX 77058, USA.

Introduction: Sample return is among the most productive approaches to Mars science; it permits a synergism between the wealth of photogeologic and remote sensing data and the extensive analytical capabilities available in the laboratory. One example of a possible Mars sample return mission is currently under study at the Johnson Space Center [1]. The concept includes a lander supporting one or two small rovers. Rock, soil, and atmosphere samples would be collected from the vicinity of the lander. Sample selection would be controlled from Earth, based on multispectral imaging.

The mission is designed to return approximately 2.5 kg of material. This would include 10–20 rocks, several samples of soil, and a single atmosphere sample. The solid samples would be documented, stored separately, and shielded from ionizing radiation. The outside of the sample container would be biologically sterilized, but the rocks and soil would be preserved at or below –10°C. The sample container would be opened in a suitably isolated terrestrial laboratory.

Samples from such a mission could provide solutions to many fundamental problems in Mars science. As applied specifically to martian volatiles these include the ages and alteration histories of martian rocks, surface-atmosphere interactions, and details of atmospheric composition.

Ages and Alteration Histories of Martian Rocks: Our direct knowledge of martian rocks comes from orbiter and lander photographs and from laboratory analysis of the martian meteorites [2]. Orbital mapping has defined the major geologic provinces, determined relative ages of surface units, and inferred rock compositions from morphologies and spectral signatures. The Viking landers documented the sizes and textures of a vide variety of rocks, but unfortunately provided no chemical data. The martian meteorites have yielded compositions and ages of samples from a few unidentified locations.

Our understanding of martian volatile history will improve dramatically when the absolute ages of surface units are established. Relative dating by crater count statistics is quite accurate, but absolute age calibration is uncertain. The leading models for Mars [3,4] differ dramatically in their recommended ages for many surfaces. For instance, the central shield of Arsia Mons could be as old as 3.4 Ga or as young as 0.6 Ga. This age uncertainty translates into uncertainty in almost every quantitative aspect of martian evolution, including duration of volcanism; sources, sinks, and abundances of volatiles; volatile loss mechanisms; and the persistence of environments suitable for life. To calibrate martian crater counts requires at least one returned sample. A carefully selected Middle to Early Amazonian surface would provide the highest degree of differentiation between the leading crater chronologies.

Rocks on the martian surface have undergone limited physical and chemical alteration [5]. Some rocks at the Viking landing sites show evidence of wind erosion, mechanical breakage, and possible weathering rinds. Signs of aqueous chemical alteration have been documented in some of the martian meteorites [2]. Secondary sulfate and carbonate minerals, clearly of preterrestrial origin, line cracks within several of these rocks.

The sampling mission discussed here would return a number of 100–200-g rocks. Such small samples are likely products of mechanical weathering. Each may well show evidence of surface and possibly interior alteration. Data from these rocks and the soil samples discussed below could elucidate the physical and chemical weathering environment at the martian surface.

Surface-Atmosphere Interaction: The martian surface material was characterized by instruments onboard both Viking landers [6]. Major-element compositions of the fines were determined by X-ray fluorescence spectrometry. Additional data include volatile release upon heating and reaction with water, abundance of the magnetic component(s), approximate grain size, mechanical properties, and spectral signatures. Soils from the two landing sites sites proved essentially identical.

Significant gaps still exist in our understanding of the martian surface. The Viking XRF analyzers were not sensitive to the key volatile elements H, C, N, and O. In addition, the soil mineralogy was not determined and is not well constrained by existing data. A few hundred grams of surface material could identify the major soil minerals and indicate the alteration processes that have operated on Mars.

Interactions between the soil and atmosphere are poorly understood but may be fundamental to our understanding of the martian surface. An apparently oxidizing soil, combined with a high ultraviolet flux and cold temperatures, have resulted in a sterile surface layer. The nature and depth of this layer have profound implications for the possibility of current or past martian life. The near surface is also a potentially important sink for volatiles. Much of the planet's water inventory may well be trapped, perhaps reversibly, in ground ice and hydrated minerals. A combination of samples from the surface and from several centimeters in depth could provide definitive data for such studies.

Atmospheric Composition: A wealth of information already exists concerning the martian atmosphere, based on data from mass spectrometers on the two Viking spacecraft, as well as orbital and Earth-based spectral measurements. The major atmospheric components are well known, upper limits on possible minor constituents are constrained at or below the parts per million level, and the important isotope ratios for H, C, N, O, Ar, and Xe have been determined [7].

The composition of the martian atmosphere is not constant, however. As seasons change, CO_2 alternately condenses and sublimes at the poles. This mass exchange involves as much as 30% of the atmosphere. The abundance of water vapor also varies seasonally and spatially. Finally, the atmosphere always contains a suspended dust component, which can increase by orders of magnitude during planetwide storms.

A returned sample of the martian atmosphere will enable measurements of all atmospheric components at considerably improved precisions. It will provide a snapshot of the abundances of variable species under a documented set of conditions. The sample will yield "ground truth" to calibrate Earth-based spectroscopic measurements. Finally, the optical and thermal properties of suspended dust will be determined.

References: [1] Kaplan D. I. (1995) *LPS XXVI*, 723–724. [2] McSween H. Y. Jr. (1994) *Meteoritics, 29*, 757–779. [3] Neukum G. and Hiller K. (1981) *JGR, 86*, 3097–3121. [4] Tanaka K. L. et al.

(1991) in *Mars*, 345–382. [5] Gooding J. L. et al. (1991) in *Mars*, 626–651. [6] Banin A. et al. (1991) in *Mars*, 594–625. [7] Owen T. (1991) in *Mars*, 818–834.

EVOLUTION OF THE SOLAR EUV RADIATION AND ITS IMPACT ON MARTIAN EXOSPHERIC CONSTITUENTS OVER TIME. T. R. Ayres, Center for Astrophysics and Space Astronomy, University of Colorado, Boulder CO 80309, USA.

Important loss mechanisms for the key constituents (N, O, C) of the martian atmosphere are nonthermal escape to space following dissociative recombination, direct scavaging of exospheric ions by the solar wind, and sputtering by solar-wind-accelerated pickup ions [1]. These mechanisms depend critically on the solar ultraviolet radiation field and on the mass flux, speed, and entrained magnetic field of the solar wind. Because the young Sun is believed to have been considerably more active in its UV emissions and coronal-wind fluence than at present, the solar-induced erosion of the martian atmosphere undoubtedly was considerably greater during the early postbombardment era than it is now.

Previous studies [2,3] have appealed to the evolutionary history of the solar radiation field described by Zahnle and Walker [4] and that of the solar wind by Newkirk [5]. The former was written at a time when crucial information on the evolution of chromospheric and coronal activity of solar-type stars was beginning to emerge, thanks to pioneering spacecraft observations [particularly by IUE (UV spectroscopy) and Einstein (X-ray imaging)]. Many of the gaps in the developing understanding of stellar activity of that era have been filled over the intervening decade and a half, particularly in the past five years with second-generation spacecraft observatories: HST (UV spectroscopy), EUVE (EUV spectroscopy), ROSAT (X-ray imaging), and ASCA (X-ray spectroscopy). Extensive UV/X-ray studies now are available for young galactic clusters, ranging in age from 50 m.y. (Pleiades, α Persei) to 500 m.y. (Hyades), and stars of the field (mostly older than 1 G.y.). At the same time, new insights have been developed concerning the behavior of the solar wind at early times. Finally, the present-day ultraviolet spectrum of the Sun recently has been measured with very high precision by the SOLSTICE instrument on UARS [6] and by contemporary sounding rockets [7]. Thus, it seems appropriate to revisit the question of the solar-induced erosion of the martian atmosphere over time.

The new observations of the solar UV spectrum permit the calculation of accurate photoionization rates at the martian orbit for the key species H, O, O_2, N_2, CO_2, and CO. The photoionization rates can be decomposed into components that depend on flux contributions from specific zones of the solar outer atmosphere: chromosphere ($T < 10^4$ K), transition-region (10^4 K $< T < 10^6$ K), and corona ($T > 10^6$ K). The overall (magnetic) activity of a solar-mass star decays with time, owing to wind-induced angular-momentum loss, which negatively impacts the rotation-catalyzed "dynamo" [4]. However, the distinct emission layers of the star fade at different rates: the high-excitation coronal zones, rapidly; the lower-excitation chromospheric layers, more slowly. Nevertheless, the separate decay rates are believed to be highly predictable for solar-mass dwarfs older than about Hyades age (500 m.y.); thus the decomposed photoionization rates can be scaled backward in time from the accurately known contemporary values.

I will also discuss new insights concerning the properties of the young solar wind, based on recent studies of flare activity among Hyades-age G-type dwarfs.

Acknowledgments: This work was supported by NASA grant NAGW-4529 to the University of Colorado.

References: [1] Luhmann J. G. and Bauer S. J. (1992) in *Venus and Mars: Atmospheres, Ionospheres, and Solar Wind Interactions* (J. G. Luhmann et al., eds.), 417–430, Geophysical Monograph 66, AGU. [2] Luhmann J. G. et al. (1992) *GRL*, 19, 2151–2154. [3] Kass D. M. and Yung Y. L. (1995) *Science*, 268, 697–699. [4] Zahnle K. J. and Walker J. C. G. (1982) *Rev. Geophys. Space Phys.*, *20*, 280–292. [5] Newkirk G. Jr. (1980) in *The Ancient Sun* (R. O. Pepin et al., eds.), 293–320, Pergamon, New York. [6] Rottman G. J. et al. (1993) *JGR*, 98, 10667–10677. [7] Woods T. N. and Rottman G. J. (1990) *JGR*, 95, 6227–6236.

ACIDIC VOLATILES AND THE MARS SOIL. A. Banin, F. X. Han, I. Kan, and A. Cicelsky, Department of Soil and Water Sciences, Hebrew University, P. O. Box 12, Rehovot, Israel.

Acidic volatiles released to the martian atmosphere may react with exposed basaltic glass and minerals on the planet's surface. The volatiles-rock interaction may lead to acido-hydrolytic weathering of the primary minerals and the formation of various secondary minerals constituting the layer of fine soil and dust covering the planet's surface. Mars soil thus becomes a major sink for volatiles, including the derivatives of the acidic species of S, Cl, and perhaps N. In the present report we present the results of an experimental study of Mars-soil analogs weathered by acidification and touch on the potential relevance of the results to soil formation and volatile-cycling scenarios on Mars.

Mars Soil: A single "geological unit" consisting of fine, apparently weathered soil material covers large portions of the surface of Mars [1,2]. The chemical-elemental composition of the soil has been directly measured by the Viking landers, and positive detection of Si, Al, Fe, Mg, Ca, Ti, S, Cl, and Br was achieved [3–5]. Sulfur was found in martian soil at concentrations of 6–9% (as SO_3). This concentration is 2 orders of magnitude higher than for typical igneous rock and for the lithospheres of the Earth and Moon. Relatively high Cl content (0.7–0.8%) was also found. Sulfur appears to be in the form of sulfate, SO_4^{2-}, contained in various salt compounds, primarily magnesium sulfate, although the presence of Al and Fe sulfates could not be ruled out [6]. The source of the sulfate has been attributed to gases (SO_2) released during volcanic activity and oxidized in the atmosphere [7]. Likewise, Cl may be a component of volcanic gaseous emanations. Recent spectroscopic studies [8] and analyses of SNC meteorites and Mars soil analogs indicate that nanophase minerals may be prevalent in the martian soil, including nanophase Fe oxides [9,10] and silicate mineraloides [11]. The mode of formation of this somewhat peculiar type of soil is still far from being clear.

Acidification Study: To study, in enhanced mode, the weathering processes of basaltic materials due to acidic volatiles, we acidified samples of a palagonitic soil formed from volcanic tephra. The soil was sampled on the peak of Mauna Kea, on the island of Hawaii [12]. Varying inputs of sulfuric, nitric, and hydrochloric acids were used, at levels of addition covering the range from zero to the corresponding element concentration found (or estimated) in Mars soil and beyond it. The acidic solutions were sprayed onto the mineral matrix and mixed in it. The samples were stored at slightly elevated temperature (30°–40°C) for several weeks and then freeze-dried and pulverized. They were characterized by a combined com-

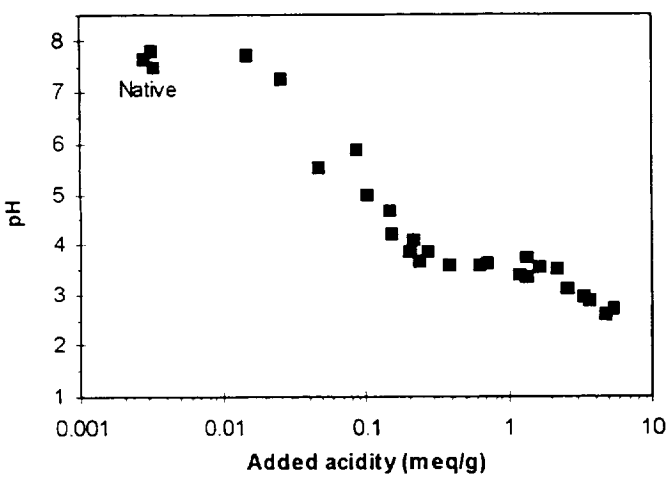

Fig. 1. Change in the pH of slurries (1%) of a palagonitized basaltic tephra from Mauna Kea, as a result of acidification with H_2SO_4, HCl, and HNO_3 and their mixtures. Each point represents a sample treated with a certain acidity dose.

puterized titration-extraction procedure that measures solid-surface and solution acidity and chemistry [13].

The palagonitic soil effectively "neutralizes" the added acidity as shown in Fig.1. At low levels of acidification the added acidity lowers the pH of the palagonitic soil; however, at additions higher than 0.3–0.4 meq/g, the soil buffering enters into effect and the pH remains between 3.0 and 4.0. At addition levels higher than 1.7–2.0 meq/g, the soil buffering is somewhat less effective and further slight lowering of pH to ~2.4 is observed (Fig. 1). (Recalculation of the Viking results for Mars soil [13] shows that the soil contains about 2.0 meq/g sulfate + chloride.) The present results show that volcanic glass/palagonite, "artificially weathered" by addition of various acids, is stabilized at pH levels buffered by the Al and Fe hydrolysis products. Titration curves (Fig. 2a) show that the total final acidity is practically equal to the added acidity if titration is conducted up to pH = 10.8–11.1. Even though the full amount of acidity added to the soil is stored in it, only a very small fraction is preserved as the original protonic acidity, the majority being present

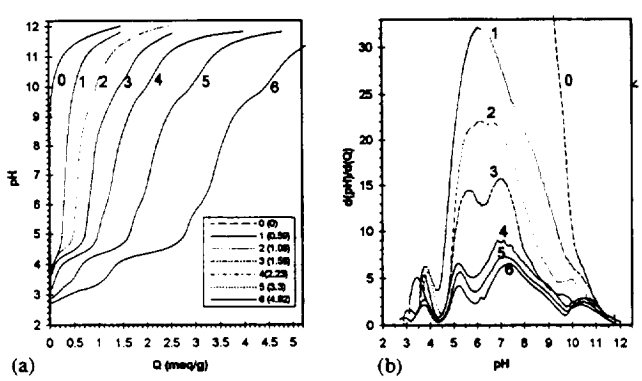

Fig. 2. (a) Acid-base titration curves (pH vs. amount of NaOH added, Q, meq/g) of palagonitized basaltic tephra treated with mixtures of H_2SO_4, HCl, and HNO_3 (at ratios of ~1:1.1:0.05). Total acidity added (meq/g) is indicated in brackets. (b) Derivatives of the titration curves (dpH/dQ) plotted against pH, in order to identify the endpoints characterizing the various acidity species and sites as defined in the text.

as hydrolytic species of Al, Fe, and Mg released from the soil minerals. At low levels of addition, the added acidity resides at the solid-phase surface. Higher acidity additions (above 0.2–0.3 meq/g) release increased proportions of matrix constituents to the solution phase. Acidity is split among four groups of species as follows (Fig. 2b): Species 1, EP (end point) at pH 3.75 ± 0.23, is assigned to H^+ and the first hydrolysis product of Fe; species 2, EP at pH = 5.48 ± 0.30, is assigned to the three major Al hydrolysis products; species 3, EP at pH = 6.95 ± 0.37, is assigned to surface Fe; and species 4, EP at pH = 10.11 ± 0.43, is assigned primarily to Mg hydrolysis products. The surface acidity amounts to about 0.25–0.35 meq/g and is split among the various species, mostly present as species 2 and 4. The sulfate and chloride added to the palagonitized tephra were present as salts and easily-solubilized minerals, electrically balanced by cationic components dissolved from the soil matrix primarily constituted of Mg and Ca, and some Fe and Al.

Relevance to Mars: The currently most accepted scenario for soil formation on Mars is that it took place during earlier epochs (3.5–4.0 b.y. ago) when Mars may have been "warm and wet" [2,14]. It is therefore puzzling that apparently only a minor portion of the oxides and silicates in the Mars soil have crystallized and developed a more thermodynamically stable mineralogical composition and particle size distribution during weathering and over the long periods of time since their formation. Banin et al. [10] recently attributed the peculiar nature of the martian dust and soil to a relatively "young" weathering product that has formed during the last several hundreds of million to a billion years. Acidic volatiles released to the martian atmosphere may produce (as a result of their neutralization-reaction with basaltic glass or rock surfaces) salts, nanophase Fe oxides, and secondary silicates. Particularly susceptible to such weathering are the more recently erupted volcanic materials [15]. Estimated at 26.4×10^6 km^3 during the Amazonian [6], these materials may have supplied both the highly unstable primary minerals and the acidic volatiles that weathered a portion of them. Due to the lack of liquid water, these mineral products have not evolved to form highly crystallized mineral grains. The global surface stability of Mars, due to lack of plate tectonics, facilitates the accumulation and piling-up of weathering products on the surface. As a result, products of extremely slow processes, which are negligible on Earth, may strongly affect the martian surface. The chemically modified weathered minerals are mixed with, and diluted by, products of physical weathering and wind abrasion, and together they form the loose topsoil of Mars, which is what was sampled by the Viking landers and studied during the last three decades by intensive Earth-based telescopic observations and flyby and orbiter missions to the planet.

The chemically weathered component of the martian soil, according to the present study and the hypothesis presented above, consists of a salt-rich mineral mixture containing the salts of the anionic-legands SO_4 and Cl resulting from volatiles emitted from volcanos during more recent eruptions (up to 1 b.y.). Its pH may be below neutrality, buffered by acidic surface and solution species, primarily the hydrolysis products of Fe and Al. The low pH of the soil destabilizes carbonates and may diminish the sorption and retention of CO_2. However, the presence of hydrous carbonates, suggested recently on spectroscopic grounds [17], may be possible due to increased stability and abundance of HCO_3 at slightly acidic environments. It appears then that the top loose soil of Mars may constitute a significant sink for volatiles recently released to the martian atmosphere.

Acknowledgments: This study was supported in part by the Exobiology Program, NASA HQ.

References: [1] Christensen P. R. and Moore H. J. (1992) in *Mars* (H. H. Keifer et al., eds.), 686–729. [2] Banin A. et. al (1992) in *Mars* (H. H. Keifer et al., eds.), 594–625. [3] Clark B. C. et al. (1976) *Science*, 194, 1283–1288. [4] Toulmin P. III et al. (1977) *JGR, 82*, 4625–4634. [5] Clark B. C. et al. (1982) *JGR, 87*, 10059–10067. [6] Clark B. C. and Van Hart D. C. (1981) *Icarus, 45*, 370–378. [7] Settle M. (1979) *JGR, 84*, 8343–8354. [8] Bell J. F. III et al. (1995) *JGR, 100*, 5297–5307. [9] Morris R. V. et al. (1989) *JGR, 94*, 2760–2778. [10] Banin A. et al. (1993) *JGR, 98*, 20831–20853. [11] Gooding J. L. (1992) *Icarus, 99*, 28–41. [12] Banin A. et al., unpublished data. [13] Banin A. et al., in preparation. [14] Gooding J. L. et al. (1992) in *Mars* (H. H. Keifer et al., eds.), 626–651. [15] Plescia P. (1990) *Icarus, 88*, 465–490. [16] Greeley R. and Schneid B. D. (1991) *Science, 254*, 996–998. [17] Calvin W. M. et al. (1994) *JGR, 99*, 14659–14675.

IMPLICATIONS OF SUBSURFACE VOLATILE DISTRIBUTION FROM MARTIAN IMPACT CRATER MORPHOLOGY. N. G. Barlow, Lunar and Planetary Institute, 3600 Bay Area Boulevard, Houston TX 77058, USA.

Cosmochemical models suggest that Mars should be volatile rich, but the amounts of volatiles in the obvious source regions of the atmosphere and polar caps are too low. However, much geologic evidence exists to suggest that the martian substrate is a major reservoir of volatiles, including large stores of H_2O. Valley networks formed by groundwater sapping processes and the large outflow channels formed by catastrophic flooding are the most obvious geomorphic indicators of the presence of subsurface volatiles. A less obvious but nonetheless important indicator of subsurface volatiles are the varying morphologies of impact craters. In many respects martian impact craters provide a more complete picture of the distribution of subsurface volatiles since they are more widespread across the martian surface than other geologic features.

Martian impact craters display a number of attributes that are distinct from impact craters on other worlds. The most obvious difference is the fluidized ejecta pattern that surrounds most fresh impact craters on Mars. Impact craters on volatile-poor bodies such as the Moon and Mercury display ejecta blankets that have been emplaced along ballistic trajectories, thus producing a radial ejecta pattern. On Mars, Venus, and some of the icy outer moons, a more lobate ejecta pattern is seen around fresh impact craters, indicating ejecta emplacement by fluidization processes. The fluidizing medium may be provided either by vaporization of subsurface volatiles [1] or by the atmosphere [2]. In the case of the outer moons, which have little to no atmosphere, the process is caused by production of a transient atmosphere from vaporization of surface ice. In the case of Venus, where the high surface temperature precludes the existence of subsurface volatiles, the fluidizing medium is the atmosphere. In the case of Mars, however, both a thin atmosphere and subsurface volatiles are present.

Fresh martian impact craters display a variety of ejecta morphologies that depend on crater size and location [3]. Lobate ejecta morphologies include those with a single lobe of material surrounding the crater (single lobe), two lobes of material (double lobe), or more than two lobes (multiple lobe). Radial morphologies are similar in appearance to ejecta blankets surrounding fresh craters on the Moon and Mercury, suggesting that ballistic rather than fluvial emplacement dominated. A minority of craters display a diverse morphology that includes both a fluvial lobe of material with a radial ejecta pattern superimposed.

A detailed study of 3819 craters ≥8 km in diameter distributed across the martian surface was conducted to determine (1) whether subsurface volatiles or atmospheric effects dominated in the formation of lobate ejecta patterns, and (2) if subsurface volatiles were suggested, what the impact crater morphologies implied about the distribution of the subsurface volatile reservoirs. The premise of the study was to look at the distribution the five major ejecta morphologies by crater size and location on the planet. If variations in ejecta pattern with latitude and crater size were detected, this would suggest an origin dominated by vaporization of subsurface volatiles. Variations in ejecta morphology with crater size but not with latitude would suggest that atmospheric processes dominate over subsurface volatiles. Elevation was not included in the original study, but is being incorporated into a follow-up study that also includes craters smaller than 8 km in diameter.

The results of the study are detailed in [3] and indicate that impact into subsurface volatiles plays the dominant role in the formation of the lobate ejecta patterns on Mars. Single lobe ejecta morphologies dominate among craters less than about 20 km in diameter in the equatorial regions, giving way to the multiple lobe ejecta pattern for craters between 20 and 45 km in diameter. Craters between 45 and 100 km in diameter show the diverse ejecta pattern, which includes elements of both lobate and radial morphologies, while most craters larger than 65 km in diameter display a radial ejecta pattern. This sequence only holds at equatorial regions, however. At higher latitudes (generally poleward of about ±40° latitude), the single lobe ejecta morphology dominates for crater diameters up through about 60 km. In the 40°–65°N latitude range, single lobe craters are replaced by the double lobe ejecta morphologies in the 8- to 50-km-diameter range. Larger craters with ejecta morphologies are too rare in the polar regions for reliable statistical analysis.

The results of this study indicate that ejecta morphologies show a strong diameter-latitude dependence, consistent with our hypothesis that the distribution of subsurface volatiles rather than atmospheric effects is the dominant parameter affecting formation of the lobate ejecta patterns. Computation of excavation depths for the crater diameters associated with specific ejecta morphologies indicate that single lobe craters excavate to depths of about 1.5 km in the equatorial regions and up to 4 km depth at high latitudes. Multiple-lobe craters excavate to depths of between 1.3 and 3.2 km in the equatorial regions and radial morphologies are associated with craters that excavate below about 4 km depth. Comparison of these depths with thermal gradient models of the distribution and phase of subsurface volatiles indicate that single-lobe craters excavate into regions dominated by ice, while multiple-lobe craters excavate to depths where liquid water reservoirs are postulated to exist in the equatorial regions. Diverse ejecta patterns are associated with craters excavating into a transition zone between volatile-rich and volatile-poor materials, and the radial ejecta morphology results from crater excavation into volatile-poor material. Quantitative analysis of the sinuosity of single-lobe, double-lobe, and multiple-lobe ejecta patterns support the idea that materials forming the single-lobe ejecta pattern are slightly more viscous than those that form the multiple-lobe pattern [4].

These results indicate that the study of impact crater morphologies, particularly the various ejecta morphologies, can provide important constraints on the distribution and phase of subsurface volatile reservoirs. A similar study, including craters smaller than 8 km in diameter and the effects of elevation, is currently being conducted, and preliminary results will be discussed at the meeting.

References: [1] Carr M. H. et al. (1977) *JGR, 82,* 4055–4065. [2] Schultz (1992) *JGR, 97,* 11623–11662. [3] Barlow N. G. and Bradley T. L. (1990) *Icarus, 87,* 156–179. [4] Barlow N. G. (1994) *JGR, 99,* 10927–10935.

THE ANCIENT MARS THERMOSPHERE. S. W. Bougher[1] and J. L. Fox[2], [1]Lunar and Planetary Laboratory, University of Arizona, Tucson AZ 85721, USA, [2]Department of Physics, Wright State University, Dayton OH 45435, USA.

The evolution of the Mars atmosphere, particularly with regard to water, is influenced by (1) nonthermal escape of O atoms created by dissociative recombination of the primary ion O_2^+, (2) O ion pickup by the solar wind, and (3) O ion sputtering [1–6]. Each of these mechanisms depends on the intensity of solar EUV radiation, which affects the neutral atmospheric structure, photoionization, and sputtering rates, and subsequently the exosphere and the fluxes of escaping atoms and ions. It is expected that the solar EUV fluxes were greatly enhanced over present-day values during the previous history of the Mars atmosphere. This paper and that of Fox and Bougher (this volume) consider the effects of higher EUV fluxes of the ancient Sun upon the neutral and ion structure of the Mars upper atmosphere. These new model simulations depart from previous one-dimensional model predictions [6] in two important ways: (1) a three-dimensional global circulation model is now used to estimate the ancient neutral densities and temperatures near the exobase, and (2) an improved one-dimensional ion model and a multistream code are now used to estimate the hot O distribution and escape fluxes for O atoms and ions from Mars.

The Mars Thermosphere General Circulation Model (MTGCM) has been used to examine three-dimensional circulation effects on the Mars dayside and nightside temperatures and densities [7,8]. The MTGCM presently calculates global winds and corresponding CO_2, CO, N_2, and O neutral density distributions and temperatures over 70–300 km, spanning the martian upper mesosphere and thermosphere. Minor species (O_2 and Ar) are also presently being simulated, along with a dayside photochemical ionosphere [9]. The MTGCM is firmly based on well-studied CO_2 energetic and chemical processes for Venus that should apply to Mars as well [10]. Adjustable parameters that can be varied for individual MTGCM cases include the F10.7 index (solar EUV-UV flux variation), heliocentric distance (orbital variation), solar declination (seasonal variation), and maximum eddy coefficient (K_t) for eddy diffusion and viscosity. The MTGCM has been validated using Mariner 9 Ultraviolet Spectrometer (UVS) data that provide dayside O mixing ratios near the ionospheric peak [11]. Also, several airglow measurements by various spacecraft (Mariner 6, 7, 9) and descent probe density profiles (Viking 1 and 2) provide scale heights and inferred temperatures for constraining MTGCM simulations [12]. In general, solar EUV forcing is the primary driver of Mars thermospheric features; however, periods are identified when upward propagating gravity waves and/or tides are surely modifying the otherwise solar-driven structure and circulation [9].

New MTGCM simulations are conducted for possible conditions occurring 3 G.y. ago. This might correspond to the period following hydrodynamic escape when it can be assumed that the composition of the upper atmosphere is basically similar to that at present. We also assume that the first-order modification to consider for addressing the ancient Mars thermosphere-ionosphere system is that of enhanced solar fluxes appropriate to 3 G.y. ago. Specifically, an average heliocentric distance (d = 1.528 AU), mean season (Equinox), and baseline solar fluxes (F10.7 = 150) are chosen for our ancient Mars simulations. These baseline EUV-UV fluxes are increased by a factor of 3.0 [13]; the solar IR fluxes are assumed to be 0.79× those at present [14]. The most up-to-date parameters are used for Mars thermospheric heating and cooling: (1) the EUV/UV heating efficiency utilized is 20/22% [15]; (2) the CO_2-O relaxation rate is chosen to be 1.5×10^{-12} cm^3/s [16]; and (3) the rather uncertain eddy coefficient for conduction is purposely held to the estimated present-day value of 1.5×10^7 cm^2/s. The feedbacks among EUV-UV-IR forcing, composition, thermal structure, and dynamics are important to monitor; i.e., it is particularly important to watch the changing impact of CO_2-O collisions and subsequent 15-μm cooling, stronger heating, and global winds upon the dayside thermal budget and atomic O distributions.

Model fields are compared for a present-day MTGCM control simulation and a MTGCM perturbation simulation for 3 G.y. ago, as described above. Midafternoon exobase temperatures near the equator are seen to increase from 270 to 440 K; corresponding nightside temperatures also increase (albeit more slowly) from 150 to 180 K. This enhancement in the day-night temperature contrast of the thermosphere results in global horizontal (and vertical) winds nearly double those predicted for present-day Mars. The stronger global winds provide enhanced adiabatic cooling (dayside), thereby regulating dayside temperatures. This thermostat also appears to be important in the present-day Mars upper atmospheric heat budget [8]. In addition, the O/CO_2 mixing ratio near the dayside ionospheric peak can be examined as an indicator of the efficiency of CO_2 net dissociation. Since solar EUV fluxes were larger 3 G.y. ago, one would expect the photolysis of CO_2 to be more efficient. This is seen in the threefold enhancement of the noontime O/CO_2 mixing ratio near the equator (2% present-day case; 6% 3-G.y. case). Subsequently, this atomic O enhancement stimulates an increase in CO_2 cooling rates above those at present. This stronger CO_2 15-μm cooling also provides a thermostatic control of dayside temperatures, a situation consistent with the present-day Venus thermospheric heat budget [6,16]. For ancient Mars, the net effect is a dual thermostat, composed of strong global winds and CO_2 cooling, that tightly regulates the Mars upper atmosphere temperatures to be much cooler than otherwise expected from one-dimensional modeling studies [6]. The O atom densities near the exobase are also modified accordingly.

The corresponding ionospheric structure also departs from previous one-dimensional model predictions [6]. The companion paper by Fox and Bougher (this volume) describes an updated one-dimensional ionosphere model [17] and its application to the ancient Mars ionosphere and O escape rates.

References: [1] Luhmann J. G. and Kozyra J. U. (1991) *JGR, 96,* 5457. [2] Luhmann J. G. and Bauer S. J. (1992) *Geophys. Monograph Series, Vol. 66,* 417. [3] Luhmann J. G. et al. (1992) *GRL, 19,* 2151. [4] Fox J. L. (1993) *JGR, 98,* 3297. [5] Fox J. L. (1993) *GRL, 20,* 1747. [6] Zhang M. J. et al. (1993) *JGR, 98,* 10915. [7] Bougher S. W. et al. (1988) *GRL, 15,* 1511. [8] Bougher S. W.

et al. (1990) *JGR, 95,* 14811. [9] Bougher S. W. et al. (1993) *JGR, 98,* 3281. [10] Bougher S. W. (1995) *Adv. Space Res., 15, #4,* 21. [11] Stewart A. I. F. et al. (1992) *JGR, 97,* 91. [12] Barth C. A. et al. (1992) in *Mars,* 1054. [13] Zahnle K. J. and Walker J. C. G.(1982) *Rev. Geophys., 20,* 280. [14] Gough D. O. (1981) *Solar Phys., 74,* 21. [15] Fox J. L. and Dalgarno A. (1979) *JGR, 84,* 7315. [16] Bougher S. W. et al. (1994) *JGR, 99,* 14609. [17] Fox J. L. et al. (1995) *Adv. Space Res.,* in press.

PRIMITIVE METHANE ATMOSPHERES ON EARTH AND MARS.

L. L. Brown and J. F. Kasting, Department of Geosciences, Pennsylvania State University, University Park PA 16802, USA.

A variety of model atmospheres have been proposed for early Earth and Mars as a means of compensating for lower solar luminosity in the past. Sagan and Mullen [1] originally proposed a reducing atmosphere containing ammonia. Others have favored an atmosphere dominated by CO_2 and H_2O [2] and containing only trace amounts of reduced gases such as ammonia and methane. As pointed out by Kasting [3], the greenhouse warming of CO_2 and H_2O alone is insufficient to provide the necessary warming on early Mars when the condensation of CO_2 is taken into account. Here we investigate the warming potential of a more reducing atmosphere with significant concentrations of methane and we investigate the photochemical stability of such atmospheres.

Using a one-dimensional radiative-convective climate model [3], we have calculated the radiative forcing of CH_4 and CO_2 in Earth's atmosphere and find that methane may have contributed more warming on early Earth than previously thought. Beginning with a temperature profile from the U.S. Standard Atmosphere and a CO_2 mixing ratio of 330 ppm, we calculated the change in the net longwave flux at the tropopause as the CH_4 mixing ratio was increased from 10^{-6} to 10^{-1}. Figure 1 is a comparison of our results and those for a similar calculation by Kiehl and Dickinson [4]. As methane concentration increases our model predicts increasingly larger changes in the tropospheric IR flux. For example, at a methane mixing ratio of 10%, we calculate ~84 Wm^{-2}, whereas Kiehl and Dickenson calculate only ~24 Wm^{-2}. The difference between these

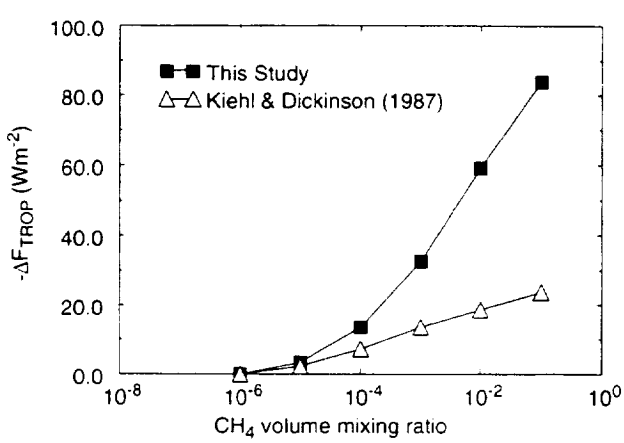

Fig. 1.

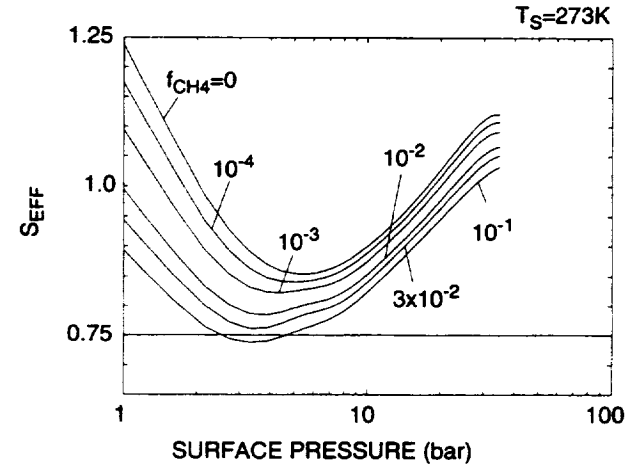

Fig. 2.

two models is apparently due to our inclusion of more methane absorption bands [5]. Methane mixing ratios of 10^{-4} or higher are possible for Earth's atmosphere between ~3.5 and 2.2 b.y. ago.

We have used this same model to calculate the concentration of methane required to maintain the surface temperature of early Mars at or above the freezing point of water. Figure 2 shows that a methane mixing ratio of ~5–10 vol%, combined with a CO_2 partial pressure of 3–4 bar, could sustain a global average surface temperature of 273 K near 3.8 b.y. ago, when the solar flux was approximately 75% of the present value. Such a methane concentration is higher than we think plausible (see below), but methane might still be responsible for part of the warming required to solve the early Mars climate puzzle. Possible sources for methane on early Mars include submarine volcanic outgassing from a reduced upper mantle or methanogenic activity by a hypothetical martian biota.

An important question that must be addressed is whether the possible sources of methane on early Mars would have been large enough to sustain methane concentrations sufficient to affect climate. To answer this question, we have constructed a photochemical model to study the lifetime of methane in possible paleoatmospheres. Preliminary results for Earth indicate that a CH_4 mixing ratio of 10^{-4} could be sustained by a methane source of 8×10^9 cm^{-2} s^{-1}, which is about 8% of the present terrestrial flux. Even higher mixing ratios are possible if the escape of H to space proceeds at less than the diffusion-limited rate. These relatively high methane concentrations are predicted by the model even though we form negligible amounts of UV-shielding hydrocarbon particles. Particle formation is effectively precluded by reaction of C_2H radicals with oxidizing species, including O_2 and O.

Photochemical destruction of methane on early Mars would be slower than on early Earth because of a lowered solar UV flux and possibly a colder, drier atmosphere. Although it is difficult to estimate the source strength of methane on early Mars, it seems plausible that methane could have played an important role in warming the early martian climate.

References: [1] Sagan and Mullen (1972), *Science, 177,* 52–56. [2] Pollack J. B. et al. (1987) *Icarus, 71,* 203–224. [3] Kasting (1991) *Icarus, 94,* 1–13. [4] Kiehl and Dickinson (1987), *JGR, 92,* 2991–2998. [5] Kiehl J. T. (1993) personal communication.

QUANTITATIVE ANALYSIS OF THE 3-μm WATER OF HYDRATION ABSORPTION FEATURE IN THE EASTERN VALLES MARINERIS. W. M. Calvin, U.S. Geological Survey, Flagstaff AZ 86001, USA.

The eastern end of the Valles Marineris, in particular Ganges, Eos, and Capri Chasmata, mark the transition from the canyon system proper to chaotic terrain and into the outflow channels. While the canyon system is largely tectonic in origin (Fig. 1), certain surface features such as streamlined highlands flow from higher to lower elevations, and scour marks have long suggested that the channels are related to the action of water in some form on the surface of Mars (Fig. 2). Chaotic terrain is characterized by slumped material and jumbled blocks, is associated with collapse after removal of subsurface material, and is consistently the source region for channels [3]. Layered deposits within the chasmata suggest a variety of origins including eolian or lacustrine deposition, mass wasting, or volcanism [4,5].

The Mariner 6 mission in 1969 obtained data over Ganges and Eos Chasmata and the chaotic terrain that begins near 40° longitude. The instrument complement included an Infrared Spectrometer (IRS), the entrance aperture of which is a slit resulting in a ground footprint approximately 150 km × 8 km, depending on the range from the planet. The groundtracks of the IRS are overlain with images from the Martian Digital Image Map (MDIM) in Fig. 1. The observations continue north and west and pass over the region where Juventae Chasma leads into the Maja Valles, and there is a second pass nearby that crosses both Aram Chaos and Iani Chaos.

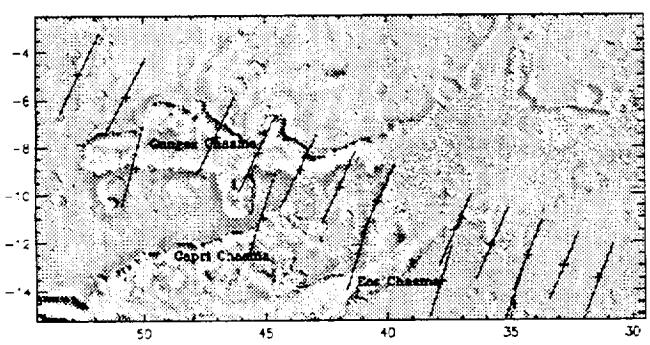

Fig. 1. Footprints of the Mariner 6 spectrometer over the eastern Valles Marineris; chasmata names are also noted.

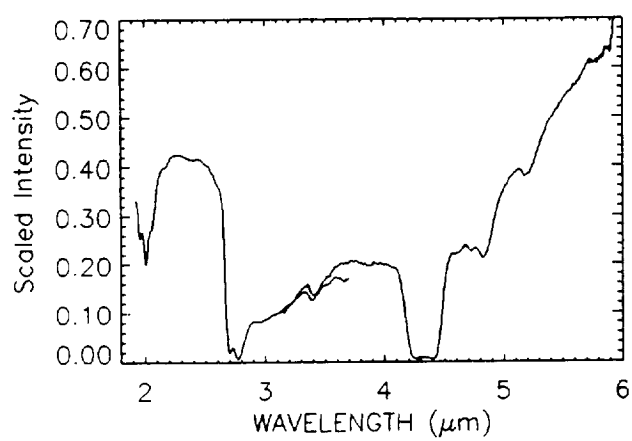

Fig. 2. Sample spectra from the Mariner 7 instrument, which is identical in design to Mariner 6. Calibration has been performed only for the 3-μm to 6-μm wavelength segment.

The IRS obtained data from 1.9 μm to 6 μm in two segments at spectral resolutions near 1.5%. Signal-to-noise can be as high as 100–150 or as low as 10, depending on the raw signal level [6]. The high spectral resolution and extended wavelength coverage allow for discrimination of atmospheric multiplets as well as features due to surface mineralogy. In particular, the broad absorption associated with water of hydration in surface minerals has long been identified in this dataset [7]. A sample spectrum for the full wavelength range is shown in Fig. 2.

Analysis of the water of hydration band has so far been restricted to band ratios of the albedos at 2.2 μm and 3.1 μm [7,8]. These studies note variability of the ratios, but it is unclear to what extent these globally binned ratios actually map variations in the water of hydration band rather than variation in the albedo at 2.2 μm. In related work, with data from the imaging spectrometer (ISM) onboard the Phobos spacecraft, Erard et al. [9] calculated similar band ratios and found variations in the state of hydration of dark regions in the canyon floors and a high degree of spectral variability that is not necessarily correlated with geomorphic units. This suggested it would be fruitful to examine the Mariner data in more detail over localized regions of similar 2.2-μm albedo. For this study a few dozen spectra over the eastern end of Valles Marineris were selected due to the high probability of the action of water in chaotic terrain and the overlap with the Phobos ISM observations.

Recently, Miyamoto and Zolensky [10] examined the integrated intensity of the water of hydration band in various carbonaceous chondrites and found an excellent correlation to bulk H content of the samples. This technique, in addition to band ratios, is applied to the Mariner data over the Eastern Valles Marineris in an effort to look for variability in the volatile abundances and to corroborate band ratios as a viable method of determining hydration state. Analysis of the data includes removal of the thermal contribution and merging the spectral segments. Initial results will be reported at the meeting.

References: [1] Lucchitta B. K. et al. (1992) in *Mars* (H. Kieffer et al., eds.), 453. [2] Baker V. R. et al. (1992) in *Mars* (H. Kieffer et al., ed.), 493. [3] Sharp R. P. (1973) *JGR, 78,* 4073. [4] Nedell S. S. et al. (1987) *Icarus, 70,* 409. [5] Lucchitta B. K. et al. (1994) *JGR, 99,* 3783. [6] Calvin W. M. et al. (1994) *JGR, 99,* 14659. [7] Pimentel G. C. et al. (1974) *JGR, 79,* 1623. [8] Blaney D. L. et al. (1994) *Bull. AAS, 26,* 1113. [9] Erard S. et al. (1991) *Proc. LPS, Vol. 21,* 437. [10] Miyamoto M. and Zolensky M. E. (1994) *Meteoritics, 29,* 849.

FORMATION OF THE MARTIAN DRAINAGE SYSTEM: REDISTRIBUTION OF GROUNDWATER IN RESPONSE TO GLOBAL TOPOGRAPHY AND COLD CLIMATES. M. H. Carr, U.S. Geological Survey, Menlo Park CA 94025, USA.

The main thesis of this abstract is that the martian drainage system represents an adjustment of the distribution of groundwater in response to (1) a major change in surface conditions at the end of

heavy bombardment, (2) the global topography inherited by the planet from that era, and (3) the declining heat flow. It is neither the product nor the cause of episodic climate changes as has previously been proposed [1].

The evidence for a dramatic change in surface conditions at the end of heavy bombardment is unambiguous. Survival of craters at the VL-1 landing site [2] and on basal Hesperian surfaces [3] indicate that the average erosion rates since the end of heavy bombardment have been no more than 10^{-2} μm yr^{-1} as compared with terrestrial rates that typically range from 10–1000 μm yr^{-1}. Erosion rates at the end of heavy bombardment are much more difficult to estimate because we do not know the cratering rates. Noachian craters tens of kilometers across are seen in all states of preservation, in contrast to almost perfectly preserved lower Hesperian craters <1 km across. Estimates of the late Noachian rates range from 0.1 to 10 μm yr^{-1} [3,4]. The cause of the change in erosion rates is unknown but a climate change is likely, particularly since water was left in terrains 3–4 km above the Mars datum, as evidenced by outflow channels and valley networks, and this is difficult to do without an atmospheric source.

At the end of heavy bombardment the planet was left with a thick and probably porous megaregolith, which is estimated to have had the capacity to hold 0.5–1.5 km of water spread over the whole planet [5]. The two most likely causes of outflow channels are massive eruptions of groundwater stored in the megaregolith and trapped beneath a thick permafrost [6] and catastrophic release of water stored in lakes [7]. A thick permafrost, and climatic conditions similar to today's, are needed for groundwater eruption in order to create the large hydrostatic pressures implied by the large discharge rates. Eruption was preferred in low areas where migration of groundwater would cause hydrostatic pressures to build below the permafrost and where the permafrost was thin, such as at low latitudes or near volcanos. Thus flood sources are mostly located in the low-latitude, low-lying areas south of Chryse and near the volcanos of Elysium and northeast Hellas. Lakes formed in the canyons and drained catastrophically to the east. The canyons extend well below the depth of any permafrost. Water could therefore have leaked into the canyons to form lakes. Such lakes would have frozen over, and may have been long-lived as ablation from the ice surface was compensated for by groundwater leakage into the lakes. The surface of the lakes would have been maintained at the level of the local groundwater table. Some lakes, such as that in the completely enclosed Hebes Chasma, may have drained noncatastrophically by subsurface flow. The water that flowed through the outflow channels formed terminal lakes that either sublimed, if formed at low latitudes, or froze in place to form permanent ice deposits, if formed at high latitudes, as most were. The outflow channels have a broad range of ages but most are Hesperian. Their rate of formation declined with time because high-standing areas became progressively depleted of groundwater, as water was transferred from the high-elevation groundwater sources, mostly in the south, to the low-elevation sinks, mostly in the north.

Valley networks have been widely assumed to be close analogs to terrestrial river valleys mainly because the planimetric patterns of branching sinuous valleys resemble branching patterns of rivers on the Earth. But the valleys also have significant differences from terrestrial fluvial valleys: (1) drainage densities are 3–5 orders of magnitude less than on Earth so that same-scale views of martian and terrestrial drainage systems look dramatically different; (2) martian valley networks in the uplands lack fine-scale (<1 km across) tributaries, i.e., they do not divide into every smaller tributaries; (3) the martian valleys have roughly rectangular cross-sections from source to mouth; (4) the flat floors of some martian valleys have longitudinal central ridges; (5) channels have not been observed within the valleys; (6) some valleys have leveelike ridges on their margins, indicating that the main valley is a true channel, not a valley in which there was a much smaller channel; and (7) the networks are much smaller than terrestrial river systems. These differences, together with good evidence for mass wasting in fretted channels, led to the suggestion that the valleys formed slowly, over hundreds of millions of years, mainly by mass wasting, aided by the presence of groundwater [8]. Once a valley was initiated, such as by slumping on an escarpment, mass-wasted debris in the valley floor acted as a conduit for groundwater. Convergence of groundwater at the valley head caused headward erosion. Most valleys are old (Noachian and lower Hesperian) because heat flows were high early in Mars' history and groundwater occurred at shallow depths. Younger valley networks occur mainly on steep slopes (canyon and crater walls) and/or volcanos where anomalously high heat flows are expected. While mass-wasting was the dominant process, water may have occasionally erupted to the surface in a manner analogous to the formation of outflow channels but on a much smaller scale. The process is envisaged to have taken place under climatic conditions similar to today's.

In summary, a dramatic change took place on Mars at the end of heavy bombardment. At that time erosion rates were at the low end of terrestrial rates. They then declined rapidly by 1–3 orders of magnitude, and very low rates have been maintained ever since. A change from a warm climate to a climate that resembled today's probably caused the decline. From the period of heavy bombardment the planet inherited a very uneven topography and a deep megaregolith that contained the equivalent of a few hundred meters of water. The water was distributed throughout the megaregolith in both the high and low areas. The distribution of water began to accommodate these disequilibrium conditions. Just after heavy bombardment heat flow was high but declined rapidly so that liquid water occurred at shallow depths. Presence of shallow liquid water enabled the formation of valley networks mainly by mass-wasting. As the heat flow declined and the permafrost thickened, the rate of valley network formation declined. Movement of groundwater beneath the thick permafrost enabled hydrostatic pressures to build, causing massive breakouts and formation of the outflow channels. Breakouts became less frequent as the groundwater table dropped and the permafrost thickened. Although lakes must have formed at the ends of the outflow channels, the validity of the interpretation of miscellaneous features in the northern plains as marking former shorelines, outlining large bodies of water [8], has yet to be demonstrated. The scenario preferred here is that the floodwaters formed modest-sized lakes (10^5–10^6 km^3) that froze to form permanent ice deposits in low-lying areas at high latitudes. Late in the planet's history, drainage of near-surface materials to form valleys could occur only where there were loose materials at the surface, steep slopes, and/or high heat flows.

References: [1] Baker V. R. et al. (1991) *Nature, 352*, 589–594. [2] Arvidson R. E. et al. (1979) *Nature, 278*, 533–535. [3] Carr M. H. (19[illegible]2) *LPS XXIII*, 205–206. [4] Craddock R. A. and Maxwell T. A. (19[illegible]) *JGR, 98*, 3453–3468. [5] Clifford S. M. (1993) *JGR, 98*, 109[illegible]–11016. [6] Carr M. H. (1979) *JGR, 84*, 1995–3007.

[7] McCauley J. F. (1978) *USGS Misc. Inv. Map I-897*. [8] Parker T. J. et al. (1993) *JGR, 98*, 11061–1078.

ATMOSPHERIC DUST-WATER ICE INTERACTIONS: DO THEY PLAY IMPORTANT ROLES IN THE CURRENT MARS CLIMATE? R. T. Clancy, Space Science Institute, Suite 294, 1234 Innovation Drive, Boulder CO 80303, USA.

The global formation of water ice clouds has recently been determined as a characteristic feature of the aphelion Mars atmosphere, on the basis of microwave temperature and water vapor profiling as well as Hubble Space Telescope ultraviolet/violet imaging [1]. The microwave temperature soundings indicate that global-scale saturation conditions for atmospheric water have descended to altitudes as low as 5–10 km during Mars aphelion periods observed in 1980, 1982, 1991, 1993, and 1995. Such cold atmospheric temperatures and low altitudes of water vapor saturation present a stark contrast to the dusty/warm atmosphere of Mars observed by the Viking mission in the aphelion periods of 1976/1978, but are quite comparable to the aphelion atmospheric conditions observed by Mariner 9 in 1972. This implies that the 0.4–0.7 dust opacities measured by the Viking landers [2] in 1976/1978 led to atypical heating conditions for the aphelion Mars atmosphere at this time. Because this level of atmospheric dust loading raised atmospheric temperatures sufficiently (15–20 K) to displace water vapor saturation conditions to altitudes above 25 km, and because the Viking mission has been so influential in shaping our understanding of the Mars climate system for the past 15 years, it was widely accepted that water vapor saturation and water ice cloud formation are not important aspects of the current Mars climate [3]. It now appears that water ice cloud formation is more typical of aphelion atmospheric conditions, and may play a key role in the extreme north-south asymmetry of Mars water vapor/ice inventories [1].

However, an increased importance for water ice clouds in the Mars climate system does not reflect a diminished frequency or significance for Mars global dust storms. The cold, cloudy aphelion periods observed in 1993 and 1995 [1] were preceded by perihelion global dust storms in 1992 and 1994 [4]. In fact, the distinctly different rates of atmospheric cooling (and, hence, dust clearing) observed after the 1972, 1977, and 1994 dust storms suggest nonlinear interdependencies between cloud formation and dust removal in the current Mars climate. Solar absorption by the atmospheric dust strongly forces atmospheric temperatures, water vapor saturation is strongly dependent on ambient temperature, and cloud nucleation is likely to occur around the very fine dust aerosols. All cloud microphysical models of Mars predict substantial downward displacement of atmospheric water (vapor + ice) in the presence of cloud formation [5–7]. As the settling timescale of the submicron dust particles can exceed one year [8], dust removal rates should be significantly enhanced by ice condensation around dust nucleation centers. Because a reduction in dust loading leads to atmospheric cooling, cloud formation may progressively cleanse atmospheric dust loading in a manner that is nonlinear and dependent on the initial dust loading and atmospheric temperature conditions.

Recent microwave temperature profiling of the Mars atmosphere during 1995 northern summer dust storm activity suggests that cloud formation may have prevented dust from penetrating to altitudes above 10–15 km. 1995 HST imaging at $L_s = 80°$ and 148° indicates both regional dust storm activity in the northern polar, Isidis, and Hellas Basin regions, as well as global-scale water ice clouds [9]. Microwave temperatures obtained for several months after these observations show substantial (~15 K) heating of the lower 10–15 km of the global Mars atmosphere at these times, but no measurable heating of the atmosphere above ~15-km altitudes. In contrast, the observed dust heating during the 1992 and 1994 perihelion dust storms extended to altitudes well above 50 km [4].

It is also worth reemphasizing that the polar ice deposits of Mars imply critical relations between atmospheric dust and volatiles. The markedly higher albedo of the southern vs. the northern seasonal ice caps is sufficient to maintain year-round coverage of the southern residual water ice cap by CO_2 ice [10]. Current explanations for the lower albedo of the northern seasonal ice cap have focused on incorporation of dust by CO_2 snowfall [11], and the fact that the northern seasonal ice accumulates during the dusty perihelion period [12]. An additional forcing may be provided by the polar hood water ice clouds, which extend over the growth and retreat of the seasonal CO_2 ice caps. The polar hood is much more substantial in seasonal and spatial extent over the northern fall/winter hemisphere as compared to the southern fall/winter hemisphere [13]. This north-south dichotomy in polar hoods may be related to perihelion-aphelion differences in the polar CO_2 cycle [14] and/or the much larger atmospheric water vapor abundances of the northern vs. the southern hemisphere [1]. If the fine dust aerosols serve as nucleation centers in the polar hood clouds, they will be incorporated in the seasonal ice caps as the polar hood ice particles precipitate to the underlying seasonal ice cap. Because the polar H_2O molecule is more effective in entraining dust than the nonpolar CO_2 molecule [13], the water ice clouds of the polar hood may play a disproportionate role in the incorporation of dust into the seasonal ice caps. Hence, dust-water ice interactions within the polar hood clouds may provide significant input into the fundamental albedo differences of the northern and southern seasonal ice caps [1].

References: [1] Clancy et al. (1995) *Icarus*, in press. [2] Colburn et al. (1989) *Icarus, 79*, 159–189. [3] Jakosky and Haberle (1992) *Mars*, 969–1016, Univ. of Arizona, Tucson. [4] Clancy et al. (1994) *Bull. AAS, 26*, 1130. [5] Hess (1976) *Icarus, 28*, 269–278. [6] Kulikov and Rykhletskii (1984) *Solar System Res., 17*, 112–118. [7] Michelangeli et al. (1993) *Icarus, 100*, 261–285. [8] Murphy et al. (1990) *JGR, 95*, 14629–14648. [9] James et al., this volume. [10] Paige and Ingersoll (1985) *Science, 228*, 1160–1168. [11] Pollack et al. (1990) *JGR, 95*, 1447–1474. [12] Barnes (1990) *JGR, 95*, 1381–1400. [13] James et al. (1992) *Mars*, 934–968, Univ. of Arizona, Tucson. [14] James (1990) *JGR, 95*, 1439–1445.

HYDRAULIC AND THERMAL CONSTRAINTS ON THE DEVELOPMENT OF THE MARTIAN VALLEY NETWORKS. S. M. Clifford, Lunar and Planetary Institute, 3600 Bay Area Boulevard, Houston TX 77058, USA.

The resemblance of the martian valley networks to terrestrial runoff channels, and their almost exclusive occurrence in the planet's heavily cratered highlands, suggested to many early investigators that the networks were the product of rainfall—relics of a significantly warmer and wetter climate that existed early in the planet's history. However, in response to mounting geologic and theoretical

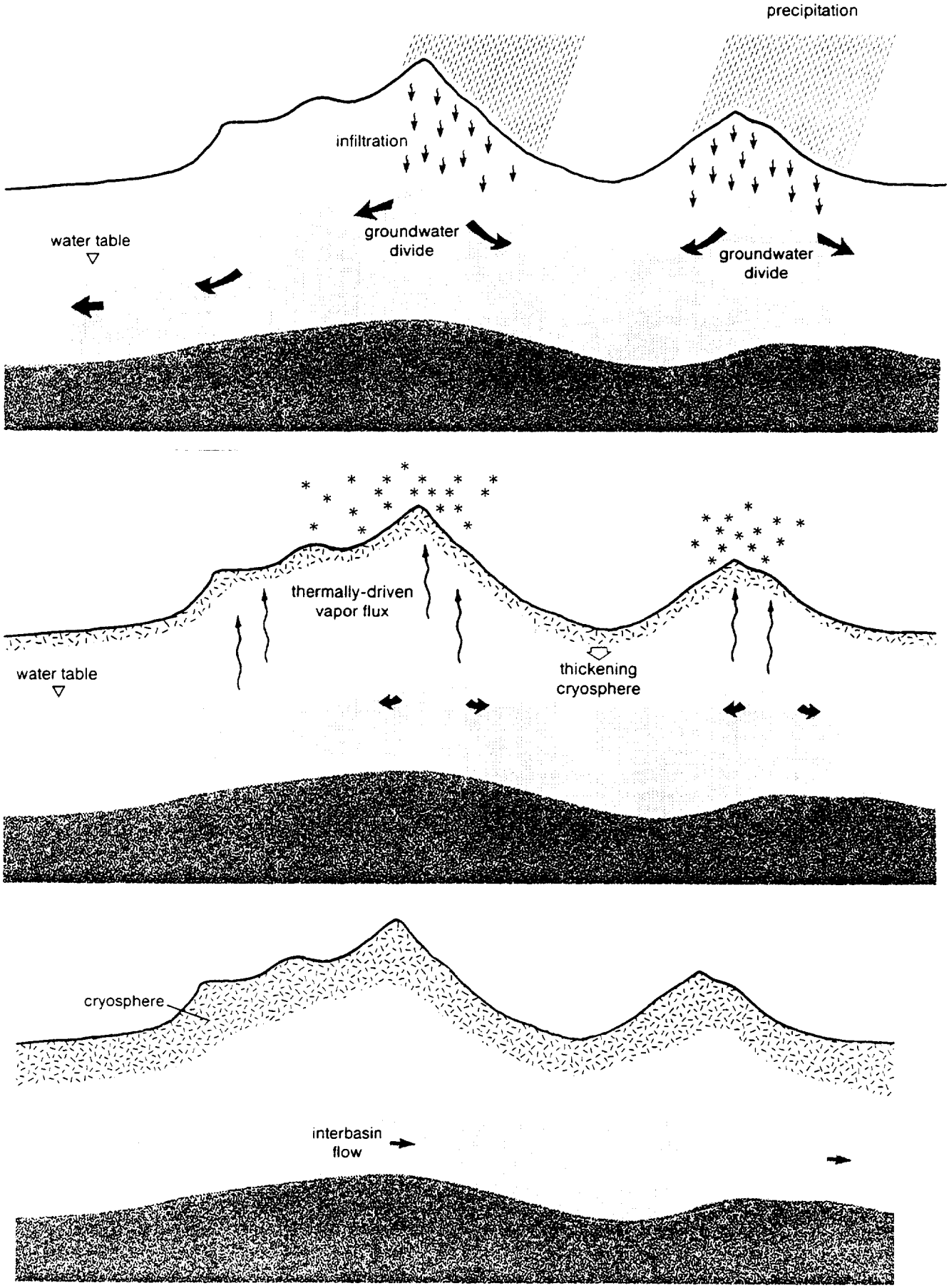

Fig. 1. The subsurface hydrologic response of Mars to the onset of a colder climate (after Clifford [3], section 6.2, Fig. 30).

arguments against the existence of a warm early Mars, efforts to explain the genesis of the networks have refocused on potential contributing endogenetic conditions and mechanisms.

An inherent assumption in many of these recent studies has been that, at the time of valley network formation, the position of the groundwater table in the cratered highlands was determined by crustal temperature alone. By this reasoning, the water table was essentially coincident with the base of the overlying frozen ground, implying a local depth beneath the terrain of as little as 100 m, given the expected 5–6× greater geothermal heatflow that is thought to have characterized the planet at this time (~4 b.y.). Under these conditions it is argued that subpermafrost groundwater may have contributed to the formation of the valleys through sapping.

However, in the absence of an active process of groundwater recharge at high elevations, the assumption of a terrain-following water table, given a planetwide subfreezing climate, appears seriously flawed. While the groundwater table on Earth often conforms to the shape of the local landscape, it does so only because it is continuously replenished by atmospheric precipitation and infiltration into the soil (Fig. 1a). However, under subfreezing conditions, the condensation of ice in the near-surface crust will effectively isolate the underlying groundwater from any possibility of atmospheric resupply (Fig. 1b). Under such conditions, groundwater will flow until any residual hydraulic head has decayed, leaving the system in hydrostatic equilibrium (Fig. 1c).

For the above reason, the identification of a vigorous recharge mechanism for groundwater in the martian highlands is a critical consideration if the valley networks were formed by the flow of liquid water. Given the concurrent existence of a subfreezing climate, the only viable candidate for this process that appears consistent with the geologic evidence is hydrothermal convection [1–3].

The arguments in favor of a hydrothermal origin of the valley networks are persuasive. Given a water-rich early crust, and the inevitable production of impact melt resulting from the formation of the craters found throughout the highlands, the development of vigorous hydrothermal systems in association with large impacts appears inescapable [1,3]. Indeed, calculations of impact melt production based on the crater size-frequency distribution of the highland crust indicate that, planetwide, impact-generated hydrothermal systems may have discharged a volume of water equivalent to a global ocean ~130 m, a volume more than sufficient to have carved the networks (section 4.4.3 of [3]). (Note that Carr [4] has recently proposed an alternative mechanism for generating the valley networks based on headward extension by groundwater-assisted mass wasting. A major strength of this idea is that the quantity of liquid water required to erode the valleys is significantly less than that required by a sapping origin, although some groundwater is still required at the base of the debris to help lubricate its transport downstream.)

Under the climatic conditions currently thought to have prevailed on Mars at the time of valley network formation, hydrothermal convection appears to be the only process capable of supplying significant volumes of water to elevated regions within the cratered highlands. Although the role of hydrothermal systems in the generation of the networks is far from proven, given a water-rich Mars, it is difficult to conceive of a scenario where the development of such systems does not naturally arise from the impact and volcanic evolution of the planet's surface [1–3].

References: [1] Newsom H. E. (1980) *Icarus, 44*, 207–216. [2] Gulick V. C. and Baker V. R. (1990) *JGR, 95*, 14325–14345. [3] Clifford S. M. (1993) *JGR, 98*, 10973–11016. [4] Carr M. H. (1995) *JGR, 100*, 7479–7508.

IS MARS WATER RICH? HYDROLOGIC, TOPOGRAPHIC, AND LATITUDINAL CONSIDERATIONS IN THE SEARCH FOR SUBPERMAFROST GROUNDWATER.

S. M. Clifford, Lunar and Planetary Institute, 3600 Bay Area Boulevard, Houston TX 77058, USA.

To date, efforts to determine whether Mars is water rich have been hampered by both the limited nature of the available data and the enormous uncertainties associated with its interpretation. However, with the advent of the Mars Surveyor Program, the potential exists for delivering electromagnetic and seismic-sounding instruments to the martian surface that can answer this question conclusively.

Because instrument mass and size constraints are likely to impose serious limits on the range and sensitivity of any geophysical sounding device, a critical factor to the success of such investigations will be the identification of landing sites where the potential depth to groundwater is minimized. Hydrologic, topographic, and latitudinal considerations suggest that the northwest interior of the Hellas impact basin (elevation < –5 km), and four low-lying sites near the equator (elevations < –2 km), are the locations best suited for the geophysical exploration of subpermafrost groundwater. The rationale behind these selections is discussed in greater detail below.

Groundwater as an Unambiguous Indicator of a Water-rich Mars: More than any other potential observation, the detection of subpermafrost groundwater would provide unambiguous evidence that Mars is water rich (sections 6.2 and 8 of [1]). This conclusion is based on the fact that the cryosphere (that region of the crust where the temperature remains continuously below the freezing point of H_2O, Fig. 1) is the primary thermodynamic sink for crustal water. That is, under the influence of the planet's geothermal gradient, water in the crust will preferentially diffuse from the higher-temperature (higher vapor pressure) depths to the lower-temperature (lower vapor pressure) near-surface crust, where it ultimately condenses in the cryosphere as ground ice. Calculations of the efficiency of this process suggest that, given a sufficiently large reservoir of groundwater at depth, a geothermal gradient of 15 K/km will supply enough H_2O to completely saturate the pore volume of the cryosphere in as little as 10^7 yr. For this reason, a necessary precondition for the widespread occurrence of groundwater is that the cold-trap represented by the cryosphere must first be saturated with ice.

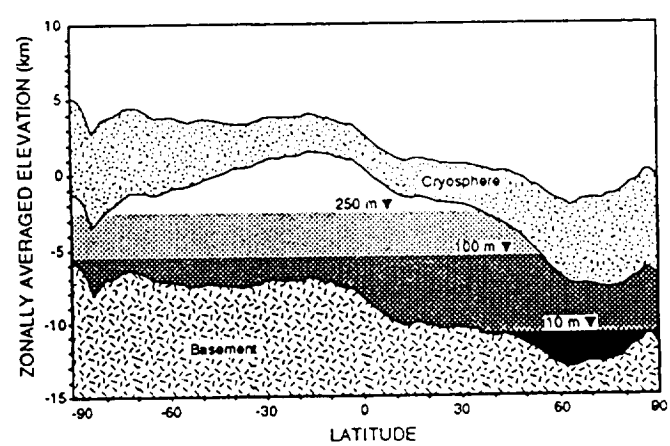

Fig. 1. A hypothetical pole-to-pole cross section of the martian crust illustrating the potential relationship of the topography, cryosphere, and groundwater for three different groundwater inventories (after [1], Fig. 7).

Given reasonable estimates of crustal pore volume, thermal conductivity, and heat flow, this appears to require an inventory of H_2O equivalent to a global ocean at least 400 m deep (section 2 of [1]).

Note that in the case where the planetary inventory of groundwater is smaller than the storage capacity of the cryosphere, virtually all the available H_2O will be rapidly cold-trapped into the frozen crust. Under these conditions, the occurrence of any subpermafrost groundwater is necessarily transient and restricted to regions of anomalous geothermal heating, where it may originate from the melting of nearby ground ice or the introduction of juvenile water in association with major volcanic centers or igneous intrusions.

Thus, the potential detection of groundwater at multiple and widely separated locations across the surface appears compatible with only one conclusion—that Mars is water rich. Yet, even in the case of a water-rich Mars, the successful detection of groundwater is not assured. Limitations of instrument range and sensitivity will require that prospective landing sites be carefully chosen to minimize the potential depth of groundwater beneath the surface. Aside from the inventory of groundwater itself, the two factors that will affect this distance most are the thickness of the cryosphere (which varies as a function of latitude) and the local elevation of the surface.

Effect of Latitude and Topography: The thickness of cryosphere at any location is essentially a function of four variables: crustal thermal conductivity, geothermal heat flow, ground-ice melting temperature, and mean temperature at the surface. Of these, only the mean surface temperature is expected to vary in a systematic way, with present-day values ranging from a high of approximately 218 K at the equator to a low of ~154 K at the poles. Given geologically reasonable values of the remaining three variables, this latitudinal decline in mean surface temperature is expected to result in a progressive thickening of the cryosphere from about 2.3 km at the equator to in excess of 6.5 km at the poles. While local values of cryosphere thickness are likely to vary significantly from these globally averaged values, it is clear that, all other factors being equal, the choice of an equatorial landing site minimizes the depth of frozen ground that must be penetrated by a geophysical sounder.

While the effect of latitude on cryosphere thickness represents an important consideration in the selection of potential landing sites, it alone is insufficient to guarantee that the depth to groundwater is minimized. This point is best illustrated by the pole-to-pole cross section of the martian crust presented in Fig. 1, which illustrates the potential relationship between the cryosphere, topography, and groundwater, for hypothetical groundwater inventories equivalent to a global layer 10 m, 100 m, and 250 m deep (for a more complete discussion, see section 2.3 in [1]). Note that for a groundwater system in hydrostatic equilibrium, the water table conforms to a surface of constant geopotential. In contrast, the base of the cryosphere mirrors the first-order variations in surface topography. As a result, the vertical distance separating the water table from the base of the cryosphere can range from zero, in regions of low elevation, to many kilometers, in regions of higher elevation (see section 2.3 and Plate 1 of [1] for a more complete discussion of potential volatile stratigraphy).

Prospective Landing Sites for the Geophysical Detection of Subpermafrost Groundwater: From the preceding analysis it is clear that low latitude and low elevation are the two most important criteria for selecting a landing site that minimizes the potential depth to subsurface water. A review of the USGS Mars Digital Terrain Model suggests that the four locations that best satisfy these criteria are Eos Chasma (9°S, 36°W), Amazonis Planitia (31°N, 158°W), Isidis Planitia (15°N, 270°W), and a region located about 1800 km southeast of Elysium Mons (6°N, 188°W). A fifth site, located in the northwest interior of Hellas (36°S, 300°W), was included because it represents the lowest spot on the planet and, despite its higher latitude, may still have the closest proximity to any reservoir of subsurface groundwater. Further details concerning each of these locations are presented in Table 1.

TABLE 1. Five potential sites for conducting geophysical soundings for subpermafrost groundwater.

Site Location	Latitude Range	Longitude Range	Elevation
Eos Chasma	6°–12°S	32°–39°W	< -3 km
Amazonis Planitia	28°–33°N	152°–163°W	< -3 km
Southeast of Elysium	2°–11°N	179°–198°W	< -2 km
Isidis Planitia	6°–22°N	263°–279°W	< -2 km
Northwest Interior of Hellas	35°–42°S	296°–307°W	< -5 km

While the design of geophysical sounders capable of detecting subpermafrost groundwater at depths of several kilometers or more may prove challenging within the mass and size constraints of the Mars Surveyor Program, it is difficult to imagine any experiment or observation that would shed more light on the current volatile inventory and hydrologic nature of Mars.

References: [1] Clifford S. M. (1993) *JGR, 98*, 10973–11016.

THE EVOLUTION OF MARTIAN WATER. T. M. Donahue, The University of Michigan, Ann Arbor MI 48109, USA.

The implications of escape of H, D, and O from Mars for the evolution of its water inventory will be examined. Particular issues to be discussed are the consequences of D/H measurements for atmospheric water vapor and hydrous minerals in SNC meteorites, and the role of atmospheric chemistry and the redox state of the atmosphere in controlling hydrogen escape. Martian water will be considered in the context of that on the other terrestrial planets.

THE ROLE OF SO_2 FOR THE CLIMATE HISTORY OF MARS. G. Dreibus and H. Wänke, Max-Planck-Institut für Chemie, Saarstrasse 23, D-55122 Mainz, Germany.

Up to 3.5 wt% S has been measured in the martian soil samples analyzed by Viking landers 1 and 2 [1]. In all likelihood S is present in the form of sulfates. A comparison of the chemical composition of the Viking soils with the composition of shergottites indicate that S might be introduced from the gas phase in the form of SO_2. As observed from SNC meteorites, martian basalts are very dry rocks compared to terrestrial equivalents [2]. The H_2O^+ abundances in shergottites range from 180 ppm up to 480 ppm [2,3]. Karlsson et al. [3], who measured the O isotope composition of water degassed from SNC meteorites at different temperatures, found that all SNC meteorites contain, besides the presence of terrestrial contamination, a large fraction of the water, which, although martian, is not derived from the martian mantle. Hence the intrinsic mantle-derived concentrations of water must be considerably lower.

Contrary to the low abundance of water, S is found in large concentrations in all shergottites, which exceeds even the concen-

tration observed for terrestrial basalts. The amount of S in basalts is generally governed by sulfide solubility. As there is clear evidence for extraction of chalcophile elements from the martian mantle due to segregation of FeS, the high abundance of S in shergottites is not surprising. This is even more true if we take into account that the solubility of S in mafic melts increases with increasing FeO content and the FeO content of shergottites exceeds that of terrestrial basalts by about a factor of 2. Reflecting the similar abundances of H_2O, CO_2, and SO_2 in terrestrial magmas, these three compounds are also found in about equal abundances in terrestrial volcanic gases. On a planet with a mantle considerably poorer in water than the Earth's mantle, but similar or richer in S, it is to be expected that SO_2 (and CO_2) will dominate the exhalation gases, although part of the S might degas in the form of H_2S and elemental S.

In order to explain the runoff channels and valley networks present on ancient, heavily cratered martian terrain, it was suggested that Mars was warmed by the greenhouse effect of a dense CO_2 atmosphere [4,5]. However, Kasting [6] has shown that this mechanism seems questionable in the early solar system history when the luminosity of the Sun was ~25–30% lower than today. SO_2 is a very efficient greenhouse gas and its importance for heating of the martian atmosphere was pointed out by Postawko and Kuhn [7].

At present, the mean surface temperature of Mars at low latitudes is –55°C, while the temperature on the poles drops to less than –140°C. Considering the lower solar luminosity 3.5 b.y. ago, the equatorial mean temperature would drop to about –73°C or close to the freezing point of SO_2. Thus without an appreciable greenhouse effect, H_2O should have been solid at all latitudes, CO_2 a solid or gas depending on latitude, and SO_2 a liquid or solid depending on latitude. On Earth, the CO_2 from erupting lavas amounts to less than 10% of the amount of CO_2 emitted to the atmosphere from fracture zones and diffusive loss through vulcano flanks. Under similar conditions on Mars, SO_2, CO_2, and H_2O from volcanic intrusions would migrate through the (mega)regolith toward the surface. Most of the CO_2 will be quickly transferred to the atmosphere, while SO_2 gas would feed solid, respectively liquid SO_2 tables at low depths. Water vapor will be trapped at even greater depths in the form of ice.

The degassing rate of SO_2 from erupting magmas is probably too small for a substantial contribution of SO_2 to greenhouse warming on a global scale. However, local warming by a volcanic intrusion will liquefy the stored SO_2 and drive it to the surface as a liquid at temperatures close to the SO_2 triple point (16 mbar and –73°C). Evaporation of stored liquid or solid SO_2 could lead to a sudden release of enough SO_2 into the atmosphere for a global temperature rise. In this way evaporation of SO_2 on a global scale might be triggered. The atmospheric lifetime of SO_2 is limited by photochemical oxidation to SO_3 and atmosphere-surface reactions. Nevertheless, the time could be sufficient to melt water ice stored at greater depths. In this way episodic eruption of larger quantities of water for comparatively short duration several times in the martian history could be explained. Water vapor in the atmosphere would further add to the greenhouse warming.

Mars contains considerable amounts of FeS [8]. Although today most of the FeS resides in the martian core a certain fraction has remained in the mantle, from which S-rich magmas were formed. The oxygen required to transform FeS to SO_2, respectively to SO_3 (sulfate), may have had an important influence on the oxygen fugacity of the martian surface and might well be the limiting factor for water.

If water was supplied by a late veneer and stored in near surface layers in form of ice, temporary greenhouse warming by SO_2 may have been responsible for melting of ice and break-out of water in areas not directly connected to volcanic activity. Aside of water, liquid SO_2 or a mixture of SO_2 and CO_2 [6] could explain some of the erosion features on the martian surface.

References: [1] Clark B. C. et al. (1982) *JGR, 87*, 10059–10067. [2] Carr M. and Wänke H. (1992) *Icarus, 98*, 61–71. [3] Karlsson H. R. et al. (1992) *Science, 255*, 1409–1411. [4] Moroz V. I. and Mukhin L. M. (1977) *Cosmic Res., 15*, 769. [5] Pollack J. B. et al. (1987) *Icarus, 71*, 203–224. [6] Kasting J. F. (1991) *Icarus, 94*, 1–13. [7] Postawko S. E. and Kuhn W. R. (1986) *Proc. LPSC 16th*, in *JGR, 91*, D431–D438. [8] Wänke H. and Dreibus G. (1988) *Philos. Trans. R. Soc. Lond., A325*, 545–557.

VOLATILES AND VOLCANOS: VERY LATE AMAZONIAN ASH DEPOSITS AND EXPLOSIVE ACTIVITY ALONG THE WESTERN FLANKS OF THE THARSIS MONTES, MARS. K. S. Edgett[1], B. J. Butler[2], J. R. Zimbelman[3], and V. E. Hamilton[1], [1]Department of Geology, Arizona State University, Box 871404, Tempe AZ 85287-1404, USA, [2]National Radio Astronomy Observatory, P.O. Box 0, Socorro NM 87901-0387, USA, [3]Center for Earth and Planetary Studies, MRC-315, National Air and Space Museum, Smithsonian Institution, Washington DC 20560, USA.

Introduction: Extensive volcanic ash deposits blanketing the youngest geomorphic units on Mars would imply that major explosive volcanic events occurred relatively late in martian history. Such eruptions would release considerable amounts of aerosols and volatiles. One probable young (<300 m.y.) ash deposit occurs on the western flank of Hecates Tholus in Elysium [1]. Mars has at least one other young, extensive ash deposit; it lies in the region known as "Stealth." It occurs west of the Tharsis volcanos, Arsia and Pavonis Montes.

Radar Stealth: The Stealth region was discovered in bistatic radar observations (3.5 cm wavelength) obtained during the 1988 Mars opposition [2]. Subsequent 3.5-cm observations from the 1992/1993 opposition refined the location of Stealth, defined as a region in which the backscatter cross section at normal incidence is very low (nearly zero, or below the 1-σ noise value [see 3]). Stealth is likely caused by the presence of an extremely underdense surface material containing no scatterers to some depth [2]. Stealth is at least 2–3 m thick, and might be 7–15 m thick [4]. It has been detected in other radio observations [e.g., 5]. Stealth covers more than 10^6 km^2 and extends about 3000 km along the equator between longitudes 115° and 215° [3].

Stealth is Not Medusa Fossae Formation: Stealth is most likely a volcanic ash deposit [2,3]. The eastern end of Stealth lies on the western slope of Pavonis Mons [3]. The southeastern end is adjacent to Arsia Mons and overlaps a region where there are small lobate features that have been interpreted as possible pyroclastic flows [6,7]. West from Pavonis and Arsia Montes, Stealth overlies a variety of geomorphic units, including lava flows and yardangs, that range from Noachian to Late Amazonian in age [8]. Stealth is one of the youngest geological features in the region [3,6,9]. Contrary to popular assumption, Stealth is not the Medusa Fossae Formation (the material in southern Amazonis Planitia that exhibits yardangs) [3,6,9].

Tharsis Montes West Flank Eruptions: Each of the Tharsis Montes has a large, lobate feature that occurs on its western flank (unit "As" in [8]). The lobes are the youngest large geomorphic features associated with each volcano [7,8]. Each of the big Tharsis Montes lobes is associated with a low radar echo: The Arsia and Pavonis Montes lobes are located at the eastern end of Stealth, and while the Ascraeus Mons lobe has a slightly higher reflectivity, it is low relative to its surroundings [3]. The implication is that Stealth consists of ash erupted from the western flanks of Arsia and Pavonis Montes. Eruptions from the west flank of Ascraeus Mons were probably smaller and had only a local effect. We invoke postcaldera flank eruptions to explain Stealth because of the stratigrapic association with the large lobe features: The lobes are younger than the calderae of Arsia and Pavonis Montes [7], and Stealth is superposed on these lobes.

Relation to Upper (Few Centimeters) Surface: Stealth has no distinguishable visual, albedo, or thermal inertia properties [3,10]. There is correlation with "rock abundance" [11]. It follows that if Stealth has no internal scatterers larger than the 3.5-cm wavelength, then there should be no "rocks" on the surface either. Some of the lowest rock abundances on Mars occur in and near (within 500 km) Stealth. These observations might indicate that the ash deposit thins toward margins that are up to 500 km outside the radar-defined Stealth area. The thermal inertia and albedo characteristics indicate that Stealth is presently overlain by a pervasive (but relatively thin) dust mantle that coats the entire Tharsis and Amazonis region [6].

Implications: The presence of Stealth in association with the western flanks of the Tharsis Montes suggests that the some of the last major events at these volcanos were probably major, explosive eruptions [6,9,12]. Explosive volcanism is expected on Mars, even in basaltic magmas [13]. Because no scatterers are seen within the 3.5-cm radar Stealth, the pyroclasts must be relatively small, even in their vent regions. Possible eolian dunes near the Arsia Mons lobe (Viking image 422A27) [14] might be composed of reworked pyroclasts. Dunes would suggest Stealth consists of grains smaller than ~1 cm. Pyroclasts should be smaller on Mars relative to similar terrestrial eruptions [13]. Stealth must consist of ash from multiple eruptions, because the width of individual volcanic airfall deposits on Mars should only be several tens to a few hundred kilometers [13], but Stealth is more than 1000 km wide. Because Stealth likely results from multiple eruptions from at least two volcanic areas (Pavonis and Arsia), the amount of volatiles that were involved in these Late Amazonian eruptions is presently unconstrained.

References: [1] Mouginis-Mark P. J. et al. (1982) *JGR, 87,* 9890–9904. [2] Muhleman D. O. et al. (1991) *Science, 253,* 1508–1513. [3] Butler B. J. (1994) Ph.D. dissertation, California Institute of Technology, Pasadena, 278 pp. [4] Muhleman D. O. et al. (1995) *Annu. Rev. Earth Planet. Sci., 23,* 337–274. [5] Harmon J. K. (1995) *Eos (Trans. AGU) Suppl., 76,* S192. [6] Zimbelman J. R. and Edgett K. S. (1994) *Eos (Trans. AGU) Suppl., 75,* 217. [7] Zimbelman J. R. and Edgett K. S. (1992) *Proc. LPS, Vol. 22,* 31–44. [8] Scott D. H. and Tanaka K. L. (1986) *USGS Map I-1802-A.* [9] Butler B. J. (1995) *LPS XXVI,* 199–200. [10] Christensen P. R. and Moore H. J. (1992) in *Mars,* 686–729, Univ. of Arizona, Tucson. [11] Christensen P. R. (1986) *Icarus, 68,* 217–238. [12] Fagents S. A. and Wilson L.(1995) *Icarus,* submitted. [13] Wilson L. and Head J. W. III (1994) *Rev. Geophys., 32,* 221–263. [14] Zimbelman J. R. (1993) *LPS XXIV,* 1575.

THE CONTRIBUTION OF VOLATILES TO THE SURFACE AND ATMOSPHERE OF MARS BY THE ACCRETION OF INTERPLANETARY DUST PARTICLES.

G. J. Flynn, Department of Physics, State University of New York–Plattsburgh, Plattsburgh NY 12901, USA.

The accretion of interplanetary dust particles (IDPs), comets, and meteorites provides a continuous addition of volatiles, including water, organics, and noble gases, to the surface and atmosphere of Mars after its formation and differentiation. The magnitude of these contributions can be estimated from the observed contributions to the Earth and Moon.

The mass distribution of extraterrestrial matter accreted by the Earth shows a bimodal distribution, sharply peaked at 10^{-7} g and 10^{18} g. The lower mass peak corresponds to the continuous, planetwide accretion of IDPs (derived from comets and asteroids), while the higher mass peak results from the infrequent impact of kilometer-size objects. Since the areas under both peaks are similar, the IDPs and the large impactors each contribute comparable masses of material to the Earth. If the IDPs and large impactors have the same composition, then each will carry roughly the same amount of water and organics to the surface. However, accretion of volatiles by the large impactors is hampered by vaporization, and possible escape, due to impact heating. IDPs, on the other hand, are gently decelerated in the atmosphere of Earth or Mars, and many IDPs arrive at the surface with their volatiles intact.

The IDPs carry with them solar wind ions, implanted while they are in space, producing concentrations of noble gases that exceed the noble gas concentrations in meteorites by several orders of magnitude. Thus, IDPs are likely to make a significantly larger contribution to the noble gas inventory of Mars than is made by the impact of the same mass of large asteroidal fragments.

Interplanetary Dust Accretion Onto Mars: The present rate of accretion of IDPs onto Mars was estimated from the flux measured at Earth using techniques described by Flynn and McKay [1]. Using this method, about 12×10^9 g of IDPs accrete onto Mars annually [2], about 75% of the 16×10^9 g/yr accreting onto the Earth [3].

Water. The chemical composition of the meteoritic component in lunar soils most closely resembles that of the CI carbonaceous chondrites [4], which have water contents ranging from 18% to 22% [5]. No quantitative water measurements have been performed on the IDPs collected at Earth, but mineralogical examination indicates that about half these IDPs contain significant abundances of hydrated silicates, the dominant water-bearing phase in CI meteorites. Taking the water abundance in the IDPs as 20%, the mean for CI meteorites, IDPs contribute about 2.4×10^9 g/yr of water, resulting in a average surface coverage of 2×10^{-9} g/cm^2 yr. Over the last 3.6 b.y. this would produce a layer of water about 7 cm thick over the entire surface of Mars.

Carbon. The C contents of CI meteorites range from 3% to 5% [5], but IDPs collected from the Earth's stratosphere have a mean C content of about 12% [6]. Using the 12% value, IDPs contribute about 1.5×10^6 kg/yr of C to the surface of Mars, or about 6×10^{15} kg of C over the last 3.6 b.y.

Noble gases. The indigenous noble gas content of meteoritic material is quite low; however, IDPs acquire noble gases from solar wind irradiation while in space. Isotopic abundances of Ne, Ar, and Xe were measured on a group of 13 IDPs from the stratosphere [7]

and He and Ne abundances have been measured on 82 individual IDPs [8]. The IDP contribution of noble gases to Mars (in Table 1) were calculated assuming these IDPs have the same noble gas concentrations as those collected from the stratosphere of Earth.

TABLE 1. Noble gas contribution by IDPs.

Isotope	Accretion Rate (cc STP/yr)	Mass Accreted Over 3.6 b.y. (g)
^{3}He	1.4×10^{6}	7×10^{11}
^{4}He	3.6×10^{8}	3×10^{14}
^{20}Ne	5.3×10^{6}	2×10^{13}
^{22}Ne	4.8×10^{5}	2×10^{12}
^{36}Ar	5.9×10^{5}	4×10^{12}
^{38}Ar	1.2×10^{5}	8×10^{11}
^{132}Xe	1.2×10^{3}	3×10^{10}

Accretion in the First Billion Years: The flux of large objects, capable of producing kilometer-sized craters, was significantly higher during the first billion years of solar system history than at present. Little is known about the flux of IDPs in that early era; however, collisions between the large asteroids and comets that produced the craters must have resulted in an abundance of dust. The accretion of meteoritic matter onto the Moon has been fit by a two-component model: a rapidly decaying flux ($t_{1/2}$ = 40 m.y.) exceeding the present flux by an order of magnitude or more 4 b.y. ago, and a relatively constant flux, near the present value, over the past 3.6 b.y. [9]. Using this model, the total accretion of IDPs from 4.0 b.y. to 3.6 b.y. ago would be about 30% of that from 3.6 b.y. to the present.

Extrapolating farther back in time, the contribution in the 200-m.y. interval from 4.2 to 4.0 b.y. ago would have been 5× that during the entire interval from 3.6 b.y. to the present. During the period from 4.5 b.y. to 4.0 b.y. ago, Mars could have acquired several meters of water, tens of centimeters of carbonaceous material, and a large inventory of noble gases from the accretion of IDPs.

References: [1] Flynn G. J. and McKay D. S. (1990) *JGR, 95,* 14497–14509. [2] Flynn G. J. (1995) in *Proceedings of the Small Bodies in the Solar System and Their Interactions with the Planets,* in press. [3] Hughes D. W. (1978) in *Cosmic Dust,* 123–185, Wiley. [4] Anders E. et al. (1973) *The Moon, 8,* 3–24. [5] Wasson J. T. (1985) *Meteorites,* 31, Freeman. [6] Thomas K. L. et al. (1994) in *Analysis of Interplanetary Dust,* 165–172, AIP Press. [7] Hudson B. et al. (1981) *Science, 211,* 383–386. [8] Nier A. O. (1994) in *Analysis of Interplanetary Dust,* 115–126, AIP Press. [9] Wasson J. T. et al. (1973) *The Moon, 13,* 121–141.

THE ANCIENT MARS IONOSPHERE. J. L. Fox[1] and S. W. Bougher[2], [1]Department of Physics, Wright State University, Dayton OH 45435, USA, [2]Lunar and Planetary Laboratory, University of Arizona, Tucson AZ 85721, USA.

The evolution of the martian atmosphere depends on nonthermal escape fluxes of species such as O and N. Nonthermal production of hot or escaping atoms may take place by photochemical processes, such as photodissociation, electron impact dissociation processes, ion-molecule reactions, and dissociative recombination; or by mechanical processes, such as sputtering and solar wind pickup. The escape fluxes due to these processes depend on the composition and temperature of the thermosphere-ionosphere and the solar fluxes, which are closely coupled. In a companion paper by Bougher and Fox (this volume) we predict, using the Mars General Thermospheric Circulation Model (MTGCM), the structure of the Mars thermosphere 3 G.y. ago, when the solar flux in the ultraviolet was about 3× more intense. Here we compute the density profiles of 14 ions and 5 minor neutral species, using densities and temperatures from the MTGCM thermospheric model. We include eddy and molecular diffusion of neutrals and ambipolar diffusion of ions. Preliminary calculations show a Venus-like, but more extended, ionosphere with an F_1 (O_2^+) peak electron density about 1.5× the present value. Due to the larger O mixing ratios, an F_2 peak appears near 300 km, where O^+ becomes the dominant ion. The escape rates of O, C, and N are enhanced for this model, and we discuss the changes and their implications for the evolution of the Mars atmosphere.

A GEOCHEMICAL MODEL FOR VOLATILE STORAGE VIA HYDROTHERMAL SYSTEMS ON MARS. L. L. Griffith and E. L. Shock, Department of Earth and Planetary Sciences, McDonnell Center for the Space Sciences, Washington University, One Brookings Drive, St. Louis MO 63130, USA.

Volatile processing on Mars has long been a topic with many questions and few solid answers. As research has progressed, it has become apparent that liquid water was involved in the evolution of Mars [1,2]. Isotopic evidence suggests that hydrothermal systems have affected the volatile evolution on the planet [2]. The O isotope data in particular imply that a reservoir other than the polar caps and atmosphere is needed to create the isotopic signatures seen in the martian meteorites and atmosphere; this reservoir could be the silicate minerals in the planet's crust [2,3]. One of the best ways to exchange isotopes between an atmosphere and silicate minerals is in moderately-high-temperature (> ~150°C) hydrothermal systems that have a "meteoric" water source. Systems of this type form as a natural consequence of volcanic activity. Volcanism has occurred on Mars throughout its history. Photogeologic evidence indicates that in the past H_2O was much more prevalent on the surface [1], and suggests that formerly there was considerable groundwater [4]. This leads to the conclusion that hydrothermal systems have operated on Mars. The question then arises: What implications do hydrothermal systems have on volatile and planetary evolution?

There are many ways to approach this issue; we have chosen to place constraints on what could have occurred on Mars by using reaction-path models to help understand the behavior of fluid/rock interactions under possible martian conditions. These calculations use irreversible thermodynamics to determine the stability of mineral phases by evaluating the extent to which a fluid has reached saturation with various minerals. At the start of a reaction-path calculation the fluid is not in equilibrium with the rock. Over the course of the calculation the equilibrium state is approached incrementally and reaction progress is monitored explicitly. Results of this type, for equilibration of shergottite with H_2O and variable partial pressures of CO_2 (P_{CO_2}), are described by Griffith and Shock [5].

We are currently expanding upon those calculations to include various plausible rock types other than shergottite and to consider differing initial fluid compositions. As in results for shergottite, we are constraining our calculations by first undertaking a comprehensive study of hydrothermal systems in Iceland. Iceland has many aspects that lend well to its use as an analog for Mars. Icelandic volcanic rocks have a fairly consistent character and are some of the most Fe rich on Earth, making them similar to martian volcanics. Most of the hydrothermal systems involve meteoric water; some appear to be recharged mostly from glacial melt waters [6], a probable characteristic of at least some martian hydrothermal systems. In addition to extensive basalt, Iceland also has localized areas of andesitic and rhyolitic volcanism, allowing us to see how varying the host-rock type affects the behavior of the system, and providing for the incorporation of other rock types into martian models.

Model results for Icelandic basalts are a close match to observations, giving confidence to our martian basaltic models [5], and permitting the investigation into the possible amount of CO_2 storage in hydrothermal carbonate on Mars. Previously, we have found that reaction path calculations for martian basalt are more "efficient" in producing carbonate than those for Icelandic basalt. For example, we find that at 250°C, 2 bar of CO_2 pressure are needed to produce carbonate during hydrothermal alteration of Icelandic basalt, but results for martian basalt yield carbonate at a $P_{CO_2} \cong 1$ bar [5]. We take this to mean that carbonate production is a likely consequence of hydrothermal interactions with basalt on Mars.

While basalt is likely a large component of the martian crust, it is probably not all of it. Photogeologic evidence suggests that several locations around Tharsis may indeed be covered by tuffaceous material [7]. On Earth, tuffs are usually rhyolitic or andesitic. Model calculations using Icelandic andesites and rhyolites do not differ greatly from the basaltic calculations. The assemblages are very similar. As the amount of SiO_2 in the host-rock increases, so do the amounts of quartz, K-feldspar, and albite in the alteration assemblage. As the amount of Mg + Fe decreases in the host-rock, so do the amounts of epidote, talc, tremolite, and chlorite in the alteration assemblage. However, the amount of carbonate is relatively unaffected by the differences in host-rock compositions. This leads to the conclusion that rock type does not greatly affect CO_2 storage in hydrothermal systems in Iceland, and most likely on Mars as well.

We have begun to look into the implications for H_2O storage via hydrothermal alteration. What is of interest is the amount of H_2O that can be stored in the hydrous alteration minerals. Some of the important phases are chlorite, epidote, kaolinite, laumontite, prehnite, talc, and tremolite. The total amount of alteration on the planet is the biggest factor in determining the amount of H_2O that could be trapped in these phases. Reliable estimates of the extent of alteration rely on several unknowns: the total amount of H_2O on early Mars, and the timing, magnitude, and distribution of heat flow when abundant H_2O was present. Another consideration that complicates these calculations is the present desiccation of the planet. A number of the hydrous phases are not stable under present near-surface conditions, and it is possible that many have decomposed and released their water, affecting the amount of H_2O stored in this manner.

A third volatile that would be affected by hydrothermal processes is S. Mars' S content seems to be higher than Earth's [8], leading to more S-rich systems. Sulfur-rich Icelandic systems produce abundant pyrite, and at springs, native S encrustations are common. Icelandic calculations that include S generate pyrite as a product, as expected, with little change in the rest of the alteration products. If Mars is indeed more S rich, as well as being more Fe rich, pyrite could be a prevalent alteration product. The total amount of "buried" S directly depends on the extent of alteration and available constraints on how S rich Mars is considered to be.

In summary, this modeling suggests that it is possible to sequester significant amounts of volatiles in martian hydrothermal systems. The extent of these systems in the martian past is unclear, but it is possible that they have affected the global budget of volatiles and moderated the isotopic exchange between the crust and atmosphere. One possibility is that hydrothermal sequestering of volatiles was extreme enough to contribute to the apparent loss from the atmosphere of H, O, and C that has been proposed to explain the isotopic data.

References: [1] Carr M. H. (1981) *Icarus, 68*, 187–216. [2] Jakosky B. M. (1991) *Icarus, 94*, 14–31, and references therein. [3] Jakosky B. M., personal communication. [4] Carr M. H. (1979) *JGR, 84*, 2995–3007. [5] Griffith L. L. and Shock E. L. (1995) *Nature, 377*, 406–408. [6] Sveinbjornsdóttir A. E. et al. (1986) *Contrib. Mineral. Petrol., 94*, 99–109. [7] McCauley J. F. (1978) *USGS Misc. Geol. Inv. Map: I-896*. [8] Anders E. and Owen T. (1977) *Science, 198*, 453–465.

THE MARTIAN CLIMATE SYSTEM AT HIGH OBLIQUITY: SIMULATIONS WITH THE NASA AMES MARS GENERAL CIRCULATION MODEL.

R. M. Haberle, Mail Stop 245-3, NASA Ames Research Center, Moffett Field CA 94035-1000, USA.

Mars' obliquity is now believed to vary chaotically on timescales of 10^7 yr [1]. On this timescale, it may have reached values as high as 60°. We have begun to explore the consequences of such high obliquities on the martian climate system using the NASA/Ames Mars general circulation model [2]. In particular, we have simulated how the general circulation and CO_2 cycle differ from the present regime when the obliquity is 60°. The simulation runs for two Mars years with all parameters as they are for current conditions (fixed atmospheric dust loading, current eccentricity, and 7.6 mbar of CO_2 available to the atmosphere + cap system).

Not surprisingly, we find a greatly amplified CO_2 cycle for the 60° obliquity simulation; the minima are deeper as the polar caps extend to 10° latitude in the each hemisphere during winter. Between ±10°, CO_2 frost condenses at night but sublimes away during the day. Thus, every location of the planet has CO_2 frost on the surface at some time of the year. Daily-averaged surface temperatures at high latitudes approach the melting point of water during summer in the north, and well exceed it during summer in the south. Thus, the seasonal variation in high-latitude surface temperatures is substantially increased compared to the present epoch.

Because of the short thermal response time of the atmosphere, the general circulation at the equinoxes is similar in structure and intensity to the present-day equinox circulation. However, at the solstices there is a major change. The cross-equatorial Hadley circulation is greatly expanded compared to present conditions. This is a consequence of the tendency of the rising branch of the Hadley circulation to track the subsolar point, which now reaches 60° at the solstices. Because angular momentum is approximately

conserved, the low-level westerly jet associated with the rising branch doubles in strength to ~40 m/s in the time and zonal-average. Surface stresses associated with this jet are more than sufficient to lift dust on a continual basis. Thus, in spite of the fact that surface pressures are lowest at this season, the winds are strong enough to lift dust; this applies to both solstices. Thus, there is no need to invoke regolith desorption as a means to increase the frequency of dust storms at times of high obliquity [3]. The greatly expanded solsticial Hadley cell, and the increased temperatures at high latitudes in the summer hemisphere, suggest that the water cycle will also be greatly amplified. One suggestion has been that at high obliquity polar water will find its way to the equatorial regions, which are more stable sites for volatiles under such conditions [4]. Another possibility suggested by these results is that water is shuffled between hemispheres each year and does not stabilize in equatorial regions. In the summer hemisphere water is mobilized and quickly transported into the winter hemisphere by the greatly expanded cross-equatorial Hadley circulation, where it precipitates out onto the seasonal CO_2 caps. In this scenario, weathering and physical erosion would be greatly accelerated compared to present-day rates.

References: [1] Tuoma J. and Wisdom J. (1993) *Science, 259*, 1294–1297. [2] Pollack J. B. et al. (1990) *JGR, 95*, 1447–1474. [3] Toon O. B. et al. (1980) *Icarus, 44*, 552–607. [4] Jakosky B. M. and Carr M. H. (1985) *Nature, 315*, 559–561.

SOME CONSTRAINTS ON THE AMOUNT OF CO_2 STORED IN THE POLAR REGIONS OF MARS.

R. M. Haberle[1] and D. Tyler[2], [1]Mail Stop 245-3, NASA Ames Research Center, Moffett Field CA 94035-1000, USA, [2]Verde Valley School, 3511 Verde Valley School Road, Sedona AZ 86351, USA.

Jakosky et al. [1] speculate that at times of high obliquity (~60°), water ice at the north pole of Mars would rapidly sublime into the atmosphere, possibly migrating to the more stable equatorial regions. In this situation, the buried polar deposits would be exposed, and if these deposits were CO_2 ice or CO_2 clathrate hydrate, then they too would rapidly sublime into the atmosphere, possibly raising global mean surface pressures by as much as 850 mbar. Storage of such large amounts of CO_2 in the current polar deposits is possible only if they are buried at depth and not in diffusive contact with the atmosphere.

Here we argue that there is an upper limit on the amount of available CO_2 stored in the polar regions that is based on the following line of reasoning. If large amounts of CO_2 have been released to the atmosphere at times of high obliquity, then it can return to the polar regions at times of low obliquity only if the heat balance permits. The major source terms in the polar heat balance are solar heating and atmospheric emission. The former is proportional to the obliquity, while the latter depends on atmospheric mass or, equivalently, the mean surface pressure. As the surface pressure increases, so does the greenhouse effect and atmospheric heat transport. Thus, a decrease in solar heating at times of low obliquity can be offset by an increase in atmospheric mass and thus prevent the formation of permanent caps and the return of CO_2 to the polar regions.

We have attempted to quantify this relationship using the energy balance model of Haberle et al. [2]. The model calculates the heat balance of the polar and equatorial regions and couples them to each other through a parameterized heat transport term that depends on surface pressure. For the current epoch, the minimum obliquity is about 11°. According to our model, permanent caps will not form at this obliquity if the atmosphere contains more than 370 mbar of CO_2. Thus, during the past obliquity cycle, no more than this amount could have been released to the atmosphere. Of course, this assumes that loss of CO_2 by weathering and escape is negligible on the obliquity oscillation timescale. This is probably a good assumption for escape, but is highly doubtful for weathering that has a nonlinear dependence on temperature.

References: [1] Jakosky B. M. et al. (1995) *JGR, 100*, 1579–1584. [2] Haberle R. M. et al. (1994) *Icarus, 109*, 102–120.

GEOLOGY OF THE POLAR LAYERED DEPOSITS ON MARS.

K. E. Herkenhoff and J. J. Plaut, Mail Stop 183-501, Jet Propulsion Laboratory, California Institute of Technology, Pasadena CA 91109-8099, USA.

It is widely believed that the martian polar layered deposits record climate variations over at least the last 100 m.y. [1–8], but the details of the processes involved and their relative roles in layer formation and evolution remain obscure [9]. A common presumption among Mars researchers is that the layered deposits are the result of variations in the proportions of dust and water ice deposited over many climate cycles [3–5], but their composition is poorly constrained [10]. The mechanisms by which material is incorporated and eroded from the layered deposits, which probably involve water ice and other volatiles, must be understood before the processes that formed and modified the layered deposits can be inferred and related to martian climate changes.

Calculations of the stability of water ice in the polar regions of Mars [5,11,12] indicate that interstitial ice is not currently stable at the surface of the layered deposits. The present water ice sublimation rate is high enough to erode the entire thickness of the deposits in about a million years. This result suggests that sublimation of water ice from the layered deposits results in concentration of nonvolatile material at the surface of the deposits. Such a lag deposit would insulate underlying water ice from further sublimation, stabilizing the layered deposits against rapid erosion. The existence of a stable, competent layer is indicated by slopes of up to 20° in exposures of the south polar layered deposits [13]. The color and albedo of the layered deposits suggest that bright, red dust is the major nonvolatile component of the deposits, and the association of dark saltating material indicates that there is at least a minor component of dark material in the deposits [14,15]. The albedo of the layered deposits does not necessarily indicate that an insulating dust layer is present, as the observed albedo only constrains the fraction of dust at the surface to be greater than 0.1% by mass if mixed with water ice grains that have radii of 0.1 mm or larger [16]. The existence of a lag deposit at least a few millimeters thick is more strongly supported by the low apparent thermal inertia of the surface of the south polar layered deposits [17]. However, a similar thermal-inertia mapping study of the north polar region indicates that water ice is present near the surface of the north polar layered deposits and is subliming into the atmosphere [18]. Hence, it appears that while the present erosion rate of the south polar layered deposits is low, the north polar layered deposits (at least in some areas) are currently being eroded by ice sublimation. These inferences have important

implications for the present water budget on Mars, and are consistent with estimates of the relative surface ages of the north and south polar layered deposits.

Using medium-resolution Viking imagery, Plaut et al. [8] found several craters in the southern layered deposits. In contrast, Cutts et al. [2] found no fresh impact craters larger than about 300 m in summertime images of the north polar layered deposits. Recent study of high-resolution springtime images confirms the lack of impact craters >100 m in diameter over most of the north polar layered terrain [19]. The uniform seasonal frost coverage, clear atmospheric conditions, and excellent resolution (20–95 m/pixel) of these springtime images make them an ideal dataset for constraining the surface age of the north polar layered deposits. This work is ongoing, but it is clear that the surface of the north polar layered deposits is much younger than that of the south polar layered deposits. Hence, erosional and/or depositional processes have been more active recently in the north polar region than in the south. The greater extent of eolian erosional features in the south polar layered terrain may be evidence that gradual erosive processes (such as eolian abrasion) have been more important than rapid ice sublimation in the evolution of the south polar layered deposits. Furthermore, the inferred average surface age of the south polar layered deposits (at least 10^8 yr [8]) is much longer than the timescales of theoretical orbital/axial variations (10^5–10^6 yr [20]). At least some areas of the south polar layered terrain have therefore not been greatly modified by global climate changes over the last 100 m.y. or so. New orbital observations of the martian polar regions from the Mars Global Surveyor and surface exploration by the Mars Volatiles and Climate Surveyor are likely to greatly enhance our understanding of the polar layered deposits and the climate changes that they record.

References: [1] Murray B. C. (1972) *Icarus, 17*, 328–345. [2] Cutts J. A. et al. (1976) *Science, 194*, 1329–1337. [3] Cutts J. A. et al. (1979) *JGR, 84*, 2975–2994. [4] Squyres S. W. (1979) *Icarus, 40*, 244–261. [5] Toon O. B. et al. (1980) *Icarus, 44*, 552–607. [6] Carr M. H. (1982) *Icarus, 50*, 129–139. [7] Howard A. D. et al. (1982) *Icarus, 50*, 161–215. [8] Plaut J. J. et al. (1988) *Icarus, 76*, 357–377. [9] Thomas P. et al. (1992) In *Mars*, 767–795, Univ. of Arizona, Tucson. [10] Malin M. C. (1986) *GRL, 13*, 444–447. [11] Hofstadter M. D. and Murray B. C. (1990) *Icarus, 84*, 352–361. [12] Paige D. A. (1992) *Nature, 356*, 43–45. [13] Herkenhoff K. E. and Murray B. C. (1990) *JGR, 95*, 14511–14529. [14] Thomas P. C. and Weitz C. (1989) *Icarus, 81*, 185–215. [15] Herkenhoff K. E. and Murray B. C. (1990) *JGR, 95*, 1343–1358. [16] Kieffer H. H. (1990) *JGR, 95*, 1481–1493. [17] Paige D. A. and Keegan K. D. (1994) *JGR, 99*, 25993–26031. [18] Paige D. A. et al. (1994) *JGR, 99*, 25959–25991. [19] Herkenhoff K. E. et al. (1996) in preparation. [20] Kieffer H. H. and Zent A. P. (1992) in *Mars*, 1180–1218, Univ. of Arizona, Tucson.

MODELING THE MARTIAN WATER CYCLE. H. Houben[1], R. M. Haberle[2], R. E. Young[2], and A. Zent[3], [1]Space Physics Research Institute, Sunnyvale CA 94087, USA, [2]NASA Ames Research Center, Moffett Field, CA 94035, USA, [3]SETI Institute, Moffett Field CA 94035, USA.

We have successfully modeled the current martian water cycle using our Mars Climate Model [1]—a spectral GCM with simplified radiation physics and a hydrological cycle, coupled to a parameterized two-layer subsurface model—provided that the adsorptivity of the martian soil is sufficient to buffer the summertime transport of atmospheric water vapor from the high northern latitude source region into the ascending branch of the cross-equatorial Hadley cell.

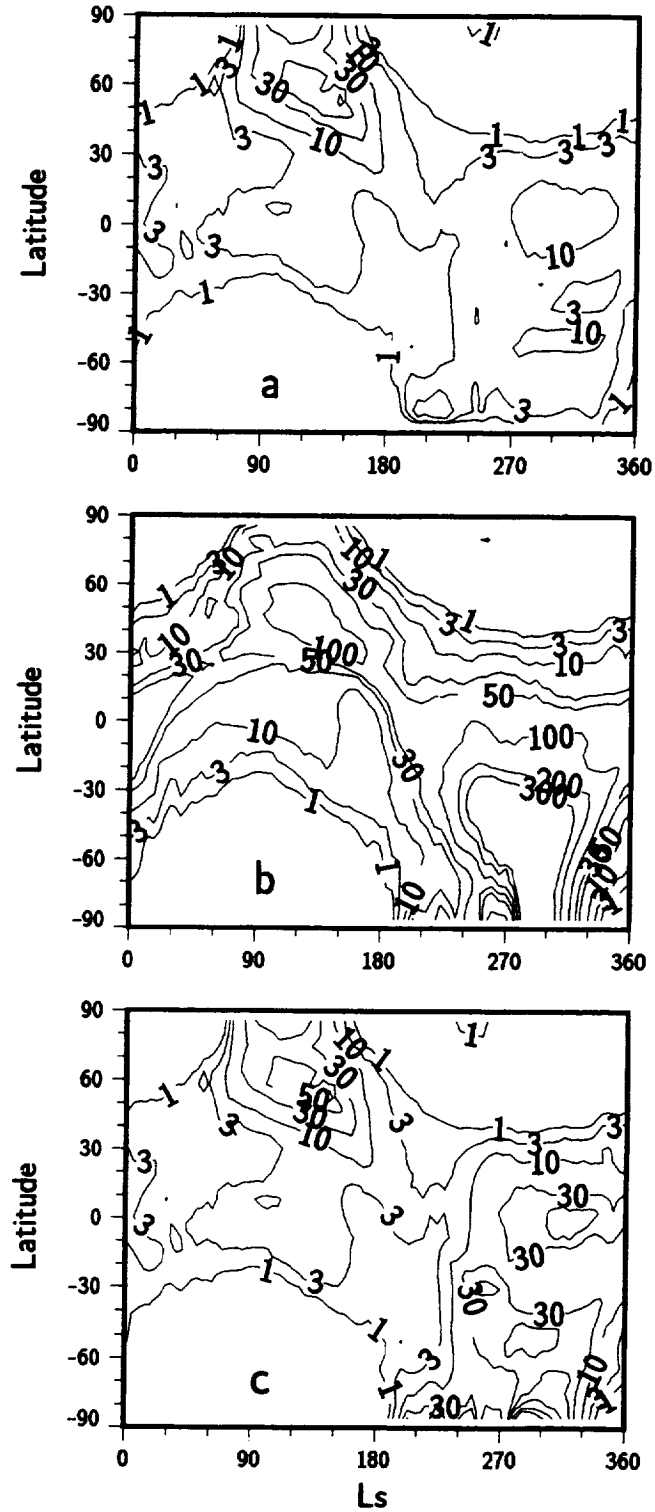

Fig. 1. Simulated martian water cycles after 10-year integrations beginning with a dry planet and atmosphere and an exposed residual water cap in the (a) northern, (b) southern, and (c) both hemispheres. Total water vapor column abundance (in precipitable micrometers) is plotted as a function of latitude and season. Note the uneven contour intervals.

In the absence of regolith adsorption, large amounts of vapor are removed from the residual polar water ice cap within only a few Mars years, resulting in a planet almost entirely covered with water frost and therefore a water vapor saturated atmosphere. The global average adsorptivity required to produce a MAWD-like [2] seasonal water cycle is approximately one-fourth of the value estimated by Fanale and Cannon [3] for basalt. In all likelihood the true martian regolith is a mixture (on an unknown scale) of a poorly adsorbing component like palagonite [4] and a small fraction of some highly adsorbing clay-like mineral. In any case, an important global-average physical property of the soil can apparently be determined from consideration of the atmospheric water cycle. Much more adsorbing soil would severely limit transport of high latitude water toward the tropics, resulting in much too dry a planet.

Our simulated seasonal cycle for the current epoch is illustrated in Fig. 1a, where we plot total column water vapor as a function of latitude and season. Our model predicts low-altitude (<20 km) saturation of the tropical atmosphere in northern summer, consistent with HST cloud observations [5], and seasonal frost deposits in midlatitudes, roughly consistent with Viking Lander 2 observations [6]. The model also predicts a significant seasonal deposit of adsorbed water in midlatitudes.

To test the stability of the current martian water system to orbital changes, we have conducted simulations that begin with a dry atmosphere and planet and an exposed residual water ice cap at the south pole (i.e., the perihelion summer hemisphere). The high temperatures and vapor pressures of the southern hemisphere overcome the buffering effects of the regolith, and water is soon spread over the planet (Fig. 1b). As in the case of our simulations with nonadsorbing regolith, almost the entire planet is covered with water frost within a few years and the lower atmosphere is saturated with water vapor. Since our model does not yet incorporate the radiative effects of greatly increased surface (frost) and cloud albedos, nor the infrared absorption by the water vapor, we cannot yet say what the eventual stable distribution of the system would be. However, it seems probable that during the cycle of its orbital evolution, Mars is at times a much wetter planet than at present.

As an intermediate case between those just described, we have conducted a simulation in which a small south polar water ice cap (of the extent of the current permanent CO_2 cap) is exposed during a single southern summer. This is meant to model the Earth-based observations of high southern summer water vapor columns in 1969 [7]. Our simulations (Fig. 1c) show a reasonable agreement with the observations for that year, with a subsequent relaxation back to the current cycle.

References: [1] Houben H. et al. (1994) *Bull. AAS, 26*, 1112. [2] Jakosky B. M. and Farmer C. B. (1982) *JGR, 87*, 2999–3019. [3] Fanale F. P. and Cannon W. A. (1974) *JGR, 79*, 3397–3402. [4] Zent A. P. and Quinn R. C. (1995) *JGR, 100*, 5341–5349. [5] Clancy R. T. et al. (1995) unpublished manuscript. [6] Wall S. D. (1981) *Icarus, 47*, 173–183. [7] Jakosky B. M. and Barker E. S. (1984) *Icarus, 57*, 322–334.

EVOLUTION OF MARTIAN ATMOSPHERIC ARGON AND NEON. K. S. Hutchins and B. M. Jakosky, Laboratory for Atmospheric and Space Physics, Department of Geological Sciences, University of Colorado, Boulder CO 80309, USA.

We have examined processes affecting isotopes of Ar (^{36}Ar, ^{38}Ar, ^{40}Ar) and Ne (^{20}Ne) in order to determine important sources and sinks of atmospheric volatiles on Mars. Our initial model for Ar and Ne atmospheric evolution [1] incorporates production of radiogenic Ar in the mantle, outgassing from extrusive and intrusive volcanism, and loss to space by collisional sputtering above the exobase. The integrated evolution of Ar and Ne species are determined in terms of four variables: (1) the planetary concentration of K, (2) the fraction of the juvenile volatile reservoir released catastrophically during the first 600 m.y., (3) potential variation in the time-history of sputtering from that suggested by Luhmann et al. [2], and (4) the volcanic factor that compares the volume of total outgassing required to match the atmospheric measurements to the volume of outgassing contributed by volcanic release. Our results indicate that sputtering has played a substantial role in modifying the martian atmosphere by removing 85–95% of the outgassed ^{36}Ar, and 70–88% of the ^{40}Ar. With this degree of loss, our calculations require outgassing of between 10 and 100× the volume of Ar species released from extrusive and intrusive volcanism. Furthermore, with loss of 100% of the atmospheric ^{20}Ne within 100 m.y. [3], Mars must have outgassed between 160 and 1820× the Ne released to the atmosphere by volcanic outgassing. Although these results must be evaluated within the context of the model uncertainties, they establish two very compelling conclusions. First, the magnitude of the Ar and Ne volcanic factors unequivocally show the existence of substantial sources of atmospheric volatiles in addition to volcanic outgassing. Second, the difference in the Ne and Ar values indicates a distinct Ne/Ar elemental fractionation (upon outgassing) on the order of 9.6 to 17.2, which can provide a framework to evaluate alternative sources of volatiles.

We have used the calculated Ar and Ne volcanic factors and the Ne/Ar fractionation as constraints to evaluate the following mechanisms for delivery of volatiles to the martian atmosphere: (1) hydrothermal or groundwater circulation, (2) melt-solubility fractionation and outgassing from quiescent volcanos, (3) delivery of volatiles by impact of comets [4], and (4) additional atmospheric modification by polar clathrate formation [5].

In hydrothermal or groundwater circulation systems, noble gas species trapped in crustal rocks and minerals at depths up to about 10 km are released into the fluid by chemical alteration and diffusion. Upon reequilibration with the atmosphere, outgassing of excess noble gases fractionates Ne/Ar in the proper direction and magnitude depending upon the initial Ne/Ar ratios in the rock and the water and the water/rock ratio. Whether hydrothermal systems can outgas enough volatiles to match the calculated volcanic factors depends upon the abundance of gas within the crustal rocks (which should be higher than for Earth due to a lack of plate tectonics) and the propensity for release of the gas from the rock during equilibration with the fluid (which will be related to the volume of water).

It has been demonstrated previously [6] that differences in the solubilities of noble gas species in magma can cause a Ne/Ar fractionation in the evolved gas phase of the right direction and magnitude dependent primarily upon the melt vesicularity. Corresponding to this fractionation mechanism, the additional source to account for the calculated volcanic factors could be outgassing from volcanos during quiescent periods (which was not accounted for the in the previous model [1], and may be as large as another factor of 10–20 in additional outgassing).

At the present there is not enough data to adequately determine the contribution of each of the aforementioned outgassing mechanisms. Martian sample return missions focusing on alteration minerals associated with hydrothermal deposits could provide further constraints on crustal exchange of volatiles. Furthermore, studies of

noble gases in comets and clathrate distribution on Mars would also be useful to better understand the entire noble gas budget.

References: [1] Hutchins K. S. and Jakosky B. M. (1995) *JGR*, submitted. [2] Luhmann J. G. et al. (1992) *GRL, 19,* 2151–2154. [3] Jakosky B. M. et al. (1994) *Icarus, 111,* 271–288. [4] Owen T. and Bar-Nun A. (1995) *Volatiles in the Earth and Solar System* (K. Farley, ed.), pp. 123–138, AJP Conf. Proc. 341. [5] Musselwhite D. and Lunine J. I. (1995) *JGR*, in press. [6] Zhang Y. and A. Zindler (1989) *JGR, 94,* 13719–13737.

MARS VOLATILE EVOLUTION FROM STABLE ISOTOPE ABUNDANCES. B. M. Jakosky[1] and J. H. Jones[2], University of Colorado, Boulder CO 80309-0392, USA, [2]Mail Code SN4, NASA Johnson Space Center, Houston TX 77058, USA.

Understanding the nature of the Mars volatile and climate system is crucial to understanding the history of the planet. Mars is the only planet other than the Earth on which water has played a significant role in the evolution of the surface. The geology suggests that the climate on Mars early in its history was substantially different from the present-day climate—degradation of impact craters suggests that erosional processes were effcient up until about 3.5 b.y. ago, and the presence of tributary systems of valleys requires liquid water to be more stable on the surface than it is today. The climate on early Mars could even have been similar to the terrestrial climate at the same time, when life was first forming on Earth, opening up the possibility that life may have formed on Mars as well.

If the early martian climate was substantially different from that of today, how can we quantify this difference? What volatiles were present on early Mars, how abundant were they, and what was their subsequent fate? We examine measurements of stable isotopes in the various components of the martian surface-and-atmosphere in order to constrain the nature and history of the reservoirs of volatiles on Mars.

Martian atmospheric volatiles are capable of exchanging with nonatmospheric reservoirs, of being lost to space by thermal and nonthermal mechanisms, and of being lost irreversibly to the crust by chemical interactions. The ability to use isotopes as a constraint on the evolution of the volatile system comes from comparisons of ratios of stable isotopes of a given element in the atmosphere, in surface alteration products thought to be derived from atmospheric gases, and from estimates of the initial isotope ratios in juvenile gases. Atmospheric ratios come from *in situ* measurements from the Viking spacecraft, from spectroscopic observations using Earth-based telescopes, and from samples of gases trapped in various components of the SNC meteorites (shergottites, nakhlites, chassignites). The SNC meteorites are convincingly of martian origin, based on their crystallization ages, O isotopes, and trapped gas composition, and were ejected to space by large impacts. Isotope ratios in crustal minerals and alteration products can be derived from them, with different components of the meteorites retaining gases or volatiles from different stages in their history. These, in turn, constrain the signatures of mantle, crustal, and atmospheric volatiles. In particular, the analysis of gas trapped in glass in one SNC (EETA 79001) has allowed the Viking measurements of the atmosphere to be considerably refined.

The ratios of D/H, $^{18}O/^{16}O$, $^{13}C/^{12}C$, $^{15}N/^{14}N$, $^{38}Ar/^{36}Ar$, and the isotopes of Xe will have the most to say about the history of martian volatiles. These gases either reside primarily in the atmosphere (N_2, Ar, and Xe) or play major roles in determining the climate (C, H, and O as CO_2 and H_2O). Whereas H and D can escape to space via thermal escape, heavier species require other mechanisms. Nitrogen, O, and C near the exobase can receive sufficient energy to escape by various photochemical reactions, such as dissociative recombination. In addition, these species and the light noble gases Ar and Ne also can be lost to space via sputtering due to the impact of O^+ ions picked up by the magnetic field of the impinging solar wind.

Based on analysis of the various isotope systems, we conclude the following: (1) There appear to be two major reservoirs of martian gases: a fractionated component that has undergone exchange with the atmosphere and a component that is unfractionated and therefore represents juvenile gases. (2) There has been substantial evolution of the atmosphere by loss to space. (3) The atmospheric species have been mixed to a large degree with crustal reservoirs of each species. Because exchange between the atmosphere and crust is not likely to occur extensively during the present climatic regime, it appears either that the climate has had occasional epochs in which liquid water was stable or that the exchange occurred through hydrothermal systems that are capable of mixing volatiles to the surface even under the present climate. The likely presence of hydrothermal systems in the crust and the weathering and hydrothermal alteration of crustal rocks argue more strongly for the latter. The occurrence of such hydrothermal systems could have substantial implications for the chemical and biological evolution of Mars.

67324

MARTIAN DUST STORMS: HUBBLE SPACE TELESCOPE OBSERVATIONS. P. B. James[1], J. Bell[2], R. T. Clancy[3], S. W. Lee[4], L. J. Martin[5], and M. Wolff[1], [1]University of Toledo, Toledo OH 43606, USA, [2]Cornell University, Ithaca NY 14853, USA, [3]Space Science Institute, Boulder CO 80309, USA, [4]Laboratory for Atmospheric and Space Physics, Boulder CO 80309, USA, [5]Lowell Observatory, Flagstaff AZ 86001, USA.

The Hubble Space Telescope (HST) acquired images of Mars several times following the 1995 opposition. Table 1 presents some of the important ephemeris parameters that characterize these observations.

TABLE 1. Post-opposition observations of Mars during 1995.

Date (UT)	Diameter (arcsec)	SE Lat (deg)	Phase (deg)	L_s (deg)	CML (deg)
April 8	9.8	18.1	32.6	81.9	282.5
May 28	6.7	23.6	38.0	104.0	272.0
July 6	5.5	26.3	35.9	122.0	275.2
July 6	5.5	26.3	35.9	122.0	32.6
July 11	5.4	26.4	35.4	124.4	159.2
Aug 2	5.0	25.9	33.0	135.0	274.2
Aug 21	4.7	24.1	30.6	144.4	272.9

The sub-Earth latitude, which was well north of the equator for all these images, provides excellent coverage of the northern hemisphere including the late phases in the recession of the north polar cap. The imaging sequences on the first two dates utilized the

WFPC2 filters 255W, 336W, 410M, 502N, and 673N. The July and August images also included the filters 953N, 1042M, LRF 7400, and LRF 8600.

Two of these sets of images, those for April 8 and August 21, reveal significant obscuration of the north polar cap. Color composites prepared using the 410M, 502N, and 673N bandpasses to represent B,G, and R strongly suggest that the cap is obscured in both cases by significant amounts of dust. Comparison of the two sets of August images also suggests dust in Isidis and other subequatorial areas. We believe that these would be classified as regional storms in the scheme of Martin and Zurek [1] based upon the area affected. Inasmuch as all of the images were acquired during one HST orbit, there are no data regarding the time evolution of these events.

Viking orbiters observed a significant regional dust storm near the north polar cap on several consecutive orbits in 1978 [2] at L_s = 65°, in the same general season as that seen in the April images. However, the late summer event seen at L_s = 144° has little precedent in previous observations [1]. This is the season of the planned Pathfinder landing in 1997, so these observations suggest that it cannot be assumed that the planned landing site will be clear at the time of the landing.

Data will be presented on the modeled optical depths of the dust for the wavelengths spanned by these observations, and the geographical extent of the storm will be constrained to the extent possible.

Acknowledgments: This research was supported by the Space Telescope Science Institute through GO grant #5832.

References: [1] Martin L. W. and Zurek R.W. (1993) *JGR, 98,* 3221. [2] James P. B. (1985) *Recent Advances in Planetary Meteorology* (G. Hunt ed.), p. 85, Cambridge; James P. B. (1993) in *LPI Tech. Rpt. 93-05,* 17.

SPUTTERING OF THE ATMOSPHERE OF MARS. R. E. Johnson, D. Schnellenberger, and M. Liu, Department of Engineering Physics, University of Virginia, Charlottesville VA 22903, USA.

O^+ "pickup" ions accelerated by the solar wind fields [1] can impact the exobase of Mars and collisionally eject atoms and molecules, a process referred to as atmospheric sputtering [2]. This erosion process has been shown to affect the isotope ratios in the martian atmosphere [3,4] and the total loss of atmosphere [5,6]. In this paper two model atmospheres are considered: an exobase dominated by O, which may resemble early martian epochs, and an exobase having a mix of O and CO_2. The Monte Carlo calculations are based on realistic interaction potentials. The results for the single-component O atmosphere are compared to the useful analytic models [2]. The results for the atmosphere having CO_2 at the exobase are compared to two earlier calculations. As expected, by including dissociation in other than the first collisions the net C loss rate is larger than that given by Luhmann et al. [5], but the net loss rate is much smaller than the order of magnitude increase obtained by assuming every energetic collision leads to complete dissociation [6].

References: [1] Luhmann J. G. and Koyzra J. U. (1991) *JGR, 96,* 5457. [2] Johnson R. E. (1994) *Space Sci. Rev., 69,* 215. [3] Jakosky B. M. et al. (1994) *Icarus, 111,* 271. [4] Pepin R.(1994) *Icarus, 111,* 289. [5] Luhmann J. G. et al. (1992) *GRL, 19,* 2151. [6] Kass D. and Yung Y. (1995) *Science, 268,* 697.

MARTIAN VOLATILES: INSIGHTS FROM THE SNC METEORITES. J. H. Jones, Mail Code SN4, NASA Johnson Space Center, Houston TX 77058, USA.

The discovery of meteorites from Mars [1] has allowed refinement of analyses from the Viking mission and has resulted in new insights that complement the Viking measurements. These insights may be summarized as follows: (1) at least two reservoirs of volatiles exist on Mars, (2) martian magmas are dry and contain little water, and (3) volatiles in martian rocks often resemble those of the atmosphere. These conclusions prompt the inference that there has been substantial interaction between volatiles in the crust and atmosphere, as well as between the SNC parent magmas and the crust.

Multiple Reservoirs: Plots of $^{129}Xe/^{132}Xe$ vs. $^{84}Kr/^{132}Xe$ indicate that at least two very different noble gas reservoirs exist on Mars [2,3]. One of these, epitomized by the shock glass in EETA 79001, appears to be representative of the martian atmosphere. Pepin has pointed out the similarity, both in terms of absolute abundances and isotopic compositions, of shock-implanted gases in EETA 79001 to those of martian air, as measured by Viking [4]. Assignment of this signature to this lithology thus allows a more precise measurement of the martian atmosphere than would otherwise be possible remotely. Experimental studies, indicating that atmospheric gases are not fractionated by shock implantation, bolster the inferences from the SNCs themselves [5].

The second reservoir, exemplified by Chassigny, is depleted in the light noble gases, relative to Xe, and its Xe isotopic composition is essentially solar. These characteristics have fueled speculation that Chassigny is representative of the depleted mantle of Mars. The absence of radiogenic contributions from ^{129}I and ^{244}Pu to Chassigny Xe indicates that this depletion occurred early in the history of the planet, in essential agreement with inferences from the shergottite Sr and Pb whole-rock isochrons [6]. This observation is also in agreement with the recent finding of a piece of the martian crust that is very ancient, ALHA 84001 [e.g., 7].

Water in SNC Magmas: The second general inference from the SNCs is that their parent magmas were rather dry. For example, in SNCs the phosphate mineral tends to be either whitlockite, which is anhydrous, or chlorapatite [8,9], which is the least-favored form of apatite after fluor- and hydroxyapatite [10]. With hindsight, this should not be surprising. The mantle source regions of the SNCs have had at least two opportunities for ridding themselves of water. The first occurred prior to core formation, when there was presumably excess metal present in the martian mantle that could react with water. The second was the early depletion event, alluded to above, that removed incompatible elements from the martian mantle. Water acts as an incompatible element during silicate partial melting, so any water that escaped core formation (or was added subsequently) should have been transported to the crust at this time. This early crust-forming event was probably quite massive. Probably half the Nd in the planet was transported to the crust at that time [e.g., 11]. Consequently, transport of water was probably at least as efficient. A consequence of this early desiccation of the martian mantle is that models of water outgassing that are tied to rates of volcanism are probably misleading [12].

Interaction Between SNC Magmas, the Crust, and the Atmosphere: Since mantle-derived magmas are expected to be dry, it perhaps not surprising that D/H in hydrous minerals from SNCs isotopically resembles water in the atmosphere [13]. The

inference therefore is that there has been a significant interaction between the crust and atmosphere, as well as between the SNC parent magmas and the crust. Most SNCs do not indicate pervasive hydrothermal alteration. Therefore, to incorporate water into the SNCs the following model is proposed:

Hydrothermal alteration of the crust occurs over geologic time, with the heat from either intrusive volcanism or impact cratering acting as the thermal driver for meteoric water circulation. In this manner, the ambient martian temperature need not be high, except locally. At some later time, the SNC magmas are transported through the crust to the surface, assimilating some crustal materials along the way. In the case of Shergotty and Zagami, this assimilation process was extensive, whereas in the case of the nakhlites and Chassigny this assimilation must have been minimal [6].

However, in one case, at least, there may have been actual hydrothermal alteration of the SNCs themselves. The nakhlites have bulk $\delta^{18}O$ values that are slightly elevated compared to that of the mantle [14]. The nakhlites also have iddingsite, a hydrous alteration product of olivine. The elevation in $\delta^{18}O$ is most pronounced for Lafayette, which is also markedly richest in the iddingsite component [15]. Isotopic analysis should be performed to discover whether this correlation between $\delta^{18}O$ and mineralogy is real or apparent.

References: [1] Bogard D. D. and Johnson P. (1983) *Science, 221,* 651–654. [2] Ott U. and Begemann F. (1985) *Nature, 317,* 509–512. [3] Swindle T. D. (1995) in *Volatiles in the Earth and Solar System* (K. A. Farley, ed.), 175–185, AIP Conf. Proc. 341. [4] Pepin R. O. (1985) *Nature, 317,* 473–475. [5] Wiens R. C. and Pepin R. O. (1988) *GCA, 52,* 295–307. [6] Jones J. H. (1989) *Proc. LSPC 19th,* 464–474. [7] Nyquist et al. (1995) *LPS XXVI,* 1065–1066. [8] Bunch T. E. and Reid A. M. (1975) *Meteoritics,* 10, 303–315. [9] McSween H. Y. Jr. (1985) *Rev. Geophys., 23,* 391–416. [10] Zhu C. and Sverjensky D. A. (1991) *GCA, 55,* 1837–1858. [11] Longhi J. (1990) *Proc. LPS, Vol. 21,* 695–709. [12] Greeley R. and Schneid B. D. (1991) *Science, 254,* 996–998. [13] Watson L. L. et al. (1994) *Science,* 265, 86–90. [14] Clayton R. N. and Mayeda T. K. (1983) *EPSL, 62,* 1–6. [15] Treiman A. H. et al. (1993) *Meteoritics, 28,* 86–97.

ISOTOPIC COMPOSITION OF CARBONATES IN SOME SNC METEORITES.

A. J. T. Jull[1,2], S. Cloudt[1], and C. J. Eastoe[2], [1]National Science Foundation, Arizona AMS Facility, University of Arizona, Tucson AZ 85721, USA, [2]Department of Geosciences, University of Arizona, Tucson AZ 85721, USA.

SNC meteorites are basaltic achondrites thought to have been ejected from the martian surface [1]. They contain minerals such as carbonates that result from aqueous alteration [2,3]. The isotopic composition of C and O can provide important information about martian H_2O and CO_2 and about weathering processes on Mars, if the carbonates can be shown to be extraterrestrial and have not subsequently exchanged with terrestrial CO_2. We will discuss the measurement of the $\delta^{13}C$, $\delta^{18}O$, and ^{14}C compositions of CO_2 released from acid-etching experiments of the SNC meteorites, ALH 84001 [4,5], Nakhla [4–6], and Zagami. The initial purpose of these experiments was to see whether the C and O isotopic composition, particularly ^{14}C, would identify the carbonate as extraterrestrial. Carbonates of this composition irradiated in space as small bodies will contain about 74 dpm/kg (3.2×10^8 atom ^{14}C/g) [4]. For 12.7% C, the calculated activity corresponds to a $^{14}C/^{12}C$ ratio (atom/atom) of 5.0×10^{-14} or 4.3% of the ratio found in modern C (~1950 AD) [4]. Twentieth-century terrestrial carbonates formed prior to atmospheric nuclear tests will have a ^{14}C content of 98–100% modern. Samples formed after 1950 AD, or which equilibrated with atmospheric CO_2 later, will contain higher levels of ^{14}C, up to 180% modern [4]. A related consideration is the decay of ^{14}C that occurs after a meteorite falls. For ALH 84001, which has a terrestrial age of about 13,000 yr [4], we would expect carbonate in ALH 84001 to have a ^{14}C activity of about 0.9% of the modern terrestrial value. No significant decay should have occurred for Nakhla and Zagami. Terrestrial weathering products introduced after the meteorite fall would lead to higher levels of ^{14}C. Carbon- and O-isotope abundances may also be affected by later isotopic exchange. The values of ^{13}C and ^{18}O that arise from weathering of meteorites are known [7,8]. The bicarbonate formed on LEW 85320 is typical of terrestrial weathering, and has $\delta^{13}C = 5.4‰$ and $\delta^{18}O = 9.4‰$. Lighter $\delta^{13}C$ values of −10 to 0‰ are observed for weathering of meteorites in warmer environments [9].

We have previously reported the results of the isotopic measurements for ALH 84001 and Nakhla [4], which showed that $\delta^{13}C$ and ^{14}C correlate inversely. The data for ALH 84001 samples and the terrestrial evaporites on LEW 85320 have a correlation coefficient, R, of 79%. High $\delta^{13}C$ values up to 45‰ correspond with low ^{14}C, indicating an extraterrestrial carbonate; low values of $\delta^{13}C$ (<5‰) show approximately modern terrestrial ^{14}C and imply a terrestrial source. Similar results were observed for Nakhla. The samples with highest $\delta^{13}C$ etched from ALH 84001 and Nakhla have very low ^{14}C activities and enrichments of ~45‰. This material is clearly extraterrestrial despite the ordinary composition of its O, $\delta^{18}O = 15$–20‰. Additionally, the isotopic data for ALH 84001 also suggest the presence of some recently formed terrestrial carbonate. This is probably the material observed filling in veins and cracks.

New results on Zagami and ALH 84001 (125–250 μm) are given in Fig. 1. Samples of crushed meteorite were treated with 100% H_3PO_4 at 25°C for times ranging from 1 to 4 days. The abundances

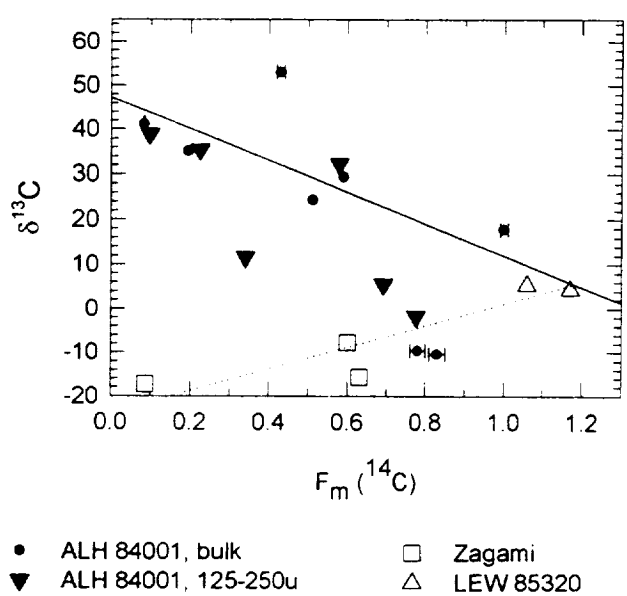

Fig. 1. Dependence of $\delta^{13}C$ on ^{14}C in CO_2 from acid etching of SNC meteorites. The units of Fm(^{14}C) are fraction of modern (1950 AD) terrestrial C.

of ^{13}C and ^{18}O were measured in purified CO_2 samples by stable-isotope mass spectrometry. After isotope analysis the CO_2 was recovered from the mass spectrometer and reduced to graphite for measurement of ^{14}C by accelerator mass spectrometry. $\delta^{18}O$ measurements are quoted relative to SMOW and assume fractionation factors [10] for calcite (for Zagami) or dolomite-ankerite (for ALH 84001). In contrast to the results obtained for ALH 84001, the CO_2 released with the lowest values of ^{14}C have the lowest $\delta^{13}C$ of –17‰ and the data appear to plot on a trend connecting $\delta^{13}C$ of –17‰ and low ^{14}C with terrestrial composition carbonates ($\delta^{13}C$ of –5 to +5‰ and ^{14}C ~ modern) at the other extreme. No correlation is evident for $\delta^{18}O$ vs. ^{14}C in any of these samples, as was also observed for ALH 84001. The $\delta^{18}O$ values found for the SNC etches differ not only from the $\delta^{18}O$ values reported in the terrestrial weathering products on LEW 85320 and EETA 79001 but also from the values characteristic of silicates in SNC meteorites [11]. These two observations suggest that the O now in the SNC carbonates was originally supplied by an extraterrestrial source external to the meteorite. Karlsson et al. [8] previously concluded that water released by pyrolysis of SNC meteorites contained O that had not equilibrated isotopically with the O present in silicates. This can be interpreted in two ways: (1) the O in the hydrothermal waters never exchanged with silicate O, thus implying a formation temperature <400°C; or (2) the O in the carbonates has subsequently exchanged with water of different isotopic composition.

The lower $\delta^{13}C$ values in ALH 84001 etch samples corresponding to carbonates incorporating some terrestrial ^{14}C are close to the earlier data for SNC meteorites [4–6,12]. In contrast, the ALH 84001 and Nakhla samples with the lowest ^{14}C compositions are higher in $\delta^{13}C$ and close to the compositions of CI and CM carbonates. Compared to carbonates found in other meteorites, the Fe- and Mg-rich carbonates in ALH 84001 are for the most part inclusions, although there are also some deposits ("late" carbonates) along cracks and grain boundaries [13]. The crystals do not contain hydrated phases, which implies a temperature of formation >~200°C [13,14]. Second, it suggests that the isotopic composition of C and O observed in the carbonate inclusions should be close to that present in the hydrothermal fluids that furnished the C. Viking spacecraft measurements suggest that atmospheric CO_2 on Mars is isotopically heavy, about 50 ± 100‰ [15]. Models also predict a high $\delta^{13}C$ value for Mars CO_2 [16] and an atmospheric source could account for the heavy $\delta^{13}C$ values. Carbonates from three presumably random samples of martian rock indicate a $\delta^{13}C$ range of –17 to +45‰ prior to any terrestrial effects. Terrestrial processes generate a wide range of carbonate $\delta^{13}C$ from +30‰ (17) to –25‰ or less, from oxidation of photosynthetic organic matter. Such extreme values are generated in small quantities by biological activity on the Earth. Most terrestrial processes generate a much more restricted range of values. If these samples truly represent martian carbonates, then the inorganic chemistry of Mars must allow a wider range of isotopic values than on Earth, unless we speculate about other processes. The alternative is that they may represent different parent objects.

References: [1] McSween H. (1994) *Meteoritics, 29,* 757–779. [2] Gooding J. L. et al. (1988) *GCA, 52,* 909–915. [3] Wentworth S. J. and Gooding J. L. (1990) *LPS XXI,* 1321–1322. [4] Jull A. J. T. et al. (1995) *Meteoritics, 30,* 311–318. [5] Romanek C. S. et al. (1994) *Nature, 372,* 655–657. (6.) Carr R. H. et al. (1985) *Nature, 314,* 248–250. [7] Grady M. M. et al. (1988) *GCA, 52,* 2855–2866. [8] Karlsson H. R. et al. (1991) *LPS XXII,* 689–690. [9] Wlotkza F. et al. (1995) *LPI Tech. Rpt. 95-02,* 72–73. [10] Rosenbaum J. and Sheppard S. M. F. (1986) *GCA, 50,* 1147–1150. [11] Clayton R. N. and Mayeda T. K. (1986) *GCA, 50,* 979–982. [12] Wright I. P. et al. (1992) *GCA, 56,* 817–826. [13] Mittlefehldt D. W. (1994) *Meteoritics, 29,* 214–221. [14] Anovitz L. M. and Essene E. J. (1987) *J. Petrol., 28,* 389–414. [15] Nier A. O. C. et al. (1976) *Science, 194,* 68–70. [16] Jakosky B. (1991) *Icarus, 94,* 14–31. [17] Martini A. M. et al. (1995) *GSA Abstr. with Progr., A-292.*

DEPOSITION AND BADLANDS EROSION OF MARTIAN CHEMICAL AND CLASTIC LACUSTRINE ROCKS.

J. S. Kargel, U.S. Geological Survey, 2255 North Gemini Drive, Flagstaff AZ 86001, USA.

Mars once had lakes and maybe seas [1–5]. Figure 1 shows an example of a radial system of valleys, which terminate in smooth and hummocky deposits. Goldspiel and Squyres [2] interpreted this landscape as an ancient drainage basin and lake bed. The region interior to the principal terminations of sapping valleys includes two morphologic units. Interior hummocky deposits, interpreted as possible eroded chemical sedimentary rocks, are surrounded by an annulus of smooth plains, interpreted as possible more resistant clastic sedimentary rocks.

Hummocky and gullied rock units are characteristic of many areas of proposed ancient martian lakes and seas. These morphologic characteristics are similar to badlands on Earth. Most badlands topography forms by erosion of poorly lithified lake and riverine sediments in arid or semiarid climates. Badlands-forming sedi-

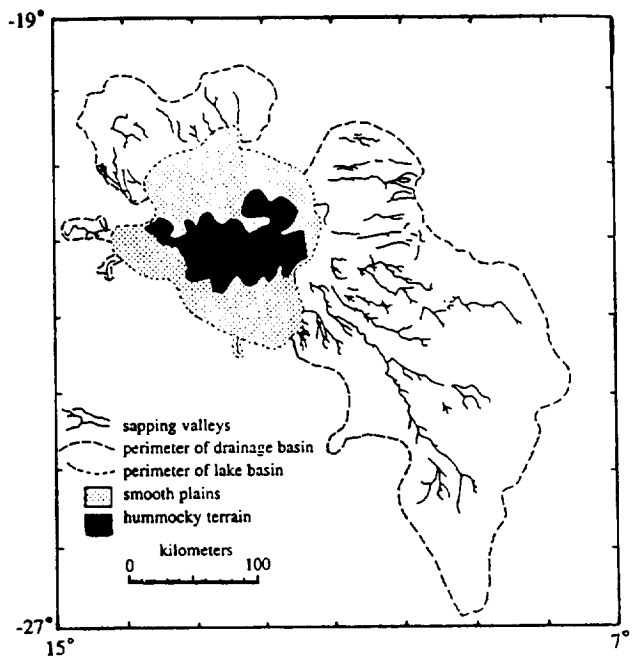

Fig. 1. Drainage basin and probable ancient lake-bed rock formations in a highlands basin, Margaritifer Sinus southeast quadrangle. Modified after Goldspiel and Squyres [2].

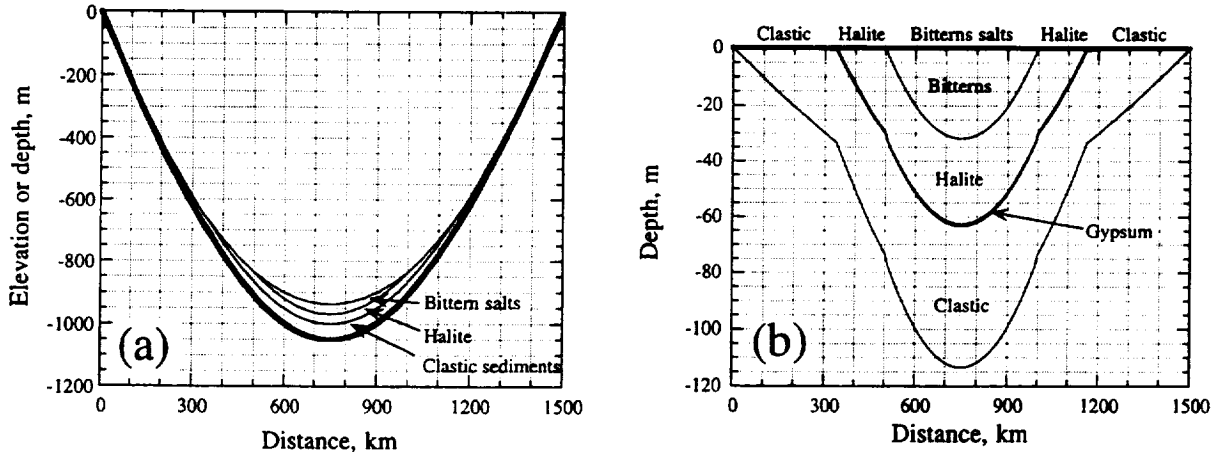

Fig. 2. Model of sediment deposition in a northern-plains lake basin such as the Chryse or Utopia Basin. Proximal coarse clastic wedge not shown. The basin cross section is assumed to be sinusoidal, its planform is cicular, and its maximum depth is 1 km after deposition of suspended mud. Brine composition is assumed to be like that of Earth's seawater, and brine volume is 8.33×10^5 km^3. Chemical precipitation in this model is forced by evaporation at 313 K. (a) Basin cross section; (b) same as (a) but basin topography has been removed and the depth axis expanded.

ments are dominantly clayey, salty muds and silts with interbeds or massive layers of carbonates, gypsum, halite, and other evaporitic salts. Wetting-drying cycles cause hygroscopic clays to expand, contract, and crumble. The high solubility of cementing salts further reduces the resistance of badlands to water erosion, which can be rapid.

I have produced chemical precipitation models of martian lake basins [6,7]. In the cases of outflow-channel-fed basins, I assumed that the basins were filled once by a brine of terrestrial seawater composition; the water then evaporated (in one model) or froze (in another model). Besides coarse clastic sediment, which was not considered in the model but would have formed a clastic wedge near the mouths of outflow channels, the first rock unit laid down would be mudstone deposited from suspension (Figs. 2 and 3). Remaining sedimentation is chemical. The resulting sedimentary rocks form a vertical and lateral (concentrically zoned) sequence from clastic to chemical sediments that progress upward (and toward the basin's center) to increasingly soluble salts. This general result applies regardless of the details of the basin, of brine composition or temperature, or of the means of forcing precipitation (evaporation or freezing).

Concentric zonation also results from classical lacustrine-evaporite-basin models, where dilute streamwater enters a lake and chemical precipitation is forced by evaporation or freezing. Figure 4 schematically illustrates results expected for a model in which rock of average SNC meteorite composition is leached by groundwater. Coarse clastic sediment is restricted to the basin's edge. Mud, dolomite, and gypsum are then deposited near the basin's center. Hydrohalite, epsomite, sylvite, and other highly soluble salts are deposited at the top of the sequence at the core of the basin. Subsequent erosion of zoned evaporites or cryogenites can produce concentric morphologies such as in Fig. 1.

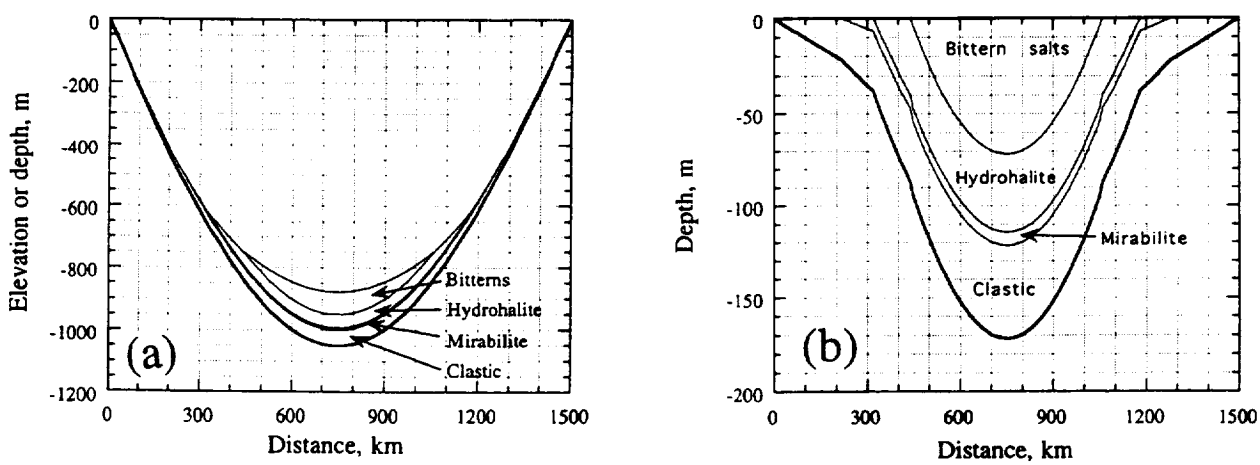

Fig. 3. Same model as in Fig. 2 except chemical precipitation is forced by freezing instead of evaporation. Chemical precipitation commences at 271 K and continues until the residual bitterns completely solidify at 221 K. (a) Basin cross section; (b) same as (a) but basin topography has been removed and the depth axis expanded.

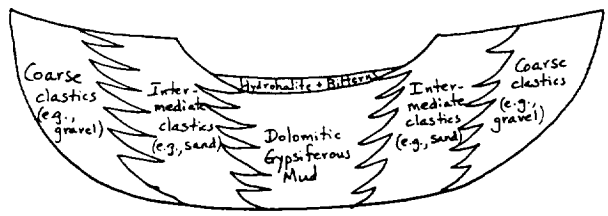

Fig. 4. Schematic drawing showing expected results of a more classical stream-fed lacustrined evaporite basin. Stream solutes consist of those predicted from the average composition of SNC meteorites. This structure results from ~10^3 basin volumes of water that have been emptied into, frozen, and evaporated from the lake basin. The clastic sediments grade from nearly pure coarse clastics near the edge to more carbonate- and gypsum-rich muddy sediments near the basin's center. The last bitterns precipitate a hydrohalite-, sylvite-, and epsomite-rich sequence of salts at the top of the sequence and near the basin's center. Modeling in progress.

References: [1] Parker T. J. et al. (1989) *Icarus, 82,* 111–145. [2] Goldspiel J. M. and Squyres S. W. (1991) *Icarus, 89,* 392–410. [3] Baker V. R. et al. (1992) *Nature, 352,* 589–594. [4] Rotto S. L. and Tanaka K. L. (1992) *LPS XXIII,* 1175–1176. [5] Forsythe R. D. and Zimbelman J. R. (1994) *JGR, 100,* 5553–5564. [6] Richardson C. (1976) *J. Glaciol., 17,* 507–519. [7] Krauskopf K. B. (1979) *Introduction to Geochemistry, 2nd edition,* p. 269, McGraw-Hill.

MINERALOGY OF THE MARTIAN SURFACE ANALYZED *IN SITU* BY MÖSSBAUER SPECTROSCOPY, AND IMPLICATIONS FOR VOLATILE EVOLUTION ON MARS.

G. Klingelhöfer[1], B. Fegley Jr.[2], R. V. Morris[3], E. Kankeleit[1], E. Evlanov[4], O. Priloutskii[4], J. M. Knudsen[5], and M. B. Madsen[5], [1]Institut für Nuclear Physics, University Darmstadt, 64289 Darmstadt, Germany, [2]Washington University, St. Louis MO, USA, [3]NASA Johnson Space Center, Houston TX, USA, [4]Space Research Instititute (IKI), Moscow, Russia, [5]University of Copenhagen, H. C. Oersted Institute, Copenhagen, Denmark.

Mössbauer (MB) spectroscopy is a powerful method for the identification of Fe-containing minerals (e.g., metal, oxide, clays, oxyhydroxides, silicates, sulfides, carbonates, etc.) in rocks and soil. The Mössbauer spectrum of a given sample immediately identifies all the Fe-bearing minerals in a sample, gives the distribution of Fe between all these minerals, and gives the oxidation state of all the Fe-bearing phases in the sample. Furthermore, MB spectroscopy can identify and determine the relative abundance of Fe atoms in different crystallographic sites (and different oxidation states) in one mineral (e.g., it can be used to distinguish Fe^{2+} in the M1 and M2 sites of pyroxene and the different amounts of Fe^{2+} and Fe^{3+} in pyroxene). Thus, in principle, MB spectroscopy is uniquely suited for studies of the mineralogy of rocks and soil on the surface of Mars because Fe is the third most abundant element (after O and Si) on the surface of Mars and is present in most of the minerals that we can imagine being present in soil.

As discussed elsewhere [1,2], the chemical weathering of primary rocks and minerals was probably an important mechanism for volatile loss from the early martian atmosphere. If such primordial chemical weathering reactions took place, relict signatures are probably preserved in the Fe-bearing minerals present on the surface of Mars, and could be detected by MB spectroscopy. As an

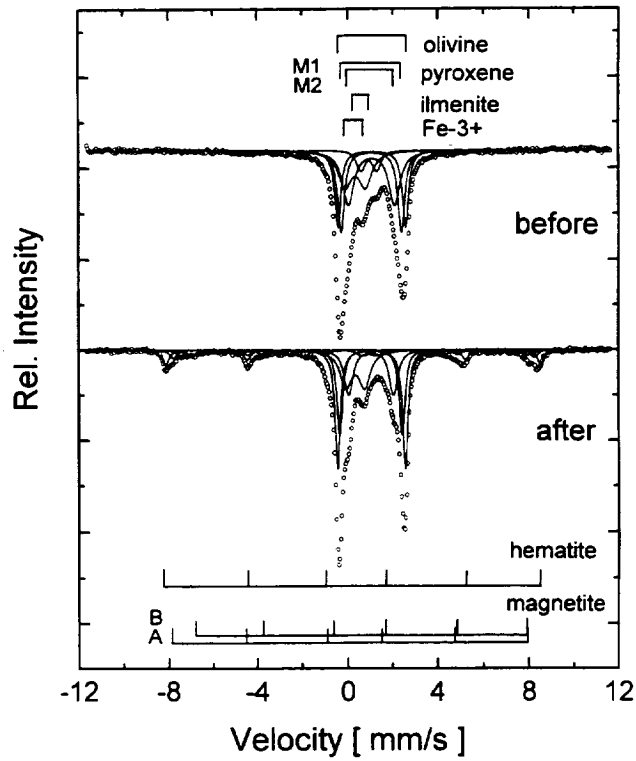

Fig. 1. Mössbauer spectra of basalt, before and after heating in CO_2 at 570°C for 19 days. The formation of hematite and magnetite is observed as well as an increase in the total amount of Fe^{3+}.

example, in Fig. 1 the MB spectra of a basalt are shown before and after heating in CO_2 at 600°C for 19 days. The shape of the spectrum changes significantly. The formation of hematite and magnetite is observed and the amount of Fe^{3+} in pyroxene is increasing. These experiments show that hematite formation via subaerial oxidation of hot basalt on early Mars was potentially an important sink for O from CO_2, H_2O, O_2, and other gases. In some cases the amount of hematite formed is equivalent to the consumption of a few milligrams of O per gram of basalt. Depending on the weathering process, different types of Fe compounds (e.g., clays, hydroxides, oxyhydroxides, oxides) may have formed. Therefore the Fe mineralogy reflects the history of water on Mars, an essential requirement for biology. Miniaturized MB spectrometers have been developed [3,4] for the *in situ* analysis of the Fe mineralogy of soil and rocks on the surface of Mars. The very lightweight modular instrument MIMOS-II, developed at the TH Darmstadt, can be adapted to the constraints due to limitations in power, mass and volume, by changing the number of detector channels of the instrument. Versions having a minimum of two and a maximum of five detector channels have been developed. The parameters of these two instruments are given in Table 1. The instrument itself can be installed either on a rover (e.g., Nanokhod, developed at Mainz, Germany [5]), a robotic arm, or on a stationary lander itself, assuming that in this case the samples will be delivered to the instrument. In all cases the MB instrument operates in backscattering mode and hence no sample preparation is required. Assuming an Fe content in martian soil similar to that detected by the Viking landers, it will take about 10–15 hr for one spectrum using the two-detector channel version (MIMOS-II-2). Further examples of MB spectroscopy for determin-

ing the Fe minerals and oxidation state for martian soil samples will be discussed at the workshop.

TABLE 1. Instrument parameters for MIMOS-II.

	MIMOS-II-2 (two detectors)	MIMOS-II-5 (five detectors)
Dimensions (mm)	48 × 32 × 80	48 × 48 × 80
Mass (kg)	0.3	0.5
Power (W)	0.5	0.8
Data/Run (kbit)	80	80
Radioactive Source	Co-57 Rhodium: 300mCi	Co-57 Rhodium: 300mCi
Data-Interface	RS-422	RS-422

Acknowledgments: This work is supported by the German Space Agency DARA, by NATO CRG No. 931476, NASA Grant NAGW-4485.

References: [1] O'Conner J. T.(1968) *JGR, 73,* 5301–5311. [2] Fegley B. Jr. et. al. (1995) *Eos (Trans. AGU), 76,* F330. [3] Klingelhöfer G. et al. (1995) *Hyp. Int., 95,* 305–339. [4] Shelfer T. D. et.al. (1995) *LPS XXVI,* 1279–1280. [5] Rieder R. et al. (1995) *LPS XXVI,* 1161–1162.

SPICAM SOLAR OCCULTATION EXPERIMENT. O. Korablev[1], M. Ackerman[2], E. Neefs[2], C. Muller[2], H. Deceuninck[2], D. Moreau[2], C. Hermans[2], W. Peertermans[2], P. C. Simon[2], S. Shadeck[2], E. Van Ransbeek[2], V. Moroz[1], A. Rodin[1], A. Stepanov[1], D. Perepelkin[1], V. Jegoulev[1], A. Krysko[1], and V. Troshin[1], [1]Space Research Institute, Russian Academy of Sciences, Profsoyusnaya 84/32, 117810 Moscow, Russia, [2]Belgian Institute for Space Aeronomy, 3, Av. Circulaire 1180 Brussels, Belgium.

Scientific Objectives: The SPICAM-S experiment is intended to operate during the Mars-96 mission as a part of the Belgian-French-Russian SPICAM occultation experiment. The experiment will study the vertical distribution of H_2O, CO, O_3, and aerosols, and will investigate their spatial, diurnal, and seasonal variations. The atmospheric constituents to be measured by SPICAM-S are listed in Table 1.

TABLE 1. Atmospheric constituents to be measured by SPICAM.

Species	Band wavelength, μm	Band strength, cm^{-1}	Number density, cm^{-3}	Detection altitude, km
Aerosol	entire range		0.1–100	0–70
CO_2	1.96	10^{-21}		
	2.0	4.5×10^{-20}		
	2.7	2.5×10^{-18}	Temperature	30–50(?)
	4.3	10^{-16}	sounding	80–110
H_2O	1.85	8×10^{-19}	10^9–10^{13}	0–60
	2.9	7×10^{-18}		0–70
O_3	0.33		$\approx 10^8$	0–70
CO	2.35	7.5×10^{-20}	10^{11}–10^{14}	0–50
	4.7	10^{-17}		20–60
HDO	2.7	1.4×10^{-21}	10^5–10^9	overlap by CO_2
	3.7	7×10^{-22}		0–20
H_2CO (?)	3.6	10^{-19}	$<10^{12}$ (?)	0–30
	0.35			
HCl (?)	3.45	4×10^{-18}	$<10^{11}$ (?)	0–30

The experiment addresses several problems of martian aeronomy. It addresses photochemistry, evolution of the atmosphere, and atmospheric stability. The intensity and Doppler broadening variations of CO_2 bands provide information on atmospheric temperature up to 100 km. Thus the thermal structure of the middle and upper atmosphere can be retrieved. Directly measured aerosol profiles at several wavelengths from 0.2 to 4.8 μm will allow study of the vertical structure of aerosols and their composition. A problem of simple organic molecules in the atmosphere reinitiated by tentative detection of formaldehyde by the Phobos mission [1] needs to be resolved.

Mars-96 mission launch is foreseen in November 1996; the spacecraft will enter the martian orbit in October 1997. The solar occultations will be observable in December 1997 for 2.5 months and then for a long period one year later.

Description of the Instrument: The SPICAM-S instrument consists of two basic parts: UV-visible and IR spectrometers. The UV-visible part is intended to measure primarily O_3 absorption in the range of 200–700 nm with a resolving power of 300. The infrared part covers the range of 1.8–5 μm with a resolving power exceeding 1000. See also the description of the SOS project [2] for the details of IR channel. A CCD camera incorporated in SPICAM-S will monitor the shape of the solar disk while entering the opaque atmosphere.

The sunlight is directed inside the instrument by a tracking system that can follow the Sun within ±1.5°. Separate lens telescopes and separate spectrometers are used for the two channels. The spectrometer's field of view is about 3 arcmin, which yields a spatial resolution of 8 km at the limb from typical Mars-96 orbit (spacecraft-to-limb distance of 10^4 km). Reticon detector of 1024 pixels accounts for the UV-visible. An infrared grating can be rotated with a precision of 12" and prepositioned with an accuracy of 12'. The IR detector is a pseudolinear PbSe array of 128 pixels. Two halves of the detector work in two diffraction orders (3.1–4.8 and 1.8–3.15 μm) simultaneously. Radiative cooling of the detector down to ≈240 K is provided by a radiator. Pixel signals form 16 channels, 8 in each diffraction order. The accumulation of signal is performed in 16 channels in parallel. The instrument signal-to-noise ratio is ≈500 at 2 μm and ≈70 at 4.7 μm.

Measurement Technique: The spectrometer is placed at solar-oriented spacecraft, and it measures the sunlight passing the atmosphere at the limb of Mars. The UV-visible channel covers its entire range by Reticon array, but the IR channel with a resolution of ≈1100 can attain limited slices of spectrum at a time. Different modes of operation allow us to meet the scientific objectives and to avoid pixel-to-pixel difference problems of IR detectors [1]. In the simplest mode the detector is read at a fixed position of the grating. Two ranges of the spectrum, ≈60 cm^{-1} in the first order and 120 cm^{-1} in the second, are measured four times per second. The resolution in this mode corresponds to the width of one pixel. In scanning mode data are obtained from 16 pixels (channels) retarded along the detector array, and the grating scans a certain number of steps (Fig. 1). This mode yields a somewhat wider spectral range and also a homogeneity of spectra specific for scanning instruments. An example of compromise mode is presented in Fig. 2; in this case the entire array is read out, while the grating is wobbling within a narrow angle. It is promising for some retrieval problems, when even limited oversampling of spectra can radically increase the accuracy.

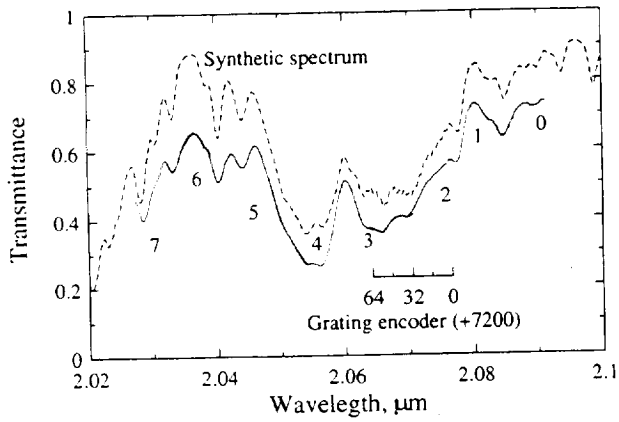

Fig. 1. SPICAM calibration spectrum. Telluric CO_2 band recorded in scanning mode. The scan includes 64 grating steps.

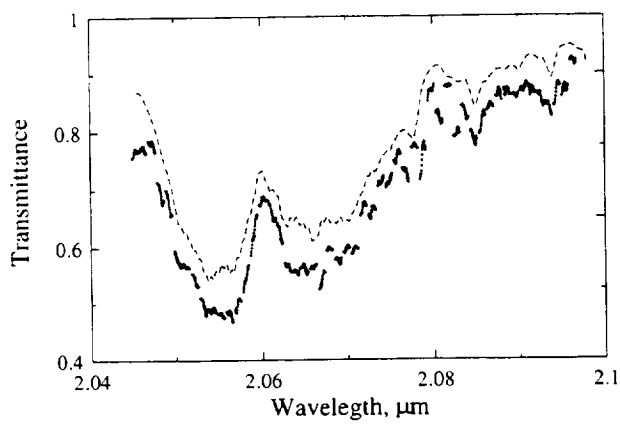

Fig. 2. The same as in Fig. 1, recorded in pixel mode combined with wobbling of grating.

Acknowledgments: The work has been supported in part by ISF grants N7T000 and N7T003.

References: [1] Korablev O. I. et al. (1993) *Planet. Space Sci., 41*, 441–451 [2] Korablev O. I. et al., this volume.

LIGHTWEIGHT SOLAR OCCULTATION SPECTROMETER EXPERIMENT.

O. I. Korablev[1], V. I. Moroz[1], M. Ackerman[2], E. Van Ransbeek[2], P. C. Simon[2], and J.-L. Bertaux[3], [1]Space Research Institute, Russian Academy of Sciences, Profsoyusnaya 84/32, 117810 Moscow, Russia, [2]Belgian Institute for Space Aeronomy, 3, Av. Circulaire 1180 Brussels, Belgium, [3]Service d'Aeronomie, B.P.3 91371 Verrieres le Buisson Cedex, France.

Introduction: An opportunity to dispose of 8 kg of Russian payload at the U.S. Mars Surveyor 1988 orbital platform was announced by NASA in June 1995. We proposed a advanced lightweight version of the SPICAM/Mars-96 [1] instrument: Solar Occultation Spectrometer (SOS) measurements of vertical profiles of H_2O, O_3, CO, and aerosols. The SOS instrument was directed to optically complement the GRS [2]. It is decided to fly the PMIRR [3] in 1998, but we hope that the possibility for SOS to fly with GRS in the next launching window (2001) remains open.

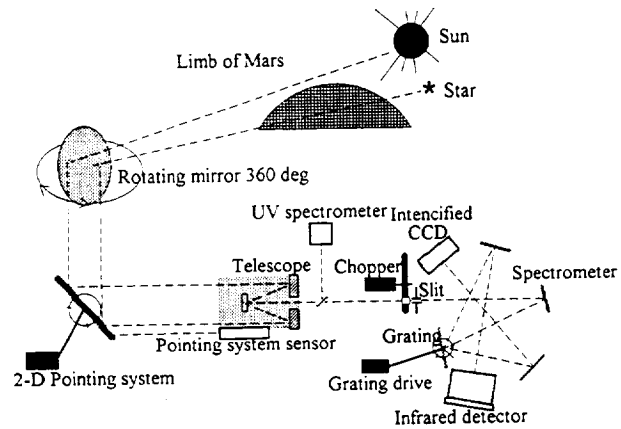

Fig. 1. Optical design of the instrument.

Low weight, high spectral resolution in the IR, and the possibility of obtaining directly the vertical profiles of the volatiles in the martian atmosphere make the SOS instrument an efficient tool for mapping and monitoring key atmospheric parameters and minor constituents. The instrument can be easily adapted for the nadir-oriented platforms, and for three-axis solar-stabilized spacecrafts. All this makes the instrument a potential candidate to be flown on any Mars orbiter within the Intermarsnet program. The measurement approach was tested during the Phobos mission (experiment *Auguste* [4]). The main components of the proposed experiment have been designed and tested for space application, and many of them are available as spare parts of the SPICAM instrumentation.

Scientific Goals: The measurement approach of the experiment is the absorption spectroscopy of the martian atmosphere from an orbiter at the limb of the planet using the Sun and stars as sources of radiation (Fig. 1). The instrumental properties of SOS are summarized in Table 1. The IR part of the experiment is dedicated to measure H_2O and CO atmospheric distributions. The measurements in the CO_2 bands allow retrieval of temperature profiles at 80–120 km. Simultaneous measurements in continuum will allow study of the detached hazes and dust vertical profiles at several wavelengths. This permits a detailed study of volatiles phase transitions [5] that might play a key role in the Mars climate system [6].

The ozone is known to be anticorrelated with the amount of water vapor in the atmosphere. The simultaneous knowledge of details of both water vapor and ozone profiles are very important for the study of atmospheric chemistry. The new ozone channel has lower reso-

TABLE 1. Instrumental properties of SOS channels.

Channel	IR	UV	UV-VIS stellar
Light source	Sun	Sun	Stars $1.5^m - 2^m$
Spectral range, μm	1.8–4.8	0.2–0.4	0.2–0.7
Resolving power $\lambda/\Delta\lambda$	≈1500	≈100	≈300
Vertical resolution for Mars-Surveyor orbit, km	2 km	0.8 km	0.25 km
Accuracy to measure atmospheric transmittance	±0.2% to ±1.5% (4.7 μm)	±0.1%	±1%

lution, compared to SPICAM, although the accuracy of measurements in the 330-nm continuum is almost identical.

In contrast to the elongated orbit of Mars-96, the MSP satellite will be on the low mapping polar orbit. At this orbit solar occultations are possible almost any time, always in polar regions. This meets the current need of experimental data on the winter polar atmosphere, which influences the entire planet in the sense of atmospheric chemistry and radiative transfer. The spacecraft-to-limb distance is 1500 km, which provides very high spatial resolution and better spectral coverage in the IR. The restraint of solar occultation to the high latitudes will be counterbalanced by combining a UV stellar occultation sensor in the same package. It will use the same optics, and will allow enhancement of latitudinal and diurnal coverage of the ozone. This channel will use the components of a specialized stellar occultation instrument, which is a part of the SPICAM/Mars-96 experiment.

Nadir orientation of the MSP platform together with the SOS pointing device will allow us to point to any direction at the limb of Mars. We can therefore observe any star entering the limb. The number of bright stars suitable for the small SOS telescope is ≈20 at sky. The light from these stars is sufficient to detect the absorption by ozone. Hence, the stellar channel will be able to sound atmosphere at any latitudes, and to measure 3–4 extra O_3 profiles per orbit.

Description of the Instrument: The simplified optical scheme of the instrument is presented in Fig. 1. The light from the source is directed inside the instrument with an elliptical mirror rotating within 360°. The optical axis of the instrument coincides with the mirror rotation axis, which greatly simplifies the design. The Sun-tracking system tracks within ±3° in elevation (Sun vertical excursion for the tangential altitude 0–120 km), and ±1.5° in azimuth. The tracking device is not used in stellar occultation mode; the capture of the star is provided by the aperture of detector.

A Ritchey-Chretien telescope has a 48-mm-diameter primary mirror. A small mirror off focal plane serves as a beam-splitter and separates the light to the infrared and UV spectrometer. The latter is a miniature spectrometer with Rouland grating and a linear CCD 256-pixel array detector.

The configuration of the infrared channel is almost equivalent to the SPICAM-S instrument, with some modifications in order to adopt components of the stellar occultation spectrometer. Chopper is placed before the slit, which is retractable for stellar occultations "window" observation mode. Joint IR-stellar UV spectrometer consists of a crossed Czerni-Turner monochromator collimator and two objectives. The second objective is used for stellar detector. One side of the grating, which can be rotated within 360°, is used for IR; another side is for stellar occultations. The IR detector consists of two PbSe 64-pixel pseudolinear arrays that are working in two orders of diffraction. Cooling of the detector is provided by a four-stage Peltier cooler. The UV stellar detector is a flat CCD matrix 288 × 384 pixels, with an image intensifier. It can operate in the spectral range 200–700 nm following the position of the grating.

References: [1] Korablev O. I. et al., this volume. [2] McCleese D. L. et al. (1992) *JGR, 97,* 7735–7757. [3] Boynton W. V. et al. (1992) *JGR, 97,* 7681–7698. [4] Blamont J. et al. (1989) *Nature, 341,* 601–604. [5] Rodin A. V. et al., this volume. [6] Clancy R. T. et al. (1995) Paper presented at IUGG meeting, Boulder, Colorado.

PHOTOCHEMICAL WEATHERING OF MARTIAN CARBONATES AND SULFATES. A. P. Koscheev[1], L. M. Mukhin[2], Yu. P. Dikov[3], J. Huth[4], and H. Wänke[4], [1]Karpov Institute of Physical Chemistry, ul. Vorontzovo Pole 10, Moscow, Russia, [2]Space Research Institute, ul. Profsoyznaya 84/32, Moscow, 117810, Russia, [3]Institute of Ore Deposits, Petrography, Mineralogy and Geochemistry, Staromonetny per. 35, Moscow, Russia, [4]Max-Planck-Institut für Chemie, Saarstrasse 23, D-55122, Mainz, Germany.

The chemical compositions of the martian surface and atmosphere as well as the intensity and spectral distribution of solar irradiation are favorable for heterogeneous photochemical processes, including reactions of martian volatiles. In a number of experimental works the potential importance of gas-solid (mainly metal oxides) chemistry and photochemistry in martian condition was confirmed [1–6]. In the present work we investigated the possibility of the production of volatiles under UV-irradiation of calcite and magnesium-sulfate in vacuum.

The release of CO_2 from calcite crystal under UV-irradiation at room temperature in vacuum conditions (10^{-8} Torr) was clearly established by mass spectrometry analysis. The photodecomposition rate was highest at the beginning of the irradiation (3×10^{15} molecules cm^{-2} h^{-1} for 250-W mercury lamp), and decreased to a near constant value after several hours of irradiation (6×10^{14} molecules cm^{-2} h^{-1}). The rate of release increased only slightly with temperature in the range 200–400 K. A linear dependence of the initial photodecomposition rate on the light intensity up to fluences of 10^{17} photon cm^{-2} s^{-1} was observed. The spectral dependence of CO_2 release clearly showed the threshold at 350–400 nm. The calculated quantum yield of CO_2 release during the initial stage was approximately $\sim 10^{-5}$ molecules per incoming photon at wavelength near 300 nm.

It was shown that the observed photodecomposition of calcite does not relate to a possible photo-induced desorption of CO_2 molecules that could be adsorbed on the cleaned sample surface from residual air in the vacuum chamber. According to our additional measurements and estimations the observed CO_2 release also cannot be explained by the heating effect of UV irradiation.

The evidence of surface damage produced by UV light was obtained by means of thermodesorption mass spectrometry when we measured the rate of CO_2 release by slow heating during evacuation of the vacuum chamber. A clear difference was observed between the two thermodesorption curves representing the CO_2 release from irradiated and nonirradiated or annealed samples and indicating the presence of some "stored" CO_2 in the irradiated surface layer. This additional amount of CO_2 is likely formed during thermo-stimulated relaxation of damaged layer with broken or weakened chemical bonds. The same result was obtained for calcite samples irradiated in 1 Torr CO_2 environment, supporting the possibility of carbonate photo-decomposition in the CO_2-rich martian atmosphere.

The same set of measurements was made with samples of $MgSO_4$ powder. The results confirmed the main trends observed for calcite, although the rate of photodecomposition for sulfate at room temperature was approximately an order of magnitude lower than for calcite and the temperature dependence was more pronounced in this case. Another difference between carbonate and sulfate was in the spectral dependences of photodecomposition. The photo-in-

duced release of SO_2 from $MgSO_4$ took place even in the wavelength range of 500–600 nm.

The observed photo-stimulated release of volatiles from carbonates and sulfates can be important for the surface-atmosphere chemistry on Mars and the problem of evolution and stability of the martian atmosphere. Assuming the integral flux of photons (190–390 nm) on Mars of ~2 × 10^{15} photon cm^{-2} s^{-1}, the carbonate abundance in martian soil between 0.01% (lower limit) [7] and ~1% (upper limit) [8], and the measured mean quantum yield for photo release of CO_2 ~10^{-5} due to photodecomposition of carbonates, one obtains fluxes of CO_2 in the near-surface atmosphere layer of about 10^8 and 10^6 molecules cm^{-2} s^{-1}. These values are high compared to the estimated CO_2 nonthermal escape rate of ~10^5 molecules cm^{-2} s^{-1} for the martian atmosphere [9], used in the recent models of atmosphere evolution and stability [10–12], and certainly should be included in these models. For martian conditions relatively high fluxes of photo released gases might be maintained due to permanent "refreshing" of the surface by windblown high-velocity dust particle bombardment with high erosion rate [13].

In the case of sulfates, the estimated rate (at room-temperature conditions) of SO_2 photo release was of 10^8 cm^{-2} s^{-1} molecules assuming 10% abundance of sulfates in martian soil [14]. At this rate it will only take approximately two years to release the amount of SO_2 (~2 × 10^9 kg) equivalent to the upper limit of total SO_2 contents (0.1 ppm [15]) in the whole martian atmosphere at the present day. However, in this case gas phase oxidation to SO_3 [16] and reactions with surface minerals can be the important limiting factors.

References: [1] Booth M. C. and Kieffer H. H. (1978) *JGR, 83,* 1809–1815. [2] Clark B. C. et al. (1979) *J. Mol. Evol., 14,* 91–102. [3] Kong T. Y. and McElroy M. B. (1977) *Icarus, 32,* 168–189. [4] Atrea S. K. and Zhen G. G. (1994) *JGR, 87,* 13133–13145. [5] Huguenin R. L. (1974) *JGR, 79,* 3895–3905. [6] Huguenin R. L. (1976) *Icarus, 28,* 203–212. [7] Gooding J. L. et al. (1991) *Meteoritics, 26,* 135–143. [8] Clark B. C. and Van Hart D. C. (1981) *Icarus, 45,* 370–378. [9] Luhmann J. G. et al. (1992) *GRL, 19,* 2151–2154. [10] Jakosky B. M. et al. (1994) *Icarus, 111,* 271–288. [11] Pepin R. O. (1994) *Icarus, 111,* 289–304. [12] Haberle R. M. et al. (1994) *Icarus, 109,* 102–120. [13] Greeley R. (1982) *JGR, 87,* 10009–10024. [14] Pollack J. B. et al. (1990) *JGR, 95,* 14595–14628. [15] Owen T. (1992) in *Mars* (H. H. Kieffer et al., eds.), 818–834. [16] Settle M. (1979) *JGR, 84,* 8343–8354.

HUBBLE SPACE TELESCOPE OBSERVATIONS OF TIME-VARIABLE REGIONAL ALBEDO FEATURES ON MARS.

S. W. Lee[1], M. J. Wolff[2], P. B. James[2], L. J. Martin[3], R. T. Clancy[4], and J. F. Bell[5], [1]Laboratory for Atmospheric and Space Physics, University of Colorado, Boulder CO 80309, USA, [2]University of Toledo, Toledo OH 43606, USA, [3]Lowell Observatory, Flagstaff AZ 86001, USA, [4]Space Science Institute, Boulder CO 80309, USA, [5]Cornell University, Ithaca NY 14853, USA.

The Mariner 9 and Viking missions provided abundant evidence that eolian processes are active over much of the surface of Mars [1–4]. The primary manifestation of this activity observable from the vicinity of Earth is in the form of variable albedo features. In 1990, a long-term program of HST observations commenced to monitor the surface and atmosphere of Mars [5]. To date, slightly more than two martian years of observations have been obtained.

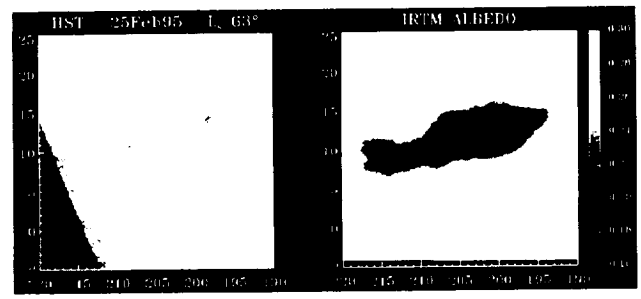

Fig. 1. Comparison of the appearance of the Cerberus albedo feature in HST and Viking observations. Maps are in simple cylindrical projection. The IRTM phase-corrected albedo map is from the Mars Consortium data collection [9]; the brightness scale to the right refers only to this IRTM map. The HST map was produced from a 673-nm image obtained in February 1995. A Minnaert correction has been applied (k = 0.65), and data at emission angles greater than 75° have been eliminated. It is evident that much of the Cerberus albedo feature is not visible at the time of the HST observations.

The Syrtis Major region exhibited a great deal of variability in albedo during the Viking missions [4], hence it was chosen as the primary target for repeated observations by HST. The appearance of this region has varied only slightly since our HST observations commenced in December 1990; the major albedo variations noted during Viking have not been evident in the HST data [5]. The variability during Viking was probably related to the massive dust storms that occurred several times during that mission. The current "stability" of the region indicates that dust activity of a magnitude comparable to that during Viking has not occurred since the HST observations commenced. The Solis Planum region, also noted for albedo variability during Viking and in historical groundbased observations, also has not undergone major changes in albedo features during the time-span current observations.

One major albedo feature that has changed dramatically between the Viking period and present is Cerberus, the prominent dark albedo feature (about 1500 × 500 km in size) that forms the southeastern boundary of the bright Elysium region. This feature was observed to be relatively constant in appearance between the Mariner 9 and Viking missions [6]. In fact, it appears to have remained fairly constant in location and appearance in telescopic observations obtained since the early 1900s [7]. However, in the February 1995 HST observations, Cerberus had virtually disappeared (see Fig. 1). This indicates that the normally dark surface has been covered with bright dust sometime during the period between Viking (ending in 1982) and present. Initial examination of our HST observations indicate that Cerberus has not been prominent in any images obtained since 1990. Earth-based observations suggest that this region has been fading for the past several years [8]. We will be collaborating with other groundbased observers to determine when this feature began to fade, and if this variability can be traced to any observed dust storm activity in the region.

References: [1] Veverka J. et al. (1977) *JGR, 82,* 4167–4187. [2] Thomas P. et al. (1981) *Icarus, 45,* 124–153. [3] Greeley R. et al. (1992) in *Mars* (H. H. Kieffer et al., eds.), 730–766, Univ. of Arizona, Tucson. [4] Kahn R. et al. (1992) in *Mars* (H. H. Kieffer et al., eds.), 1017–1053, Univ. of Arizona, Tucson. [5] James P. B.

et al. (1994) *Icarus, 109*, 79–101. [6] Chaikin A. L. et al. (1981) *Icarus, 45*, 167–178. [7] Slipher E. C. (1962) *A Photographic History of Mars, 1905–1961*, Northland Press, Flagstaff. [8] Parker D. (1995) personal communication. [9] Pleskot L. K. and Miner E. D. (1981) *Icarus, 45*, 179–201.

CO_2 ICE: RHEOLOGICAL PROPERTIES AND IMPACT CRATERING. J. Leliwa-Kopystynski, Institute of Geophysics, Warsaw University, ul. Pasteura 7, 02-093 Warszawa, Poland.

This paper is based on the experiments performed previously by the author and his co-workers [1–4]. The rheological experiments [1–3] have focused on the studies of the time-dependent, pressure-driven compaction of the granular (then porous, at least on the beginning of experimental run) mixtures of different ices. Water ice, water ice mixed with mineral grains, water-ammonia ice, and CO_2 ice have been studied. An experimental output has lead to rheological formulae that expressed density or, equivalently, porosity of the samples as the functions of time [1–3]. The kinetics of phase transitions in water ice (ice I–ice II–ice VI) have been studied as well [2]. The rheological formulae for water ice mixed with mineral grains and these for water ammonia ice were used for studies of evolution of icy satellites [2,3,5]. In particular, it was found that the presence of mineral admixture to water ice seriously decreases the rheological processes; on the other hand, admixture of ammonia increases the compaction rate of the samples and therefore it makes a faster satellite evolution rate.

Nevertheless, CO_2 ice is not a dominant building ice of the satellites of the outer planets. It is certainly important as a component of cometary nuclei [6] as well as, apart from the water ice, the most important ice candidate to be built within the martian regolith [7,8]. Therefore, rheology of the mixtures of minerals saturated with CO_2 ice can be important for studies of the evolution of martian surface features, e.g., their gravity driven relaxation. At present, I have experimental data on the rheology of pure CO_2 granular ice [3]; however, unfortunately, I have no data on CO_2-saturated analog of planetary regolith. Therefore some rough estimates deduced from the data for pure CO_2 ice and for H_2O icy/mineral mixtures are necessary. The similar situation concerns experimental data from impact experiments onto icy targets. Indeed, there are quite a lot of published results concerning impacting of H_2O ice targets [9,10], but the data of bombardment of other ices are rather scarce.

As underlined in [11], the martian crater morphology has probably been strongly influenced by subsurface volatiles. Our experimental results concerning impacts onto CO_2 targets [4] were extrapolated for a large acceptable interval of impact velocity onto the martian surface (from its minimum value, 5 km/s, to its maximum value, ≤58 km/s). Next they were compared with those concerning impacts onto H_2O targets as well as with the depth/diameter relationships for the craters on terrestrial planet surfaces [11]. On the basis of these data combined with expected values of flux of meteorites infalling onto martian surface, the production rate of gaseous CO_2 liberated from impacted regolith is calculated.

References: [1] Leliwa-Kopystynski J. and Maeno N. (1993) *J. Glaciol., 39*, 643–655. [2] Leliwa-Kopystynski J. et al. (1994) *Planet. Space Sci., 42*, 545–555. [3] Leliwa-Kopystynski J. and Kossacki K. J. (1995) *Planet. Space Sci., 43*, 851–861. [4] Brooke-Thomas W. et al. (1995) *Icarus*, submitted. [5] Kossacki K. J. and Leliwa-Kopystynski J. (1993) *Planet. Space Sci., 41*, 729–741. [6] Prialnik D. et al. (1993) *Icarus, 106*, 499–507. [7] Squyres S. W. et al. (1992) in *Mars* (H.H. Kieffer et al., eds.), 523–554, Univ. of Arizona, Tucson. [8] Zent A. P. et al. (1995) *JGR, 100*, 5341–5349. [9] Lange M. A. and Ahrens T. J.(1987) *Icarus, 69*, 506–518. [10] Kato M. et al. (1995) *Icarus, 113*, 423–441. [11] Strom R. G. et al. (1992) in *Mars* (H.H. Kieffer et al., eds.), 383–423, Univ. of Arizona, Tucson.

HYDROGEN ISOTOPE GEOCHEMISTRY OF SNC (MARTIAN) METEORITES AND THE HISTORY OF WATER ON MARS. L. A. Leshin[1], S. Epstein[2], and E. M. Stolper[2], [1]Department of Earth Space Sciences, University of California, Los Angeles CA 90095, USA, [2]Division of Geological and Planetary Sciences, California Institute of Technology, Pasadena CA 91125, USA.

Water in the present martian atmosphere is enriched in D relative to water on Earth, with a D/H ~5× greater than terrestrial [1], corresponding to a δD value of 4000. This has been interpreted to result from preferential loss of H relative to D from the martian atmosphere throughout geologic time from an initially terrestrial-like reservoir (δD ~ 0) [2,3]. The 12 "SNC" or "martian" (shergottites, nakhlites, chassignite, and ALH 84001) meteorites are igneous rocks widely believed to be samples from Mars [4]. Measurements of the D/H of hydrous components in SNC meteorites place constraints on the interactions between crustal rocks, fluids, and the atmosphere [5,6]. Here, we focus on two observations that are especially relevant to understanding the history of martian volatiles: the D/H of water in presumably ancient ALH 84001, and the poor correspondence of H [5] and O [7] isotopic studies on water in whole-rock SNCs.

We have measured the D/H of water released from eight whole-rock SNC samples by conventional vacuum-extraction/mass spectrometry [5]. The general pattern observed for all SNC extractions is that, with the exception for water released from the samples at low temperatures (thought to represent terrestrial contamination), the released water is enriched in D relative to terrestrial water with δD values reaching as high as ~2000. This implies that the weathering products that likely contribute the majority of the water released from the whole rocks were produced by preterrestrial alteration of the samples on Mars and probably reflect the action of hydrothermal circulation of aqueous fluids in the martian crust. The elevated D/H values signify that water that once resided in the atmosphere or has isotopically exchanged with atmospheric water was involved in this alteration.

The extraterrestrial H released from ALH 84001 is essentially identical in δD to that observed in the nakhlites [5,8], reaching values of ~800, but ALH 84001 appears to have crystallized at ~4.5 Ga [e.g., 9], while the nakhlites formed at 1.3 Ga [e.g., 10]. Based on the observation of "iddingsite" in the nakhlites [11,12] and carbonates in ALH 84001 [13], these samples were altered after they crystallized. If this alteration took place soon after igneous crystallization, and is responsible for the introduction of D-rich water into the samples, then the presence of D-rich water in a >4-Ma sample implies that the assumption of an initially terrestrial δD value for the martian water system may be in error.

The similarity of the extraction procedure for several of our samples to that used by Karlsson et al. [7] allows a direct comparison between the H and O isotopic measurements on water released from

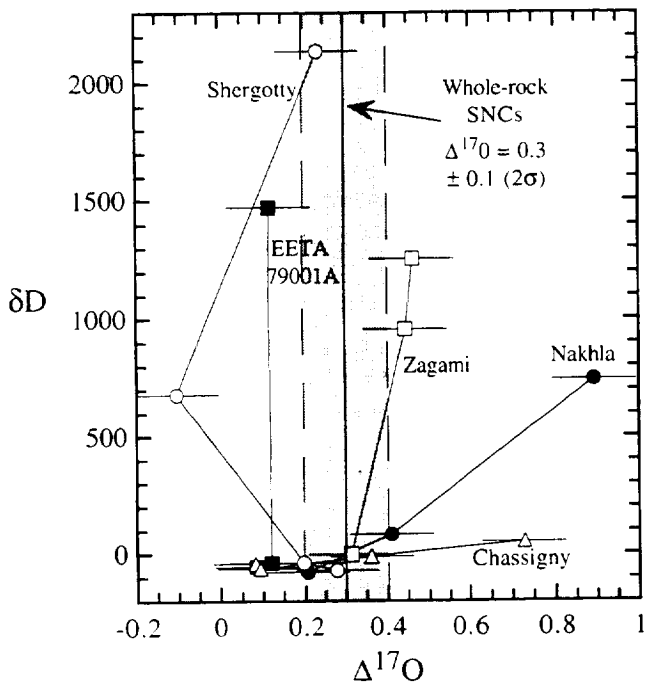

Fig. 1. Isotopic composition of SNC water.

SNC meteorites. Figure 1 shows the $\Delta^{17}O$ measurements of extracted water [7] for individual temperature steps plotted against the δD values measured by us for five SNCs (see [5] or [7] for experimental details). The SNC silicates are grouped along a mass-dependent fractionation line that is displaced from the terrestrial fractionation line by ~ 0.3‰ on a $\delta^{17}O$ vs. $\delta^{18}O$ diagram (i.e., $\Delta^{17}O$ = 0.3) [15]. Thus, any water in equilibrium with the O in the rock should have a $\Delta^{17}O$ value of ~0.3. Terrestrial contamination should have a $\Delta^{17}O$ value of 0.0. Karlsson et al. measured values of $\Delta^{17}O$ higher than 0.3 for high-temperature water aliquots in Nakhla, Chassigny, and Lafayette and suggested that this water is not in equilibrium with the host rock, but may have evolved isotopically as a separate reservoir related to the martian atmosphere. If the D-rich high-temperature H in the SNC samples also reflects an atmosphere-related component (as discussed above), the distinctive O and H isotopic characteristics of the high-temperature water would be expected to be correlated. As shown by Fig. 1, the correspondence is imperfect. For example, we observe increasing δD values with temperature for all our samples, interpreted to represent mixing between water with a terrestrial signature at low temperature and an extraterrestrial component released at high temperature. $\Delta^{17}O$ values, however, increase with temperature only for Nakhla, Lafayette (not plotted in Fig. 1), and Chassigny, while values for Shergotty and Zagami are not significantly higher in $\Delta^{17}O$ than whole rock, and show no particular pattern with temperature. Thus the elevated δD values in water released at high temperatures that are indicative of a martian atmospheric component are not always associated with elevated $\Delta^{17}O$ values. Implications of the lack of correlation of these two datasets will be discussed.

References: [1] Bjoraker G.L. et al. (1989) *Bull. AAS, 21, 991.* [2] Yung Y. L. et al. (1988) *Icarus, 76,* 146–159. [3] Owen T. et al. (1988) *Science, 240,* 1767–1770. [4] McSween H. Y. Jr. (1994) *Meteoritics, 29,* 757–779. [5] Leshin L. A. et al. (1995) *GCA,* submitted. [6] Watson L. L. et al. (1994) *Science, 265,* 86–90. [7] Karlsson H. R. et al. (1992) *Science, 255,* 1409–1411. [8] Watson L. L. et al. (1994) *LPS XXV,* 1471–1472. [9] Jagoutz E. et al. (1994) *Meteoritics, 29,* 478–479. [10] Nakamura N. et al. (1982) *GCA, 46,* 1555–1573. [11] Treiman A. H. et al. (1993) *Meteoritics, 28,* 86–97. [12] Gooding J. L. et al. (1991) *Meteoritics, 26,* 135–143. [13] Romanek C.S. et al. (1994) *Nature, 372,* 655–657.

THE MARTIAN NOBLE GAS ISOTOPE PARADOX.

L. K. Levsky, Institute of Precambrian Geology and Geochronology, St. Petersburg, 199034, Makarova 2, Russia.

The ratio of ^{36}Ar (terrestrial atmosphere)/^{36}Ar (martian atmosphere) is $\approx 10^2$. The deficiency in ^{36}Ar and other noble gases can be explained by a scenario of martian parent bodies' degassation that was unlike that for terrestrial parent bodies. The loss of volatiles from chondritic materials was longer, "hotter," and more effective in the case of martian evolution before accumulation. It applies not only to noble gases but also to moderately volatile elements such as Rb and K. It may be that the loss of the latter can partly explain the comparatively low ^{40}Ar concentration in the martian atmosphere.

In the martian atmosphere the ratio $^{129}Xe/^{132}Xe \approx 2.9$ is higher than that for the terrestrial atmosphere (0.98) and the ratio $\Delta^{129}Xe_r$ (martian atmosphere)/$\Delta^{129}Xe$ (terrestrial atmosphere) is equal to ~60. At the same time, $\Delta^{136}Xe_{fiss}$ (martian atmosphere)/$\Delta^{136}Xe_{fiss}$ (terrestrial atmosphere) is equal to ~6. This difference can be explained by a specific style of the martian primitive mantle depletion and degassation. The degassation of the martian mantle was comparatively short (≤50 m.y.) and ineffective. Nevertheless, the main part of $^{129}Xe_r$ (daughter of ^{129}I) was expelled in the martian atmosphere, contrary to the $^{136}Xe_{fiss}$ (daughter of ^{244}Pu) that was left in the mantle.

TRACE-ELEMENT GEOCHEMISTRY OF MARTIAN WEATHERING PRODUCTS IN LAFAYETTE.

D. J. Lindstrom[1], A. H. Treiman[2], and R. R. Martinez[3], [1]Mail Code SN4, Planetary Science Branch, NASA Johnson Space Center, Houston TX 77058, USA, [2]Lunar and Planetary Institute, 3600 Bay Area Boulevard, Houston TX 77058-1113, USA, [3]Lockheed-Martin, Houston TX 77058, USA.

Secondary minerals have been identified in several of the SNC meteorites, and it has been convincingly argued that these are the products of martian weathering [1]. As such, they may retain geochemical signatures of the aqueous solutions in the martian crust. The Lafayette meteorite was chosen for this study because it contains more of the secondary minerals than the others, amounting to about 1–2% of the meteorite.

Sampling and Instrumental Neutron Activation Analysis (INAA): Samples of the orange-brown weathering products ("iddingsite" [2,3]), along with some olivine and pyroxene grains, were hand-picked from a crushed sample of Lafayette (ME2116 from the Field Museum, Chicago, Illinois). Fourteen grains of the weathered material weighing a total of 0.12 mg were packaged in sealed high-purity quartz tubes and irradiated for 96 hr at a thermal flux of about 7.5×10^{13} $cm^{-2}s^{-1}$. After irradiation, the samples were

removed from the tubes and weighed into new tubes for g ray assay, which was done using intrinsic Ge detectors in the low-background Radiation Counting Laboratory at JSC. Because the samples were so friable, individual 1–10-μg samples were weighed directly into the tubes, which themselves weighed about 100 mg, or ~10^5 larger than the samples. The weighing uncertainties were too high, so sample weights were obtained instead by calculation, assuming that the samples contained 29% FeO [1]. Satisfactory standards are not available for some elements (Br, Hg, Se), so abundances of these elements were estimated based on published cross sections [4].

Results: Discussed below are preliminary results for 16 of the 19 samples analyzed. The other three had much higher Sc contents (16, 21, and 29 ppm) than the rest, and are thought to contain substantial amounts of pyroxene.

Alkalies (Na, K, Rb, Cs). The alkalies are important because of their relatively high solubilities in aqueous solutions and their well-known affinity for clay minerals.Sodium concentrations of about 2100 ppm are somewhat lower than the bulk meteorite (3220 ppm [5]), while K contents of 3000–7000 ppm are higher by about a factor of five. Rubidium concentrations are close to INAA detection limits. An error-weighted mean of 34 ± 5 ppm Rb was obtained on 6 of the 16 particles that had Rb concentrations greater than the 2σ uncertainties; upper limits for Rb in the other 10 samples are in agreement with this estimate, which is about an order of magnitude higher than Rb in bulk Lafayette. Cesium enrichments are even greater, the average value of 20 ppm amounting to 60× bulk.

Transition metals (Sc, Cr, Co, Zn). Scandium concentrations in the iddingsite vary considerably, even after the three highest-Sc samples are excluded. The spread in values suggests the approach to a lower limit of about 0.2 ppm, much lower than the clinopyroxene and olivine (65 and 8 ppm Sc respectively) that make up the bulk of the meteorite. Chromium contents are highly variable, ranging from values (or lower limits) of about 3 ppm up to 5800 ppm. As with Sc, the low values are probably characteristic of the iddingsite, with the higher values representing the presence of small amounts of other phases in the analyzed sample. It is not surprising, considering the normalization to Fe, that Co values are quite constant at 56 ± 5 ppm. This is a factor of 2 lower than the Co content of the olivine, and represents a Co/Fe ratio about 14% lower than the olivine. Zinc concentrations average 137 ppm, or about 2× the value for bulk Lafayette.

Rare earths (La, Ce, Sm, Eu, Yb, Lu). Most of the samples do not have detectable abundances of rare earths. Detection limits for the heavy REE, Yb and Lu, are about 1–2× CI chondrite values, just below bulk Lafayette abundances. One sample is enriched in light REE (La ~ 50× CI), but the rest are at or below bulk Lafayette values of 7–8× CI for La and Ce. Samarium, the best-determined of the REE, varies from the bulk Lafayette level of 4× CI to as low as 0.2× CI.

Other elements detected in most samples (As, Br, W, Hg). Arsenic might be expected to be a tracer for sulfides in the fluids. Most of the As values obtained are in the range 0.5–1.5 ppm, with a few lower still. Many elements are not sufficiently abundant in igneous rocks for detection by INAA, although the sensitivity of the techniques for elements are actually quite good. The other three elements in this list fall into this category. Bromine abundances are typically 2–4 ppm, and W is observed at about 0.5–3 ppm. Detection of very high levels of Hg (20–100 ppm) is quite surprising.

Elements for which only upper limits were obtained (Hf, U, Th, Sb, Se). These elements are usually detected by INAA, but are too low in these weathering products to be observed. Upper limits in parts per million (compared to bulk Lafayette values in parentheses) are Hf < 0.3 (0.34), Th < 0.3 (0.2), U < 0.3 (0.05), Sb < 0.2 (0.03), and Se < 5 (0.07).

Discussion: These results illustrate that the weathering products are quite low in incompatible trace elements, but are enriched in heavy alkalies (K, Rb, and especially Cs). Mercury is highly enriched, and while terrestrial contamination is perhaps the most likely source, there are reasons to believe that the elevated Hg may be real. Bromine is detected, but is apparently not as concentrated as Cl [1] in the iddingsite.

References: [1] Treiman A. H. et al. (1993) *Meteoritics, 28,* 86–97. [2] Bunch T. E. and Reid A. M. (1975) *Meteoritics, 10,* 303–315. [3] Boctor N. Z. et al. (1976) *EPSL, 32,* 69–76. [4] Mughabghab S. F. (1984) *Neutron Cross Sections*, Academic, New York. [5] Treiman A. H. (1986) *GCA, 50,* 1061–1070.

ROLE OF THE MARTIAN MAGNETIC FIELD HISTORY IN LOSS OF VOLATILES TO SPACE.

J. G. Luhmann, Space Sciences Laboratory, University of California, Berkeley CA 94720-7450, USA.

The efficacy of atmospheric ion scavenging by the solar wind and the related sputtering process for loss of martian volatiles over time is closely tied to the history of the Sun and the history of the planet's magnetic field. Solar evolution is being discussed elsewhere in this workshop, but it is also important to consider how the decay of the martian dynamo phases with the solar history, and in particular with the early period of enhanced EUV flux when the above loss mechanisms would have been most effective. Schubert and Spohn [1] proposed a model for the early field of Mars based on assumptions about the postaccretionary cooling of the core and the subsequent onset of solid inner core formation. Using this model as an example, coupled with models for the solar EUV and solar wind histories, we show how exposure of the upper atmosphere to the solar wind, and hence ion "pickup" and its sputtering effects, would be altered if the magnetic field was significant in Mars' early life (~2–3 G.y. ago). These examples illustrate the value of paleomagnetic studies at Mars and on dated martian samples for the historical assessment of atmosphere loss to space.

References: [1] Schubert G. and Spohn T. (1990) *JGR, 95,* 14095–14104.

WATER ICE IN THE MARTIAN ATMOSPHERE AS DERIVED FROM PHOBOS/KRFM DATA.

W. J. Markiewicz[1], H. U. Keller[1], E. Petrova[2], N. Thomas[1], and M. W. Wuttke[1], [1]Max-Planck-Institute for Aeronomie, Postfach 20, 37189 Katlenburg-Lindau, Germany, [2]Space Research Institute, Russian Academy of Sciences, Profsoyuznaya Ulitsa 84/32, Moscow 117810, Russia.

During the 1989 Phobos mission, the KRFM instrument observed the equatorial region of Mars in eight spectral bands from 315 to 550 nm. From three subsets of the KRFM data, the present work infers the presence of various forms of water ice in the Mars atmosphere.

1. Access above mean brightness and its decrease to mean level was observed in the morning UV profiles. Explaining these variations with a model of a homogeneous constant silicate haze does not

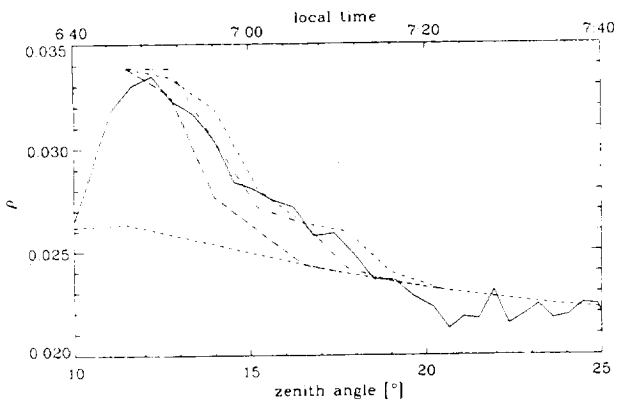

Fig. 1. Morning part of UV profile, measured by KRFM instrument on March 6, 1989. Solid line indicates a solid curve; dashed curve corresponds to a model of a constant dust haze with $\tau = 0.20$, $m_i = 0.035$; dotted curve corresponds to the model that includes near-surface particles with ice shells with $\Delta = 5.0$, but no sublimation; remaining three curves are models with $\Delta = 5$ and including sublimation for $\alpha_s = 0.8$ (dash-dot), 1.0 (dash-dot-dot-dot), and 1.5 (long dash) $\times 10^{-15}$ g $\mu m^{-2} s^{-1}$. The particles are assumed to be coated by water ice condensing during the night according to $R = (R^2_{core} + \Delta)^{1/2}$, where Δ is the thickness of the ice mantle. This ice mantle is assumed to sublimate after sunrise according to $d/dt\, M_{ice} = -\alpha_s\, 4\pi R^2(t)$.

seem possible for two sessions. A model including a time-evolving, near-surface layer of silicate particles covered with water ice provides a better fit to the data. The inferred column density of water vapor that condensed overnight on the dust particles is about 0.5×10^{-5} g cm^{-2}, and the sublimation rate of these ice mantles after sunrise is of the order of 10^{-15} g μm^{-2} s^{-1}. The ice haze contribution to the total optical depth decreases from about 0.05 at dawn to zero within about an hour.

2. A brightness increase of another type, observed in the afternoon UV profiles of the Valles Marineris, is shown to be consistent with the presence of water-ice clouds. The dependence on the

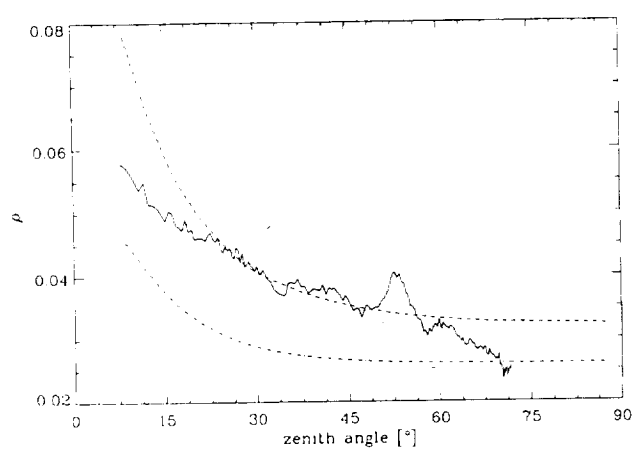

Fig. 2. Solid curve is evening part of UV profile measured by KRFM instrument on March 21, 1989, at Valles Marineris. Other curves are calculated brightness for models with a cloud ($\tau = 0.05$) placed at an altitude of 50 km, and composed of spherical ice particles with a broad size distribution (dotted) and a narrow size distribution (dashed), and of irregular ones with narrow size distribution (dashed-dotted).

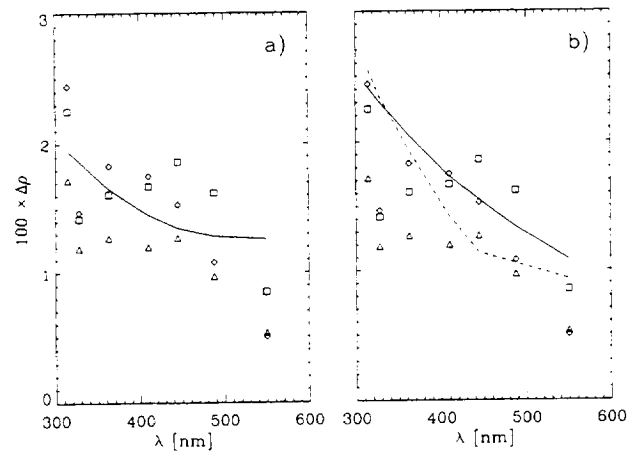

Fig. 3. The spectral dependence of brightening at the mountains. Measured values are shown by symbols: Pavonis Mons on 26.02 with diamonds, Arsia Mons on 13.03 with triangles and on 14.03 with squares. (**a**) Ice particles with silicate cores with $\tau = 0.05$, $\Delta = 0.5$, and core size of 0.8 µm (solid) and 0.5 µm (dotted). (**b**) Pure ice particles with radius R_{eff}, with $\tau = 0.10$ and $R_{eff} = 0.8$ µm (solid), $\tau = 0.2$, and $R_{eff} = 0.5$ µm (dashed), and $\tau = 0.10$ and $R_{eff} = 0.5$ µm (dotted). $P_{gas} = 2.0$ mbar in the models shown.

properties of the clouds is discussed. The size distribution of the cloud particles seems of secondary importance. Their assumed shape, however, is critical. For spherical particles, the optical depth of the cloud is deduced to be 0.05 and the water content within the cloud to be 0.54×10^{-5} g cm^{-2}. For particles with a slightly irregular shape and rough surface, both of these estimates are 3× higher.

3. The photometric profiles of the Tharsis Ridge, where the KRFM traces passed over the martian volcanos, exhibit an increase in brightness in all wavelengths, but stronger in shorter wavelengths. The spectral dependence of the measured brightening is analyzed to extract the properties of the clouds around Arsia Mons and Pavonis Mons. The effective radius of the cloud particles is estimated to be <1 µm. The corresponding optical depth of the cloud is 0.05, but it could be as large as 0.2 if smaller particles are assumed. The column density of the water ice within the cloud is estimated to be in the range 1.5–4.1×10^{-6} g cm^{-2}, depending on the assumed properties of the particles.

All the estimates given are approximate, partly because of the limited information in the KRFM data, and possibly more importantly, because of the discussed complexities of the martian atmosphere. Models of the KRFM photometric profiles of the morning haze reveal that even slight amounts of ice condensing on and subsequently sublimating from atmospheric dust can have a great influence on the measured brightness. Similar statements can be made with respect to the assumed shape for the particles within the clouds. This confirms the complexity of the Mars atmosphere-surface system and points out the necessity of careful analysis of imaging data of this planet.

NASA'S MARS SURVEYOR PROGRAM: FOCUS ON VOLATILES. D. J. McCleese, Jet Propulsion Laboratory, California Institute of Technology, Pasadena CA 91109, USA.

Mars Surveyor is a continuing program of Mars exploration employing investigations conducted from landed and orbiting plat-

forms. The program focuses on the themes of life, climate, and resources. These themes are connected by the common thread of water on Mars. The missions to be launched in 1998 as part of this program focus specifically on volatiles and climate history of Mars. This paper focuses on the anticipated studies of martian volatiles to be made by Mars Surveyor.

The first mission in the program is the Mars Global Surveyor (MGS), an orbiter to be launched in 1996 that recovers much of the science lost with the failure of Mars Observer. MGS has a strong volatile research component. The mission includes investigations of volatiles (both CO_2 and H_2O) on the surface and in the atmosphere, utilizing the thermal emission spectrometer (TES) and high-resolution and global imaging from the Mars Orbiter Camera (MOC).

In the 1998 opportunity, a lander will be placed on the layered terrain of the south polar region of Mars. The Mars Volatile and Climate Surveyor (MVAC) focuses on understanding the form, quantity, and behavior of surface volatiles using a payload of integrated instruments. The lander will also carry the Mars descent imager (MARDI), which provides contextual information for the lander. In orbit, the pressure modulator infrared radiometer (PMIRR) and Mars color imager (MARCI) will map the sources and sinks of volatiles, as well as track their transport over the planet.

Mars Surveyor mission plans include an orbiter and lander to be launched in 2001. The orbiter will carry an improved γ ray spectrometer (GRS) that will map reservoirs of surface and near-surface water. While subject to an upcoming Announcement of Opportunity, and consequently not defined, the lander science may continue the *in situ* study of martian volatiles.

NASA is also pursuing a joint program with ESA in 2003 that would provide a small network of three landers, carrying geochemistry instruments as well as other geophysics and geology sensors. The three surface stations will be supported by an orbiter carrying an atmospheric sounder. Candidate sounders for the orbiter are capable of observing atmospheric water vapor.

Return of a sample from the surface of Mars is planned for 2005. It is possible that samples of the atmosphere and of volatiles will be preserved within the return capsule.

LIMITS ON THE CO_2 CONTENT OF THE MARTIAN POLAR DEPOSITS. M. T. Mellon, Mail Stop 245-3, NASA Ames Research Center, Moffett Field CA 94035, USA.

It has recently been suggested that large quantities of CO_2 could be sequestered within the martian polar deposits as CO_2 ice or CO_2 clathrate hydrate, stabilized against sublimation by a nonporous overburden of water ice. I investigate the phase stability of CO_2-bearing polar ices and place limits on the quantity of CO_2 that can be sequestered. The magnitude of this limitation follows from CO_2-bearing ices having thermal conductivities on the order of 5–6× smaller than that of water ice, producing a higher geothermal gradient. By calculating the effective thermal conductivity of a mixture of ices and the resulting temperature-pressure profile of the polar deposits and comparing these profiles with the phase diagrams of water ice, CO_2 ice, and CO_2 clathrate hydrate, I set limits on the quantity of CO_2 in the polar deposits.

The abundance of past fluvial activity on Mars has led many investigators to conclude that Mars once had a warmer and wetter climate than it has today, maintained by a dense atmosphere containing greenhouse gases. Owing to the current atmospheric composition, CO_2 has been included as the primary greenhouse gas in the early martian atmosphere and as much as several bars would have been required to bring the global temperature above the freezing point of water. Today the climate is colder, and only 5–6 mbar of CO_2 is present in the atmosphere. Therefore, if Mars once had a warm, wet climate caused by a thick CO_2 atmosphere, nearly all that CO_2 would need to have been subsequently lost to space and/or be currently sequestered in some nonatmospheric reservoir. Recent attention has been brought to possible polar deposits of CO_2 ice and CO_2 clathrate hydrate, where sublimation of the polar cap as a whole, during times of extremely high obliquity, could provide a mechanism for periodic climate change.

Upper limits on the CO_2 content of the polar deposits can be obtained from calculating the temperature-pressure profile within the deposits. Mixtures of water ice and CO_2-bearing ice will affect the thermal conductivity of the deposit. Water ice alone will have a high thermal conductivity and result in a low geothermal gradient. Adding low thermal conductivity CO_2-bearing ice (CO_2 ice and CO_2 clathrate hydrate) will lower the conductivity, raising the geothermal gradient and raising the polar basal temperature. By requiring that the polar deposits consist of a solid phase of the volatiles, an upper limit on the CO_2 content is obtained.

Assuming a nominal surface heat flow of 30 mW/m^2 and a long-term mean surface temperature of 155 K, I find that in a 4-km-thick north polar deposit 112 mbar (equivalent atmospheric pressure) of CO_2 can be sequestered in the form of clathrate or 254 mbar in the form of CO_2 ice. Less CO_2 is also allowed. To obtain these values required optimum (and probably unrealistic) conditions; I assumed a lower limit on the maximum thickness of the deposit, low values of heat flow (ignored frictional heating), and low surface temperature (ignored insulating polar firn deposits), excluded salts and dust, and assumed perfectly random and isotropic CO_2-bearing ice inclusions with no layering or contact resistance. Any one or combination of these effects are probable and will reduce the allowed CO_2 content of the polar deposits. With more realistic conditions it is unlikely that the north polar deposit can contain more than a few tens of millibars of CO_2, with less also being allowed. No CO_2 is required by existing observations.

A similar quantity might be expected in the south polar deposit due to similar climate conditions accounting for its formation and similarities in its present state and structure; however, the smaller thickness of the deposit does not allow for direct constraints as in the north.

The most important implication of these results is that the polar deposits of Mars do not contain large quantities of CO_2 that could be periodically available for climate change during periods of high obliquity, or as a relic of an early warm, wet climate. Models of the climate evolution of CO_2 are correct to reject results predicting a thick CO_2-ice polar cap at present and should be cautious of past thick CO_2-bearing deposits. Nevertheless, periodic release of even a few tens of millibars of CO_2 during high obliquity would have a notable effect on the martian climate and surface-atmosphere interactions.

IRON, SULFUR, AND CHLORINE PHASES ON MARS.
R. V. Morris[1], D. C. Golden[2], D. W. Ming[1], and J. F. Bell III[3], [1]Mail Code SN, NASA Johnson Space Center, Houston TX 77058, USA, [2]Dual Inc., Houston TX 77058, USA, [3]Center for Radiophysics and Space Research, Cornell University, Ithaca NY 14853, USA.

Introduction and Background: Spectral data of weathered martian surface material (martian bright regions) obtained from Earth-based telescopes are, in general, characterized by a shallow absorption band centered near 860 nm, a relative reflectivity maximum near 750 nm, and an absorption edge extending from ~400–750 nm with inflections near 600 and 520 nm [1,2,4]. Spectral data from the Phobos-2 spacecraft [3] confirm the ~860-nm band minimum and also show for certain regions that the shallow band minimum is located near 900 nm. It is not known whether the other spectral features also change position because the Phobos-2 data do not extend to wavelengths shorter than ~800 nm.

An important basis for specific mineralogical assignments for these spectral features has been analyses of terrestrial analog samples where the mineralogy of Fe-bearing phases could be determined. Samples that contain palagonite (weathering product of basaltic glass) have received considerable attention, in part because many palagonitic samples are reasonable martian spectral analogues [5–10] and in part because processes favorable to palagonite formation are considered to be active on Mars, both now and in times past. Samples of palagonitic tephra collected from the same location on the Puu Nene cinder cone, Hawaii, are among the best spectral analogs and have been studied in detail as sample Hawaii-34 [5], VOLO2A [7], and PN-9 [11]. Collectively, these studies show that the visible absorption edge results predominantly from Fe^{3+} present as discrete particles (dimensions < ~20 nm) embedded in a hydrated aluminosilicate matrix. In addition to these nanophase ferric oxide particles, subordinate amounts of well-crystalline hematite (α-Fe_2O_3) are also indicated for martian bright regions where the hematite spectral features at ~860 nm (minimum of shallow band), 750 nm (relative reflectivity maximum), and 620 and 520 nm (inflections in the absorption edge) are present [8,11,12].

The Viking XRF experiment showed that martian dust and soil contains significant quantities of S and Cl [13]. Mineralogies containing these elements have not been found in the Puu Nene samples discussed above. Do martian bright regions that have the band near 900 nm have Fe mineralogies that contain these volatiles, as suggested by [3]? We report here spectral and other data for two samples of volcanic tephra from Hawaii (HWMK24 and HWMU1), where S and Cl participated in the weathering.

Results and Discussion: HWMK24 is a sample of yellow-colored tephra collected from a cone on the summit of Mauna Kea. HWMU1 is a sample of orange-brown tephra collected from a steam vent on the Mauna Ulu cinder cone on Kilauea Volcano. All analyses were done on the <1-mm size fraction of tephra. Diffuse reflectivity spectra between 350 and 2100 nm are shown in Fig. 1. Spectra of PN-9 and PH-1 are also given for comparison to palagonitic tephra samples where the dominant iron mineralogy is nanophase ferric oxide [10,11]. Note that the spectra for HWMK24 and HWMU1 are different from each other and both are very different from the spectra for PN-9 and PH-1. Both HWMK24 and HWMU1 have a band minimum near 910 nm. HWMK24 also has a well-defined band minimum near 430 nm. HWMU1 has an unresolved band minimum near 460 nm. XRD, Mössbauer, and electron microprobe data all show that the dominant Fe-bearing phases are jarosite [$(H_3O, Na,K)Fe_3(SO_4)_2(OH)_6$] for HWMK24 and akageneite (β-FeOOH) for HWMU1. These mineralogies are consistent with spectral data for the pure phases [14,15]. Chloride is apparently vital for the formation of akageneite and also stabilizes its structure [16].

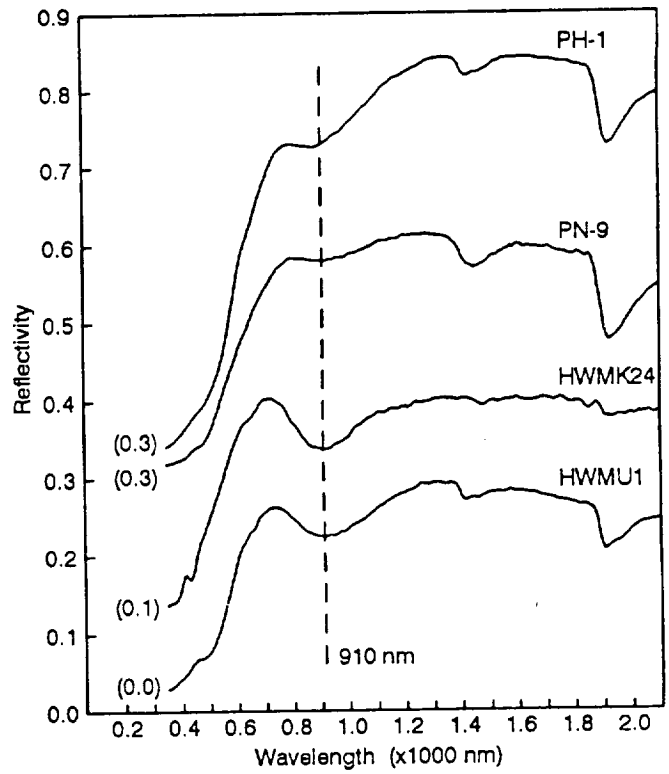

Fig. 1. Diffuse reflectivity spectra for samples of palagonitic tephra from Hawaii.

These results show that weathering of volcanic tephra in the presence of S and Cl can produce Fe-bearing weathering products that contain these elements. The source of the S and Cl is most likely local occurrences of S- and Cl-rich magmatic gases and/or fluids. Given the Viking lander S and Cl results, it is possible that the ~910-nm band minimum observed in certain martian bright regions result from jarosite and/or akageneite, and that the weathering results from hydrothermal processes driven by the heat associated with either volcanic or impact processes.

References: [1] Singer R. B. et al. (1979) *JGR, 84*, 8415–8425. [2] Bell J. F. III et al. (1990) *JGR, 90*, 14447–14461. [3] Murchie S. et al. (1993) *Icarus, 105*, 454–468. [4] Mustard J. F.and Bell J. F. III (1994) *GRL, 21*, 3353–3356. [5] Evans D. L. and Adams J. B. (1979) *Proc. LPSC 10th*, 1829–1834. [6] Allen C. C. et al. (1981) *Icarus, 45*, 347–369. [7] Singer R. B. (1982) *JGR, 87*, 10159–10168. [8] Bell J. F. III et al. (1993) *JGR, 98*, 3373–3385. [9] Golden D. C. et al. (1993) *JGR, 98*, 3401–3411. [10] Morris R. V. et al. (1990) *JGR, 95*, 14427–14434. [11] Morris R. V. et al. (1993) *GCA, 57*, 4597–4609. [12] Morris R. V. and Lauer H. V. Jr. (1990) *JGR, 95*, 5101–5109. [13] Clark B. C. et al. (1982) *JGR, 87*, 10059–10067. [14] Clark R. N. et al. (1990) *JGR, 95*, 12653–12680. [15] Sherman et al. (1982) *JGR, 87*, 10169–10180. [16] Murray J. W. (1979) *Marine Minerals*, 47–98, MSA.

OBSERVATIONAL TESTS FOR THE IDENTIFICATION OF SHORE MORPHOLOGY ON MARS. T. J. Parker, Jet Propulsion Laboratory, California Institute of Technology, Pasadena CA 91109, USA.

The northern plains of Mars received tremendous quantities of water and sediment from channel discharges that were so large that vast lakes or even an ocean, either partially or completely frozen, must have formed, at least temporarily. I previously focused work on sites along the margin of the northern plains where plains boundary morphology, suggestive of shore morphology, was imaged by the Viking Orbiters at high resolutions. In many instances, the plains boundaries are found at heights of several tens to hundreds of meters above the surrounding plains.

Coastal morphology is probably the most diagnostic evidence of former lakes that we can expect to find on Mars, at least until unequivocal surface compositional information becomes available. The following points should be noted when evaluating a potential shoreline on Mars.

1. Water is an environmentally abundant volatile at Mars' position in the solar system, and liquid water has probably been stable at its surface at various times in the past. Other liquid volatiles are less abundant and, in most cases, less stable at Mars' surface than water.

2. Free-standing liquid water is confined by gravity to an equipotential upper surface that intersects topography at an essentially constant elevation over large regions. Other liquid volatiles would be similarly confined, but gases would not, so eolian erosional boundaries are not topographically confined and are often indistinct or gradational.

3. Winds blowing across open water generate ripples and waves (or transport rafted ice in cold environments) that transfer their energy to the land, resulting in erosion, sediment transport, and deposition that is focused within a few meters of the water level. In contrast, in fluvial and glacial settings the entire column of water or ice is in motion, so erosion and deposition occurs from the high water line (fluvial) or trim line (glacial) to the base of the column. Regions subjected to fluvial and glacial processes commonly exhibit evidence of scour parallel to the direction of flow over their entire surfaces. Basins that once contained lakes (including glaciolacustrine and fluviolacustrine settings) or oceans may show signs of extensive erosion and deposition at or near the water level (at their margins and on islands), but the basin interior more than a few meters below water level would have experienced low-energy sediment deposition that would tend to drape preexisting topography with fine material. This fine material could subsequently become the site of desiccation, periglacial and thermokarst modification, and a source for eolian deflation.

4. Longshore transport moves sediment eroded from headlands into embayments, producing beaches that transit from erosional to depositional, with wave-cut cliffs grading along shore into constructional barriers and spits. Spits and coastal barriers remain as large, often arcuate or cuspate sets of beach ridges (resulting from wave refraction) after recession of the lake.

Point 2 makes it possible to distinguish shorelines from fault scarps where both feature types occur in association, such as in the Great Basin of the southwestern United States. Fault scarps cross undulations in topography with little or no lateral deflection, whereas even minor topographic undulations profoundly affect the lateral position of a shoreline. Similarly, point 2 would suggest that horizontal benches in tilted craters, in which the continuity of the bench appears uninterrupted by the presence of the crater, suggests a shoreline in which the crater was partially inundated and eroded by standing water.

Several locations where benches transit laterally into ridges (point 4) have been described [1–3]. Longshore trends from erosion to deposition distinguish wave-cut and wave-built terraces from structure-controlled benches in sequences of layered rocks. Horizontal benches "cut" at a definite angle to recognizable strata, though uncommon in Viking images (requiring dipping strata), are most easily explained as paleoshorelines.

Shore platforms and sedimentary bedforms associated with gently sloping, dissipative shorelines [e.g., 4] can be extensive, so many terrestrial paleolakeshores can be seen in moderate- to high-resolution orbiting spacecraft image data. Steeply shelving shore zones dominated by wave reflection are much narrower in plan view, so that many steep mountain-front paleolakeshores may be undetectable in orbiter images. Narrow shore platforms require high spatial resolutions to be recognizable, typically moderate- to high-resolution aerial photographs. Many terrestrial paleoshorelines appear discontinuous in satellite and aerial photographs for this reason.

References: [1] Parker T. J. et al. (1989) *Icarus, 82,* 111–145. [2] Parker T. J. et al. (1993) *JGR, 98,* 11061–11078. [3] Parker T. J. (1994) *Martian Paleolakes and Oceans*, Ph.D. thesis, Univ. of Southern California, 200 pp. [4] Wright L. D. et al. (1979) *Marine Geol., 32,* 105–140.

THE RICH GEOMORPHIC LEGACY OF THE ARGYRE BASIN: A MARTIAN HYDROLOGIC SAGA. T. J. Parker, Jet Propulsion Laboratory, California Institute of Technology, Pasadena CA 91109, USA.

Argyre Planitia is the second largest well-defined impact basin in the southern highlands of Mars. Both Argyre and Hellas, the largest highland basin, received sediment from large channels draining into them. The floors of both basins exhibit etched layered material that is probably thick sedimentary deposits from these channels. Unlike Hellas, Argyre also has a large channel, Uzboi Vallis, that flowed out of the basin, strongly suggesting overflow of a lake within the basin. This makes it the largest impact basin on Mars, with channels both draining into it and flowing out from it. Mapping the basin at the 1:500,000 scale and comparing the results with the surrounding region, both up-channel into the large valley networks south and east of Argyre, and down-channel through Uzboi Vallis and the Chryse Trough, has revealed a long, complex, and fascinating history of water and wind-related processes acting to shape the region over martian geologic time from the Noachian through the present day. This work is based on careful examination of the Viking images and relative age determinations of major geomorphic/geologic units based on superposition relationships and crater counts. This writeup summarizes my inferences about the geologic history of Argyre and the Chryse Trough and what implications they might provide about the ancient martian climate. The more important inferences are highlighted in the following paragraphs.

1. There is no real evidence to suggest that Argyre Planitia is any younger than any other large impact basin on Mars. The basin itself

is a very ancient structure that has been broadened and filled in through mass-wasting, fluvial, lacustrine, and eolian erosion. Many of the Nereidum and Charitum rim mountains are flat-topped erosional remnants of the surrounding Noachian plateau surface. Previously, the highland surface probably sloped gently into the basin intereior, such that Argyre topography may once have been similar to that of the nearby, very degraded Ladon Basin. The tallest of the rim mountains that I've measured, at several kilometers high, are along the inside southern rim. Several of the mountains in this area have large, knobby terraces some distance below the highest peak that may be the erosional remnants of an earlier stage of broadening (and thus local deepening) of the basin. Therefore, the modern "fresh" appearance of Argyre is due to erosional "enhancement" of the basin rim during the Noachian and Hesperian, rather than due to the "pristine" nature of the impact-fractured highlands. Argyre's rim is, in essence, a scale model of the extensive fretted terrains along the lowland/upland boundary, and may have formed in the same way. Any proposed paleoclimate model must account for the removal of several kilometers of rock from the basin's rim while preserving the flat-topped mesa surfaces. The most efficient mechanisms, fluvial and lacustrine erosion, would focus erosion at the bases of the rim mountains.

2. Surius, Dzigai, and Palacopas Valles, the three large valley networks flowing into Argyre from the south and east, are subsequent streams that developed after the elevated rim of Argyre had been eroded by networks draining inward and outward from a previous drainage divide at the basin's rim. Though these three channels are Hesperian in age, they probably occupy valleys formed during the Noachian. Formerly outward-draining networks may have been captured by the inward-draining systems at this time. Surius and Dzigai Valles (and Doanus Vallis, a tributary to Dzigai) head near smooth, flat-surface deposits of the Dorsa Argentea Formation. This material embays topography in such a way as to suggest a lacustrine origin, implying that global temperature ranges may have been relatively moderate in a thicker atmosphere well into the Hesperian.

3. Uzboi Vallis appears to be late Noachian in age, and probably drained a lake within Argyre northward through Ladon Valles, Margaritifer Valles, through a predecessor to Ares Valles and into Chryse Planitia. At least two episodes of flow through this system are evident in Uzboi, Ladon, and Margaritifer Valles in the form of terraces and abandoned channels. Ladon Valles exhibits as many as five terrace levels.

4. The layered material in the basin interior is probably lacustrine and is Hesperian in age, though the plains surfaces in reentrants into the rim mountains are late Noachian in age. The interior deposits are etched, possibly by eolian deflation, such that the crater size-frequency curve is "rounded off" at small diameters. This etching appears to date to the late Hesperian or early Amazonian, and may be active to this day.

5. The sinuous ridges in the basin are integral to the layered deposits and emanate from Surius Vallis, and are thus Hesperian in age. They are likely aqueous sedimentary structures, either lacustrine barriers or glacial eskers.

6. Nia Valles (southwest of Galle Crater) is a small early Amazonian outflow channel that flowed into the basin interior, forming a small lake within the basin (evidenced by local layered deposits within etched depressions on the older, more extensive layered deposits). The deposits from this flood episode are also etched.

7. The prominent debris aprons in Charitum Montes are very young (late Amazonian), but not modern, as they are lightly cratered. These aprons are similar to debris aprons in the fretted terrains around the northern plains. They occur only in association with mountains south of –55° latitude, and only within about 200 km of the basin interior.

ARE THE MARTIAN VALLEY NETWORKS REALLY SAPPING CHANNELS? J. W. Rice Jr., Department of Geography, Arizona State University, Tempe AZ 85287, USA.

The valley networks bear mute testimony to a drastic climatic change on Mars. These landforms may hold the key to unlocking the paleoclimatic history of Mars; however, there is still no consensus among investigators regarding the formation (runoff vs. sapping) of these features. An attempt will be made here to point out some major flaws associated with the sapping hypothesis based on terrestrial analog field studies and laboratory experiments.

It has been argued that the valley networks were formed primarily by groundwater seepage [1]. This is based on morphologic characteristics such as U-shaped valleys with theater heads and steep walls, low drainage density, irregular junction angles, and short tributaries. The evidence for sapping is in some cases convincing (i.e., Nirgal Vallis), but it does not explain many of the dendritic valley systems, e.g., those located in the Margaritifer Sinus region.

Some problems with the sapping model will be discussed below. First, the measurement of junction angles between individual intersecting tributaries of the valley networks does not provide evidence to refute the view that the networks were formed by rainfall/snowmelt-fed erosion [2–4]. Stream junction angles are controlled by slope, structure, lithology, and basin development stage, not precipitation [5]. Sapping requires that zones of low hydraulic head somehow be established to support the gradients needed to allow groundwater flow, and that zones of high hydraulic head be recharged, presumably by precipitation. Additionally, some of the valley networks whose channels originate on crater rim crests indicate that the local water table must have intersected the surface high on the crater wall if sapping was involved [4]. This would mean that the crater was once filled with water but there is no evidence, such as inflowing channels, to support this condition.

The sapping process also requires large volumes of water in order to produce a well-developed sapping network. The most efficient process of sapping erosion occurs in unconsolidated sediments, where the limiting factor is the transporting capacity of the spring-fed flows. Experiments [6] suggests that a minimum of 10× more water than volume-eroded sediment must be discharged in order to form a sapping valley network. This work had sediment concentrations in the outflows between 1% and 10%. In unconsolidated sediments a ratio of 100 to 1000-fold is more reasonable. For consolidated rocks, valley erosion is limited by the rate of weathering of the rocks at the sapping face. These weathering processes (solution of cement/melting of ice, salt fretting, and or freeze thaw cycles) are very slow and require water to eroded rock ratios of 10^5 or greater.

Field work on channel systems located on the Canterbury Plain, New Zealand [7], indicate that these systems are of a composite origin. These features occupy U-shaped valleys with theater heads and steep walls and have low drainage densities and short tributar-

ies. The above-mentioned characterisitics are often cited as evidence for sapping, but these channels are in fact formed predominantly by surface runoff and subsequently modified by groundwater sapping. The smaller channels are being formed by seepage and mass movement, but they stagnate when an armor is formed that cannot be breached by seepage flow.

Finally, drainage system studies have been conducted on Earth and Mars using drainage density and drainage pattern characteristics. The density of drainage may provide information on permeability and texture of materials, thus inferring the identity of materials [8]. The patterns that streams form are determined by inequalities of surface slope and rock resistance [9]. Therefore, based on terrestrial drainage system studies, this paper will make the first attempt at suggesting what geologic materials and slopes the martian valley networks may have eroded. Most of the martian valley networks have drainage patterns that fit the following patterns as described by terrestrial researchers [8,9]: subdendritic and subparallel, which are modifications of the basic drainage systems classified as dendritic and parallel respectively.

Subdendritic drainage develops where rocks offer uniform resistance in a horizontal direction. This suggests nearly horizontal sedimentary rocks, superposed drainage on folded sedimentary rocks of equal resistance, or massive igneous rocks of gentle regional slope at present or at time of drainage inception.

Subparallel drainage implies either pronounced moderate to steep regional slopes or slope controlled by parallel topographic features. This pattern usually ocurs in sedimentary, volcanic, and metasedimentary rocks that have been faulted and folded.

Another useful drainage system characteristic is that of drainage texture [9]. Drainage texture describes the relative spacing of drainage lines using the relative terms fine, medium, and coarse. Drainage texture is controlled by (1) climatic factors such as the amount and distribution of precipitation and permafrost; (2) rock characteristics, including texture and size of weathered fragments; (3) infiltration capacity; (4) topography; and (5) stage and number of erosion cycles. In unconsolidated sediments the drainage texture is directly related to grain size.

Fine texture describes a system that has a high degree of ramification of drainage lines. This results in a dense network involving multitudes of small streams. This texture type is typically observed in fairly impervious materials (shale, clay, and silt). The low infiltration capacities of fine-grained materials allow for more surface runoff, hence a denser network of surface drainage.

Coarse textures exhibit very little ramification and longer, more widely separated valleys. Permeable materials such as sand, gravel, and rocks that weather into coarse fragments exhibit coarse textures. The higher infiltration capacities of coarse-grained materials readily absorb precipitation and have fewer surface streams and display coarse drainage texture. Medium texture is the intermediate of the above-mentioned textures.

The above-mentioned drainage basin characteristics will also be combined with an age reassessment of the valley networks on Mars. This involves examining both the stratigraphic age and morphologic preservation "age" of the valley networks. Recent work [10] indicates that many of the valley networks are in fact younger than Noachian. This is contrary to most valley network studies and carries with it important implications to the geologic, climatic, and possibly biologic evolution of Mars.

References: [1] Pieri D. C. (1980) *Science, 210,* 895–897. [2] Jakosky B. M. and Carr M. H. (1985) *Nature, 315,* 559–561. [3] Rice J. W. (1993) *LPI Tech Rpt. 93-03,* 22–23. [4] Clow G. D. (1987) *Icarus, 72,* 95–127. [5] Schumm S. A. (1956) *GSA, 67,* 597–646. [6] Howard A. D. (1988) *NASA Spec. Rpt., 491,* 71–83. [7] Schumm S. A. and Phillips L. (1986) *Geology, 14,* 326–329. [8] Howard A. D. (1967) *AAPG, 51,* 2246–2259. [9] Zernitz E. R. (1932) *J. Geol., 40,* 498–521. [10] Scott D. H et al. (1995) *U.S. Geol. Surv. Misc. Inves. Series Map,* in press.

CONDENSATION-DRIVEN VERTICAL PROFILE OF WATER IN MARS TROPOSPHERE: PHOBOS REVISITED.

A. V. Rodin, O. I. Korablev, and V. I. Moroz, Space Research Institute, Russian Academy of Sciences, Profsoyusnaya 84/32, 117810 Moscow, Russia.

We present new analyses of the solar occultation infrared spectroscopy experiment, performed onboard the Phobos-2 orbiter in 1989. The instrument sounded the evening limb of Mars in two narrow spectral ranges, 2710–2740 and 5280–5370 cm^{-1}, with the resolving power of 1100. Water vapor absorption at 1.87 μm results in a set of vertical profiles of water in the altitude range 10–50 km measured with a vertical resolution of ≈4 km. First analysis of these data [1] yielded water vapor distributed with a mean scale height of 6 km. The absolute photometry in spectral continuum at 1.9 and 3.7 μm resulted in vertical profiles of dust [2]. The main reasons for revisiting the data are to introduce corrections of instrumental errors [2,3] and a new technique of vertical profile retrieval. After correction of the instrumental errors, their uncertainties were incorporated into a statistical procedure that estimates the maximum likelihood of synthetic spectra and the observed data. Variation of the water vapor mixing ratio gives its best fit and error bars.

Water Vapor Profile: Application of the described procedure to the full domain of data has revealed a new characteristic feature of the profile (Fig. 1): The mixing ratio is nearly constant below 20–25 km with a steep decrease above 30 km. At the upper

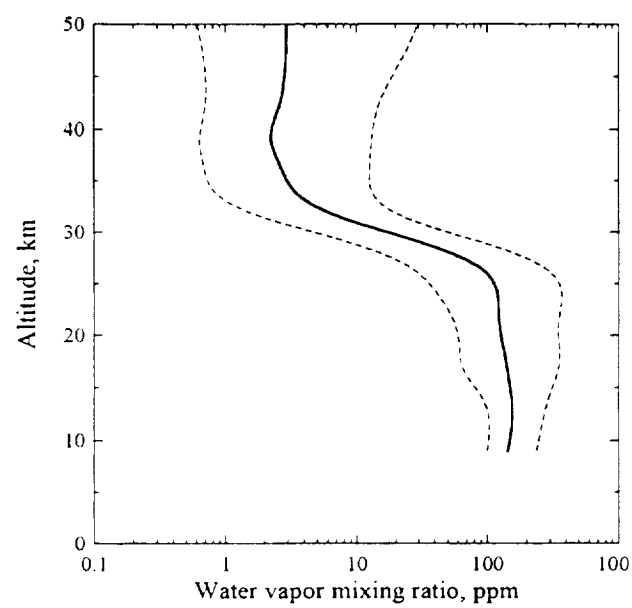

Fig. 1. Vertical distribution of H_2O averaged over the full domain of Phobos data. Solid curve shows maximum likelihood values, dashed curves are lower and upper limits.

part of the profile some increase is observed, albeit far below the uncertainty of the retrieval. The quality of data corresponding to individual occultations prevents reliable analysis of latitudinal and temporal variations. Extrapolation of the retrieved profile down to the surface, assuming that the mixing ratio is constant below 10 km, results in a total column abundance of $8.3^{+2.5}_{-1.5}$ pr.μm.

The decrease of water vapor vertical profile at 25–35 km provides an evidence of saturated atmosphere above 25 km. A condensation level and formation of clouds should therefore be expected at this altitude. Below this level a uniformly mixed profile is mantained by eddy diffusion and downward transport of water in the condensed phase. This mixing cycle is faster than any other process that may affect water profile, such as regular convection, horizontal heat transfer by winds, etc. Condensation absorbs the upward diffusion flux and explains the steep gradient of mixing ratio above the cloud layer. Based on a water vapor scale height of 2.5 km at 30 km, the condensation rate is $\approx 8 \times 10^{-12}$ g cm^{-2} s^{-1}.

Aerosol: The condensation processes can be separately constrained based on the continuum data. The nine most successful occultations resulted in vertical profiles of the extinction at 1.9 and 3.7 μm. In the previous work [2], measurements were interpreted in terms of a pure dust model, including a weak downward flux. This flux is required to explain the bend of the extinction profiles near 22 km and an extinction scale height below this bend larger than an atmospheric one, usually 15–20 km. Since the vertical profile of H_2O suggests condensation close to the altitude of the bend, we suppose that the mass loading of aerosol is provided by the release of water ice onto dust particles as condensation nuclei. In turn, the excess of extinction responsible for the bend of the profile may be caused by the presence of icy clouds. The dust downward flux required by a pure dust model is typically 3×10^{-12} g cm^{-2} s^{-1}, which is close to the value derived above for the water vapor condensation rate.

Cloud properties can be constrained by applying the dust model [2] without any flux: An excess of measured extinction above the modeled dust extinction profile is typically $(0.3–1) \times 10^{-3}$ km^{-1} within a layer 18–25 km. The number density of aerosol particles derived from the upper part of the extinction profile, which is not affected by ice fraction or dust flux, is 0.2 cm^{-3}. Since these particles are assumed to be condesation nuclei, they constrain the number density of dust + ice particles. We can then estimate the effective radius of cloud particles, ≈2 μm, and an approximate column content of water in a cloud, 10^{-6}–10^{-5} g cm^{-2}. Compared to the condensation rate we found that the time required for the cloud formation is of an order of one week; this time, in accordance with modeling results [4], shows the stability of the cloud layer. A comparable duration is required for a particle to drift down along the atmospheric scale height and to establish observed vertical distribution. Vertical distribution of water in gaseous and condensed phases are also in a good agreement with the results of this simulation.

Only long-living icy fraction is observed in solar infrared occultations, corresponding to the evening terminator. The diurnal temperature variations result in morning haze with smaller particles radii [5]. Evidence for the condensation sink of water vapor in the midaltitude atmosphere relates to the vertical transport of water controlled by the local temperature profile, which might be an important aspect of the global water cycle on Mars [6]. Monitoring of water vapor and aerosol vertical distribution with a wide latitudinal and seasonal coverage is apparently necessary for insight into the role of fine heterogeneous processes. One of the opportunities for this insight is the SPICAM solar occultation experiment [7], to be flown on the upcoming Mars-96 mission.

Acknowledgments: The work has been supported by ISF grants N7T000 and N7T003.

References: [1] Krasnopolsky V. A. et al. (1991) *Icarus, 94,* 32–44. [2] Korablev O. I. et al. (1993) *Icarus,* 102, 76–87. [3] Korablev O. I. et al. (1993) *Planet. Space Sci., 41,* 441–451. [4] Michelageli D. V. et al. (1993) *Icarus, 100,* 261–285. [5] Petrova et al. (1994) Paper presented at EGS meeting, Wiesbaden, Germany. [6] Clancy et al. (1995) Paper presented at IUGG meeting, Boulder, Colorado. [7] Korablev O. I. et al., this volume.

OXYGEN ISOTOPES IN MARTIAN SNC METEORITES.

C. S. Romanek[1], E. K. Gibson Jr.[2], R. A. Socki[3], and E. C. Perry[4], [1]Savannah River Ecology Laboratory, University of Georgia, Aiken SC 29802, USA, [2]Mail Code SN4, Planetary Sciences Branch, NASA Johnson Space Center, Houston TX 77058, USA, [3]Lockheed Engineering and Sciences Company, Houston TX 77058, USA, and [4]Department of Geology, Northern Illinois University, DeKalb IL 60115, USA.

Clues to a better understanding of volatile evolution on Mars may be found in the low-temperature mineral assemblages of the martian meteorites. Foremost among these is the SNC meteorite ALH 84001, which contains an unusual abundance of C- and S-bearing minerals and a suite of physically and chemically distinct silica-rich glasses. While the chemistry and isotopic composition of carbonates have been studied in detail [1,2], little attention has been paid to other secondary minerals. The measurement of $^{17}O/^{16}O$ and $^{18}O/^{16}O$ in glass separates may place tighter constraints on the isotopic and thermal evolution of fluids that have circulated through the martian crust.

The C and O isotopic composition of volatiles on Mars (mainly water and CO_2) is based primarily on Viking lander measurements, spectroscopic studies, and the stable isotopic analysis of trapped gases and solids in the martian meteorites. Relaying on C isotopic measurements, Romanek et al. [1] suggested that martian atmospheric CO_2 may be the source of C for carbonates in ALH 84001, while heterogeneous multistage fluids may be responsible for the observed range in $\delta^{18}O$ (~10–20‰ SMOW). Formation temperatures cannot be highly constrained from these measurements because of the large uncertainties in the isotopic composition of martian atmospheric CO_2 and water vapor.

The stable isotopic composition of carbonate in ALH 84001 falls within the range of that for other martian meteorites (Fig. 1). If it is assumed that all minerals in ALH 84001 precipitated from a single homogeneous reservoir, the difference in $\delta^{18}O$ between primary orthopyroxene and secondary carbonate (5–15‰) is compatible with the carbonate being a low-temperature precipitate. This interpretation becomes much more complicated if Mars is shown to contain more than one isotopically distinct reservoir of O as Karlsson et al. [3] suggest.

In addition to carbonate, ALH 84001 contains at least two physically and chemically distinct glasses. One glass is translucent and has a chemistry typical of maskelynite (An_{33}) while the other is transparent and silica-rich (~78% SiO_2). While the paragenetic

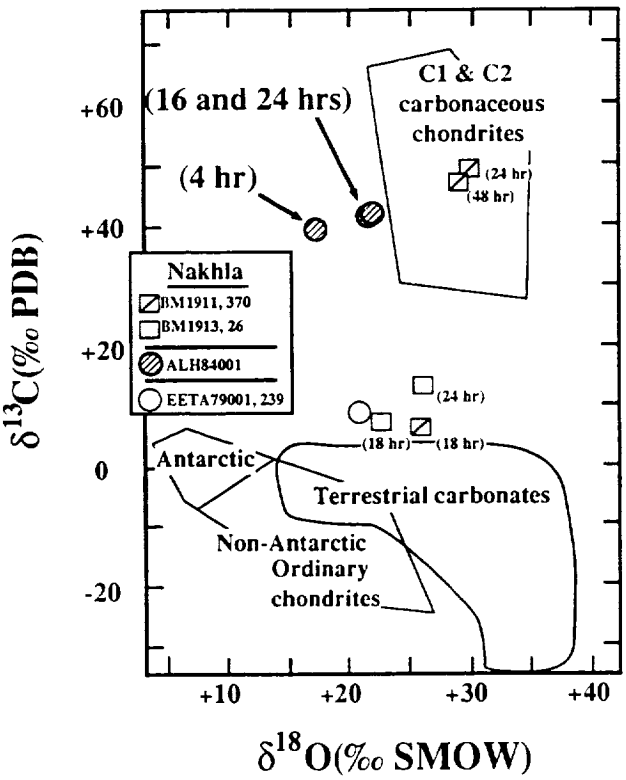

Fig. 1. Carbon and O isotopic compositions of martian and other meteorite carbonates. For the samples shown, the number of hours at each data point represents the amount of time the meteorites underwent acid digestion to release CO_2 from the different carbonate phases.

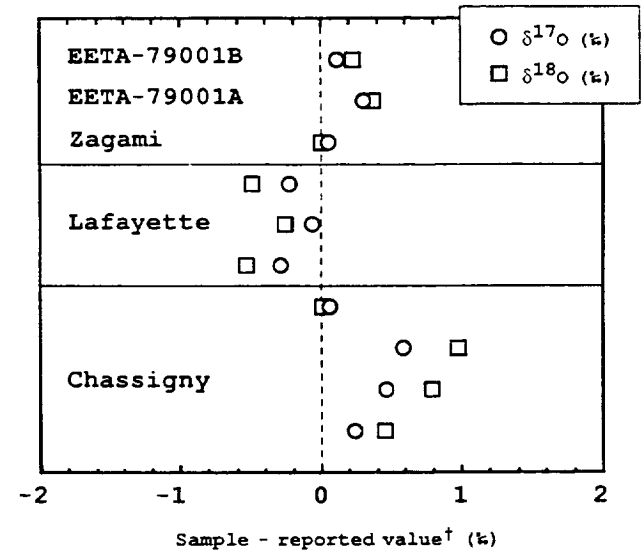

Fig. 2. Deviations from normalized literature values for O isotopic compositions of martian meteorites measured at JSC, using the newly developed laser fluorination technique.

sequence of glass formation cannot be distinguished at this time, dissolution features found within the orthopyroxene groundmass (e.g., hillocks) suggest that corrosive fluids may have remobilized a reactive silicate fraction prior to the precipitation of carbonate. If so, the potential exists for significant isotopic variability to occur in glasses from ALH 84001.

Glasses, analogous to those in ALH 84001, have been found in other SNC meteorites. Clayton and Mayeda [4] identified two chemically and isotopically distinct generations of glass in Shergotty; one with a typical maskelynite chemistry and an average $\delta^{18}O$ of 4.6 ± 0.2‰ (n = 4) and the other, a silica-rich glass, with a $\delta^{18}O$ of 5.8‰. Interestingly, one anomalous maskelynite fraction had a $\delta^{18}O$ of 9.0‰, while whole-rock samples averaged 4.6 ± 0.2‰ (n = 3). Given the isotopic variability in Shergotty glasses, the $\delta^{18}O$ of glasses in ALH 84001 may provide insights into the isotopic composition and thermal history of aqueous alteration that preceded or accompanied the precipitation of carbonate.

A state-of-the-art laser fluorination extraction line has recently been constructed that permits the direct $\delta^{17}O$ and $\delta^{18}O$ measurement of O_2 in silicates [5]. With this technique, ultrasmall (<1-mg) O-bearing samples are reacted with BrF_5 in an isolated sample chamber using CO_2 laser irradiation as a heat source. This reaction generates diatomic O, which is then purified and frozen into a microvolume cold finger held at 25°K. The temperature of the trap is raised to 85°K, and O_2 is vaporized and expanded directly into the source of an isotope ratio mass spectrometer for analysis. At this temperature, almost all other gases, including potential isobaric interferences (e.g., NF_3), are kept frozen. The precision and accuracy of this novel technique was quantified by analyzing international standards and martian meteorites of known isotopic composition. Accuracy for $\delta^{18}O$ is ±0.2‰ (1σ) for quartz and garnet standards (NBS-28 and UWG-2 respectively) while the difference between bulk samples and reported values for martian meteorites [3] was less than 1‰ (Fig. 2).

Maskelynite and silica-rich glass separates will be hand-picked from splits of ALH 84001 and analyzed using the laser fluorination technique. The results will be reported and compared with previously published $\delta^{18}O$ values for other mineral separates from ALH 84001 to better constrain the nature of fluid/rock interactions on Mars.

References: [1] Romanek C. S. et al. (1995) *Nature, 372,* 655–657. [2] Jull A. J. T. et al. (1995) *Meteoritics, 30,* 311–318. [3] Karlsson H. R. et al. (1992) *Science, 255,* 1409–1411. [4] Clayton R. N. and Mayeda T. K. (1986) *GCA, 50,* 979–982. [5] Romanek C. S. et al. (1995) *Geol. Soc. Am. Prog. with Abstr., 27,* A-421.

IRON FORMATIONS ON MARS? M. W. Schaefer, Department of Geology and Geophysics, Yale University, P.O. Box 208109, New Haven CT 06520-8109, USA.

In the surface of Mars we see a relict of the early evolution of the planet. During the early history of the solar system, conditions were probably not dissimilar on the surface of Earth and Mars, but as time passed, the two planets diverged. Earth, larger and with a greater source of internal heating, stayed active and its surface kept evolving. Mars, on the other hand, smaller and with less internal heating, froze and its surface almost completely stopped evolving. There-

fore, when we look at the surface of Mars, we have the opportunity not only to observe the early history of Mars itself, but also to observe a landscape perhaps more similar to that of early Earth than is the present terrestrial landscape. By studying processes that occurred on the early Earth, we may gain insight into what processes were important on early Mars. Conversely, as we obtain more detailed information about the present surface of Mars, we will learn more about the early history of both planets.

Some of the oldest surviving sedimentary features on Earth are the banded iron formations (BIFs), chemically precipitated sedimentary deposits containing layers of silica-rich and Fe-rich bands. Although BIFs are agreed to be chemical precipitates of Fe, the mechanism by which the precipitation occurs is a controversial topic. Both organic [1–5] and inorganic [6–11] mechanisms have been proposed.

The major idea behind both these classes of theories is that the atmosphere of the early Earth was depleted in O_2, compared to the present atmospheric level (PAL). Under conditions of low O fugacity, especially in an acidic environment, Fe exists in the ferrous form, and is highly soluble in water. Thus any Fe input into a lacustrine or oceanic system by weathering or other process will stay in solution in the water until it reaches saturation, or is oxidized to form ferric Fe, which is relatively insoluble in water. Then, for any of a variey of reasons, depending on the model, the Fe is oxidized, and precipitates out, forming the extensive deposits that still exist today.

For Fe to be deposited from waters rich in ferrous Fe, it must be oxidized by some process. There are three inorganic processes that are capable of oxidizing Fe to form BIFs. (1) Dissolved oxygen—Although this is also descriptive of what happens when photosynthesis produces O, there are inorganic reactions that may produce free O. (2) Ultraviolet irradiation—Ultraviolet (UV) radiation is capable of directly oxidizing ferrous Fe in solution. (3) Hydrogen peroxide—Hydrogen peroxide (H_2O_2) is a strong oxidant and is also able to directly oxidize ferrous Fe in solution. In all these cases, gasous H is produced, which will then be lost from the upper atmosphere, contributing to the oxidation of the planet.

Even under anoxic conditions, if the pH is low and the fCO_2 content high, siderite (Fe carbonate) can be precipitated. Both these conditions should have been met in an early martian ocean [12].

Burns [13] suggested that Fe formations may have been deposited on Mars. If conditions on early Mars were such that large bodies of water were present, then any of the mechanisms mentioned above could have produced Fe formations there, similar to those found on Earth. The goethite or siderite deposited originally in lacustrine or oceanic basins would have altered to hematite in the present martian environment, and could have provided one source for the widespread hematite thought to exist on the surface today. The formation of these deposits on Mars would have had a significant effect on the evolution of its atmosphere and hydrosphere.

References: [1] Cloud P. (1973) *Econ. Geol., 68,* 1135–1143. [2] Garrels R. M. Jr. et al. (1973) *Econ. Geol., 68,* 1173–1179. [3] LaBerge G. L. (1973) *Econ. Geol., 68,* 1098–1109. [4] LaBerge G. L. et al. (1987) in *Precambrian Iron Formations,* 69–96. [5] Robbins E. I. et al. (1987) in *Precambrian Iron Formations,* 97–139. [6] Braterman P. S. and Cairns-Smith A. G. (1987) in *Precambrian Iron Formations,* 215–245. [7] Cairns-Smith A. G. (1978) *Nature, 276,* 807–808. [8] Eugster H. P. and Chou I.-M. (1973) *Econ. Geol., 68,* 1144–1168. [9] Francois L. M. (1986) *Nature, 320,* 352–354. [10] Holland H. D.(1973) *Econ. Geol., 68,* 1169–1172. [11] Towe K. M. (1983) in *Developments and Interactions of the Precambrian Atmosphere, Lithosphere, and Biosphere,* 53–62. [12] Schaefer M. W. (1993) *GCA, 57,* 4619–4625. [13] Burns R. G. (1993) *GCA, 57,* 4555–4574.

SPECTROSCOPIC MEASUREMENTS OF MARTIAN ATMOSPHERIC WATER VAPOR. A. L. Sprague, D. M. Hunten, and R. E. Hill, Lunar and Planetary Laboratory, Kuiper Space Sciences Building, The University of Arizona, 1629 E. University Boulevard, Tucson AZ 85721-0092, USA.

We report measurements of martian atmospheric water vapor for the period 1991–1995. Our measurements indicate abundances (pr μm) that are quite similar, overall, to those of the Viking MAWD experiment and to other groundbased measurement programs [1–4]. Latitudinal profiles are routinely obtained and we can monitor the seasonal shifts and variations between hemispheres. Diurnal variations in abundance are also noted, with lowest abundance near the morning terminator. A listing of observations and measured abundances for a subset of the data obtained between January 1991 and June 1995 is given in Table 1.

Measurements that showed equivalent widths of less than 1 mÅ were not converted to pr μm and are not listed on Table 1 but will be included in a forthcoming publication. Strong latitudinal variations were observed for all L_s (seasons), with late spring and summers wet in both hemispheres but northern latitudes up to 5× wetter than southern. Equatorial regions (+30° to −30°) show a rather stable abundance of atmospheric water varying between 2 and 20 pr μm, while much larger variations are observed at high latitudes. Our high northern measurements show as much as 80 pr μm in northern summer. Southern atmospheric water drops below 10 pr μm rapidly in early autumn and is below our measurement threshold by late autumn.

We have not observed another wet southern summer (L_s 290–340) like that measured in 1969 [1]. It is interesting that our measured abundances during the clear atmosphere period observed during the 1994–1995 apparition are about the same as those measured by MAWD in the dusty atmosphere conditions. This is notable because it is generally thought that the dusty atmosphere is warmer than when clear, yet no apparent difference in water vapor is observed among the datasets.

Our measurements are made with a high-resolution (R ~ 180,000) échelle spectrograph with a cooled CCD data acquisition system at the 1.5-m Catalina Observatory on Mt. Bigelow, Arizona. Because our equipment has a high quantum effciency, and the chip is quite sensitive in the spectral region used (8177–8199 Å), we can obtain high signal-to-noise spectral images with integration times of 10–15 min.

References: [1] Barker E. et al. (1970) *Science, 170,* 1308–1310. [2] Jakosky B. and Farmer B. (1982) *JGR, 87,* 2999–3019. [3] Rizk et al. (1988) *Icarus, 90,* 205–213. [4] Clancy T. et al. (1992), *Icarus, 100,* 48–59.

TABLE 1. Martian water vapor measurements.

Frame #	Date	UT h m	L(s)	Dia. (")	Slit Orient.	Sect. Lat.	Sect. Long.	Equiv. Width mA	Abun. pr µm
1991									
25jan123.fit	01-23	06 21	010	10.6	N/S_CM	-61.4	097.7	0.4363	0.7874
25jan123.fit	01-23	06 21	010	10.6	N/S_CM	-36.8	097.7	0.8227	3.326
25jan123.fit	01-23	06 21	010	10.6	N/S_CM	-13.9	097.7	1.620	8.502
25jan123.fit	01-23	06 21	010	10.6	N/S_CM	+09.2	097.7	2.166	10.96
25jan123.fit	01-23	06 21	010	10.6	N/S_CM	+38.6	097.7	1.790	6.586
1992									
mars001.fit	07-22	10 39	292	6.02	N/S_CM	+48.2	240.9	0.4370	0.5798
mars001.fit	07-22	10 39	292	6.02	N/S_CM	+25.6	240.9	0.2649	1.001
mars001.fit	07-22	10 39	292	6.02	N/S_CM	+04.7	240.9	0.8158	4.211
mars001.fit	07-22	10 39	292	6.02	N/S_CM	-10.8	240.9	1.737	9.930
mars001.fit	07-22	10 39	292	6.02	N/S_CM	-27.6	240.9	1.957	11.20
mars001.fit	07-22	10 39	292	6.02	N/S_CM	-44.9	240.9	7.923	48.86
mars001.fit	07-22	10 39	292	6.02	N/S_CM	-68.8	240.9	5.301	20.43
1993									
09mar30.fit	03-09	04 10	050	9.48	N/S_CM	-55.1	171.5	4.991	0.8362
09mar30.fit	03-09	04 10	050	9.48	N/S_CM	-36.0	171.5	0.6604	2.844
09mar30.fit	03-09	04 10	050	9.48	N/S_CM	-20.9	171.5	0.8852	6.354
09mar30.fit	03-09	04 10	050	9.48	N/S_CM	-07.4	171.5	1.480	10.37
09mar30.fit	03-09	04 10	050	9.48	N/S_CM	+05.3	171.5	2.077	11.22
09mar30.fit	03-09	04 10	050	9.48	N/S_CM	+18.1	171.5	2.106	14.29
09mar30.fit	03-09	04 10	050	9.48	N/S_CM	+31.5	171.5	2.618	19.33
09mar30.fit	03-09	04 10	050	9.48	N/S_CM	+46.7	171.5	3.608	16.15
09mar30.fit	03-09	04 10	050	9.48	N/S_CM	+65.9	171.5	3.524	15.91
09mar33.fit	03-09	05 20	050	9.48	N/S_CM	-53.0	181.0	5.208	1.105
09mar33.fit	03-09	05 20	050	9.48	N/S_CM	-35.9	181.0	0.6280	0.6348
09mar33.fit	03-09	05 20	050	9.48	N/S_CM	-20.8	181.0	0.1883	4.254
09mar33.fit	03-09	05 20	050	9.48	N/S_CM	-07.4	181.0	0.9604	6.165
09mar33.fit	03-09	05 20	050	9.48	N/S_CM	+05.4	181.0	1.215	11.68
09mar33.fit	03-09	05 20	050	9.48	N/S_CM	+18.1	181.0	2.119	17.36
09mar33.fit	03-09	05 20	050	9.48	N/S_CM	+31.5	181.0	3.050	17.94
09mar33.fit	03-09	05 20	050	9.48	N/S_CM	+46.6	181.0	3.290	21.20
09mar33.fit	03-09	05 20	050	9.48	N/S_CM	+65.4	181.0	4.410	17.30
10mar23.fit	03-10	03 05	050	9.32	N/S_CM	-55.0	146.9	0.2922	0.3174
10mar23.fit	03-10	03 05	050	9.32	N/S_CM	-32.8	146.9	0.9754	3.345
10mar23.fit	03-10	03 05	050	9.32	N/S_CM	-16.3	146.9	1.320	5.927
10mar23.fit	03-10	03 05	050	9.32	N/S_CM	-01.6	146.9	1.708	8.734
10mar23.fit	03-10	03 05	050	9.32	N/S_CM	+12.7	146.9	2.287	12.38
10mar23.fit	03-10	03 05	050	9.32	N/S_CM	+27.5	146.9	3.452	18.77
10mar23.fit	03-10	03 05	050	9.32	N/S_CM	+43.9	146.9	3.620	17.53
10mar23.fit	03-10	03 05	050	9.32	N/S_CM	+65.9	146.9	3.451	10.60
10mar24.fit	03-10	03 25	050	9.32	N/S_CM	-55.1	150.6	0.0768	0.0854
10mar24.fit	03-10	03 25	050	9.32	N/S_CM	-32.8	150.6	1.176	4.028
10mar24.fit	03-10	03 25	050	9.32	N/S_CM	-16.3	150.6	1.571	7.074
10mar24.fit	03-10	03 25	050	9.32	N/S_CM	-01.6	150.6	3.163	16.77
10mar24.fit	03-10	03 25	050	9.32	N/S_CM	+12.7	150.6	3.122	17.24
10mar24.fit	03-10	03 25	050	9.32	N/S_CM	+27.5	150.6	3.487	18.94
10mar24.fit	03-10	03 25	050	9.32	N/S_CM	+43.9	150.6	3.032	14.42
10mar24.fit	03-10	03 25	050	9.32	N/S_CM	+66.0	150.6	2.580	7.867
11mar22.fit	03-11	05 49	050	9.22	N/S_CM	-43.2	176.6	1.617	3.436
11mar22.fit	03-11	05 49	050	9.22	N/S_CM	-17.0	176.6	2.023	9.058
11mar22.fit	03-11	05 49	050	9.22	N/S_CM	+05.7	176.6	2.300	12.23
11mar22.fit	03-11	05 49	050	9.22	N/S_CM	+28.4	176.6	3.398	18.27
11mar22.fit	03-11	05 49	050	9.22	N/S_CM	+55.8	176.6	4.061	15.93
08apr31.fit	04-08	02 30	063	7.30	N/S+1"	+58.8	224.2	2.912	11.24

TABLE 1. (continued)

08apr31.fit	04-08	02 30	063	7.30	N/S+1"	+30.1	224.2	3.418	18.70
08apr31.fit	04-08	02 30	063	7.30	N/S+1"	+08.9	224.2	2.855	15.06
08apr31.fit	04-08	02 30	063	7.30	N/S+1"	-13.6	224.2	1.771	7.617
08apr31.fit	04-08	02 30	063	7.30	N/S+1"	-42.8	224.2	0.7407	1.007
08apr35.fit	04-08	03 08	063	7.30	N/S_CM	+58.8	233.7	2.822	11.12
08apr35.fit	04-08	03 08	063	7.30	N/S_CM	+30.1	233.7	1.929	10.11
08apr35.fit	04-08	03 08	063	7.30	N/S_CM	+08.9	233.7	1.573	8.032
08apr35.fit	04-08	03 08	063	7.30	N/S_CM	-13.6	233.7	1.668	7.172
08apr35.fit	04-08	03 08	063	7.30	N/S_CM	-42.8	233.7	0.8568	1.190
04may02.fit	05-04	03 47	074	6.16	N/S_CM	-26.3	354.3	1.226	3.527
04may02.fit	05-04	03 47	074	6.16	N/S_CM	+01.5	354.3	2.430	11.86
04may02.fit	05-04	03 47	074	6.16	N/S_CM	+28.5	354.3	3.755	20.92
04may02.fit	05-04	03 47	074	6.16	N/S_CM	+58.5	354.3	5.931	27.50
04may09.fit	05-04	04 16	074	6.16	N/S_CM	-27.6	001.6	0.5149	1.324
04may09.fit	05-04	04 16	074	6.16	N/S_CM	+01.3	001.6	2.781	13.68
04may09.fit	05-04	04 16	074	6.16	N/S_CM	+28.5	001.6	3.681	20.47
04may09.fit	05-04	04 16	074	6.16	N/S_CM	+58.6	001.6	4.776	21.34
05may40.fit	05-05	02 58	074	6.10	N/S_CM	-28.2	332.2	0.6606	1.642
05may40.fit	05-05	02 58	074	6.10	N/S_CM	+01.4	332.2	1.288	6.085
05may40.fit	05-05	02 58	074	6.10	N/S_CM	+28.6	332.2	2.336	12.52
05may40.fit	05-05	02 58	074	6.10	N/S_CM	+58.5	332.2	4.931	22.20
05may41.fit	05-05	03 14	075	6.10	N/S-1.5"	-27.9	337.3	1.007	2.435
05may41.fit	05-05	03 14	075	6.10	N/S-1.5"	+01.4	337.3	2.671	13.09
05may41.fit	05-05	03 14	075	6.10	N/S-1.5"	+28.2	337.3	4.631	26.47
05may41.fit	05-05	03 14	075	6.10	N/S-1.5"	+58.3	337.3	5.466	25.13
06may62.fit	05-06	02 39	075	6.02	N/S_CM	-28.4	318.9	0.5155	1.221
06may62.fit	05-06	02 39	075	6.02	N/S_CM	+01.6	318.9	1.525	7.263
06may62.fit	05-06	02 39	075	6.02	N/S_CM	+28.8	318.9	2.725	14.76
06may62.fit	05-06	02 39	075	6.02	N/S_CM	+59.6	318.9	5.492	24.77
06may63.fit	05-06	03 14	075	6.02	N/S_CM	-28.6	327.5	0.9245	2.161
06may63.fit	05-06	03 14	075	6.02	N/S_CM	+01.6	327.5	1.665	7.959
06may63.fit	05-06	03 14	075	6.02	N/S_CM	+28.8	327.5	2.799	15.20
06may63.fit	05-06	03 14	075	6.02	N/S_CM	+59.8	327.5	5.850	22.53
02jun18.fit	06-02	03 42	087	5.30	N/S_CM	-28.7	073.9	0.2544	0.6409
02jun18.fit	06-02	03 42	087	5.30	N/S_CM	-02.2	073.9	0.6701	3.076
02jun18.fit	06-02	03 42	087	5.30	N/S_CM	+20.6	073.9	1.212	6.409
02jun18.fit	06-02	03 42	087	5.30	N/S_CM	+43.1	073.9	2.526	12.94
02jun18.fit	06-02	03 42	087	5.30	N/S_CM	+69.4	073.9	5.038	20.78
02jun19.fit	06-02	03 57	087	5.30	N/S+1.3"	-28.8	076.8	0.7097	1.782
02jun19.fit	06-02	03 57	087	5.30	N/S+1.3"	-02.2	076.8	0.6932	3.186
02jun19.fit	06-02	03 57	087	5.30	N/S+1.3"	+20.5	076.8	1.4020	7.446
02jun19.fit	06-02	03 57	087	5.30	N/S+1.3"	+43.0	076.8	2.1690	11.02
02jun19.fit	06-02	03 57	087	5.30	N/S+1.3"	+69.5	076.8	5.5020	22.96
03jun85.fit	06-03	03 13	087	5.26	N/S_CM	-31.0	058.4	0.5758	1.306
03jun85.fit	06-03	03 13	087	5.26	N/S_CM	-02.3	058.4	0.5982	2.740
03jun85.fit	06-03	03 13	087	5.26	N/S_CM	+20.5	058.4	1.588	8.484
03jun85.fit	06-03	03 13	087	5.26	N/S_CM	+43.2	058.4	2.433	12.43
03jun85.fit	06-03	03 13	087	5.26	N/S_CM	+70.8	058.4	4.250	16.67
03jun86.fit	06-03	03 25	087	5.26	N/S-1"	-30.9	060.3	0.6110	1.398
03jun86.fit	06-03	03 25	087	5.26	N/S-1"	-02.3	060.3	0.6048	2.771
03jun86.fit	06-03	03 25	087	5.26	N/S-1"	+20.6	060.3	1.177	6.226
03jun86.fit	06-03	03 25	087	5.26	N/S-1"	+43.6	060.3	2.635	13.51
03jun86.fit	06-03	03 25	087	5.26	N/S-1"	+71.3	060.3	3.159	11.91
03jun87.fit	06-03	03 37	087	5.26	N/S-1"	-31.1	065.9	1.159	2.637
03jun87.fit	06-03	03 37	087	5.26	N/S-1"	-02.3	065.9	1.481	6.934
03jun87.fit	06-03	03 37	087	5.26	N/S-1"	+20.5	065.9	2.093	11.33
03jun87.fit	06-03	03 37	087	5.26	N/S-1"	+43.2	065.9	2.586	13.28
03jun87.fit	06-03	03 37	087	5.26	N/S-1"	+70.9	065.9	3.175	12.06
1994									
19sep36.fit	9-19	11 30	349	5.64	N/S_CM	+62.2	217.6	0.4667	0.8178

TABLE 1. (continued)

19sep36.fit	9-19	11 30	349	5.64	N/S_CM	+34.6	217.6	0.0754	0.3356
19sep36.fit	9-19	11 30	349	5.64	N/S_CM	+11.7	217.6	0.2912	1.556
19sep36.fit	9-19	11 30	349	5.64	N/S_CM	-11.1	217.6	0.2912	2.893
19sep36.fit	9-19	11 30	349	5.64	N/S_CM	-38.9	217.6	0.5490	0.2319
21nov26.fit	11-21	10 57	020	7.96	E/W+30	+10.9	384.7	1.844	6.885
21nov26.fit	11-21	10 57	020	7.96	E/W+30	+17.3	361.1	1.906	10.27
21nov26.fit	11-21	10 57	020	7.96	E/W+30	+20.2	342.5	1.584	8.881
21nov26.fit	11-21	10 57	020	7.96	E/W+30	+21.1	325.1	1.665	8.765
21nov26.fit	11-21	10 57	020	7.96	E/W+30	+20.2	307.6	1.834	8.008
21nov26.fit	11-21	10 57	020	7.96	E/W+30	+17.3	289.0	1.925	5.084
21nov26.fit	11-21	10 57	020	7.96	E/W+30	+10.8	265.1	1.949	1.141
21nov30.fit	11-21	11 46	020	7.96	N/S_CM	-36	337.0	0.7109	2.130
21nov30.fit	11-21	11 46	020	7.96	N/S_CM	-13	337.0	0.9160	4.163
21nov30.fit	11-21	11 46	020	7.96	N/S_CM	+05	337.0	0.9352	4.779
21nov30.fit	11-21	11 46	020	7.96	N/S_CM	+21	337.0	1.595	8.398
21nov30.fit	11-21	11 46	020	7.96	N/S_CM	+38	337.0	1.077	5.267
21nov30.fit	11-21	11 46	020	7.96	N/S_CM	+55	337.0	0.3570	1.404
21nov30.fit	11-21	11 46	020	7.96	N/S_CM	+77	337.0	0.4318	0.9583
28dec21.fit	12-28	10 20	038	10.72	N/S_CM	-39.3	329.8	0.0232	0.0610
28dec21.fit	12-28	10 20	038	10.72	N/S_CM	-19.5	329.8	0.3936	1.703
28dec21.fit	12-28	10 20	038	10.72	N/S_CM	-04.3	329.8	0.4598	2.356
28dec21.fit	12-28	10 20	038	10.72	N/S_CM	+09.3	329.8	0.8618	4.797
28dec21.fit	12-28	10 20	038	10.72	N/S_CM	+21.9	329.8	1.048	5.951
28dec21.fit	12-28	10 20	038	10.72	N/S_CM	+34.6	329.8	1.721	9.479
28dec21.fit	12-28	10 20	038	10.72	N/S_CM	+48.1	329.8	1.409	6.909
28dec21.fit	12-28	10 20	038	10.72	N/S_CM	+63.3	329.8	1.742	6.873
28dec21.fit	12-28	10 20	038	10.72	N/S_CM	+80.6	329.8	1.108	2.789
28dec24.fit	12-28	11 14	038	10.72	E/W	+10.3	280.0	1.539	1.044
28dec24.fit	12-28	11 14	038	10.72	E/W	+16.3	299.7	1.324	3.632
28dec24.fit	12-28	11 14	038	10.72	E/W	+19.5	315.0	1.137	4.803
28dec24.fit	12-28	11 14	038	10.72	E/W	+21.3	329.2	1.117	5.750
28dec24.fit	12-28	11 14	038	10.72	E/W	+21.9	342.9	1.220	6.964
28dec24.fit	12-28	11 14	038	10.72	E/W	+21.3	356.6	1.391	8.289
28dec24.fit	12-28	11 14	038	10.72	E/W	+19.5	370.9	1.447	8.435
28dec24.fit	12-28	11 14	038	10.72	E/W	+16.2	386.4	1.479	7.745
28dec24.fit	12-28	11 14	038	10.72	E/W	+10.4	405.5	1.855	6.750
1995									
20mar18.fit	03-20	02 01	074	11.52	N/S_CM	-36.6	200.3	0.0946	0.2380
20mar18.fit	03-20	02 01	074	11.52	N/S_CM	-17.7	200.3	0.0154	0.0671
20mar18.fit	03-20	02 01	074	11.52	N/S_CM	+00.7	200.3	0.1470	0.7629
20mar18.fit	03-20	02 01	074	11.52	N/S_CM	+17.0	200.3	0.4720	2.637
20mar18.fit	03-20	02 01	074	11.52	N/S_CM	+33.5	200.3	0.6638	3.662
20mar18.fit	03-20	02 01	074	11.52	N/S_CM	+50.9	200.3	2.625	13.53
20mar18.fit	03-20	02 01	074	11.52	N/S_CM	+72.3	200.3	3.259	11.87
18apr06.fit	04-18	04 32	086	9.54	N/S_CM	-34.1	263.8	1.825	3.876
18apr06.fit	04-18	04 32	086	9.54	N/S_CM	-10.4	263.8	1.277	5.475
18apr06.fit	04-18	04 32	086	9.54	N/S_CM	+09.6	263.8	2.274	12.16
18apr06.fit	04-18	04 32	086	9.54	N/S_CM	+28.4	263.8	2.831	15.97
18apr06.fit	04-18	04 32	086	9.54	N/S_CM	+48.1	263.8	5.050	28.22
18apr06.fit	04-18	04 32	086	9.54	N/S_CM	+72.4	263.8	5.050	20.01
19may18.fit	05-19	03 22	100	7.16	N/S_CM	-26.5	383.6	1.561	4.004
19may18.fit	05-19	03 22	10[illegible]	7.16	N/S_CM	+00.4	383.6	1.879	8.539
19may18.fit	05-19	03 22	10[illegible]	7.16	N/S_CM	+22.6	383.6	3.108	16.82
19may18.fit	05-19	03 22	10[illegible]	7.16	N/S_CM	+44.9	383.6	5.095	28.47
19may18.fit	05-19	03 22	10[illegible]	7.16	N/S_CM	+71.2	383.6	8.309	36.40
22jun12.fit +22jun13 .fit									
22jun12/13.fit	06-22	04 22	115	5.90	N/S_CM	-19.0	071.5	1.364	4.407
22jun12/13.fit	06-22	04 22	115	5.90	N/S_CM	+12.1	071.5	0.4099	2.002
22jun12/13.fit	06-22	04 22	115	5.90	N/S_CM	+39.5	071.5	1.126	5.798
22jun12/13.fit	06-22	04 22	115	5.90	N/S_CM	+69.2	071.5	5.900	25.12

DIURNAL VARIABILITY OF THE ATMOSPHERIC WATER CONTENT ON MARS: OBSERVATIONS AND DESORPTION MODEL. D. V. Titov, Space Research Institute (IKI), Profsoyuznaya 84/32, Moscow 117810, Russia.

Introduction: The laboratory modeling showed that such analogs of the martian soil as montmorillonite clays and basalt powders are able to keep significant amounts of water in the adsorbed phase [1,2]. The water molecules can be involved in the regolith atmosphere exchange induced by the changes in surface insolation. Thus, the martian regolith can be an important buffer of atmospheric water. The evidences of the presence of exchange processes were found in the observations onboard Viking and Phobos-2 spacecraft.

Observations: The Mars Atmospheric Water Detector (MAWD) onboard Viking orbiters provided the observations of atmospheric water for about 1.5 martian years. Analysis of the spatial and seasonal variations of vapor amount led to the conclusion that martian regolith plays an important role in the seasonal atmospheric water cycle [3]. Together with the polar caps this reservoir provides the increase in the atmospheric water abundance in the spring-summer season. Another important conclusion was related to the diurnal behavior of the atmospheric water. Tharsis and Lunae Planum regions revealed the increase in water vapor column density by a factor of 2–4 during several hours from morning to noon [4]. This trend, atypical of the martian atmosphere, was observed in spring.

The Infrared Imaging Spectrometer (ISM) onboard Phobos-2 carried out the spectral mapping of several sites in the equatorial zone of Mars, including Tharsis region. Its measurements yielded the spatial distribution of the atmospheric water with resolution of about 20 km. The observed spatial variations reached a factor of 2 and even more at some specific sites. The atmosphere above the Tharsis volcanos and Olympus Mons was found to be anomalously enriched in water vapor: The mixing ratio was about a factor of 3 higher relative to the surrounding lowlands [5]. Pavonis Mons and its vicinity were observed twice, at ~10^h a.m. and at ~2^h p.m., which allowed us to follow the diurnal changes. The factor-of-2 increase in water vapor column density was observed above the volcanic flanks, while above the surrounding plateau it remained almost unchanged [6].

Desorption Model: We tried to account for the observed spatial variations in the frames of the model of water vapor exchange between regolith and atmosphere. This process is induced by the time-of-day changes in surface temperature and is controlled by the diffusion of molecules through the regolith skin layer a few tens of centimeters thick [5]. The ingress of water molecules into the atmosphere occurs with a timescale $\tau_{dif} = (\pi H^2\tau)/(4\gamma\varepsilon D)$, where D, ε, and τ are the diffusivity of pure CO_2, porosity, and tortuosity of the regolith. The buffering coefficient γ defines the adsorption properties of the soil. For clays its value is about 1.5 orders of magnitude greater than for basalt powders, which results in the faster release of water molecules from clay regolith as compared to basalt 1. Thus, a clay surface would respond to the subnoon surface-temperature rise much more intensively, providing higher abundance of water in the atmosphere above it. The observed spatial variations can be treated as a snapshot of the water distribution generated by desorption from regolith with different properties. Starting from a uniform background distribution of water at night the variations in regolith desorption properties would result in the corresponding vapor variations in daytime. Table 1 shows predicted by the model response to the subnoon temperature rise in two extreme cases of underlying regolith: montmorillonite clay and basalt powder. Assuming the background level of 10 pr.μm at night, this value will increase by noon by a factor of 3 or by several tens of percent depending on the regolith composition.

TABLE 1. Response of the regolith with different composition to the subnoon surface temperature rise.

	γ	τ_{dif}, S	L_{H_2O}, pr.μm
Clay	10^6	4.7×10^5	~20
Basalt powder	3×10^4	1.6×10^7	~4

Discussion: The "desorption model" yields the values of variations of the atmospheric water content on Mars consistent with the spacecraft observations. However, the actual adsorption properties of martian regolith are unknown. This increases the uncertainty of the results of the model. Recently, Zent [7] has argued that the ISM observations can be also explained by the "ice-rich regolith model," in which water accumulates in the regolith as ice rather than adsorbate. It seems likely that both mechanisms can be responsible for the observed phenomena. We believe that further progress in this subject could be achieved in the following studies: (1) The analysis of the MAWD data with an emphasis on the fine-scale variability in the data. (2) The search for possible correlations of the atmospheric water amount with the surface properties (albedo, thermal inertia, mineralogical spectral details) in the ISM data. (3) A detailed study of regolith-atmosphere exchange processes can be carried out onboard Mars '96 spacecraft by the Planetary Fourier Spectrometer (PFS) and Infrared Imaging Spectrometer (Omega).

References: [1] Anderson D. M. et al. (1978) *Icarus, 34*, 638–644. [2] Fanale F. P. et al. (1971) *Nature, 230*, 502–504. [3] Jakosky B. M. (1985) *Space Sci. Rev., 41*, 131–200. [4] Jakosky B. M. et al. (1988) *Icarus, 73*, 80–90. [5] Titov D. V. et al. (1994) *Planet. Space Sci., 42*, 1001–1010. [6] Titov D. V. et al (1995) *Adv. Space Res., 16*, 23–33. [7] Zent A. (1995) personal communication.

AN EARLY WARM, WET MARS? LITTLE SUPPORT FROM THE MARTIAN METEORITE ALH 84001. A. H. Treiman, Lunar and Planetary Institute, 3600 Bay Area Boulevard., Houston TX 77058, USA.

A critical question in understanding martian climate evolution is just how warm and wet the surface and atmosphere were during Mars' first 500 m.y. [1,2]. The martian meteorite ALH 84001 formed during this interval, and so might bear witness to hydrologic and climatic processes on early Mars. However, ALH 84001 shows no evidence for aqueous alteration between 4.55 and 4.0 Ga, and evidence for only a single groundwater infusion since then.

ALH 84001: The meteorite ALH 84001 is a sample of the martian crust, based on the isotopic compositions of O, C, N, Xe [3–8], bulk composition, mineral compositions, and oxidation state [3,9]. Radiometric ages for ALH 84001 center on 4.55 Ga from Sm-Nd and Rb-Sr chronometers [10,11] and on 4.0 Ga from ^{39}Ar (i.e., K)–^{40}Ar [12]; the former age probably represents cooling after

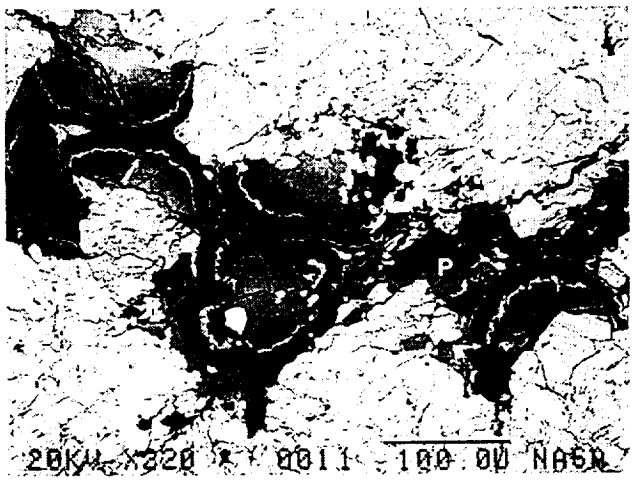

Fig. 1. Meteorite ALH 84001: backscattered electron image (BSE) of a polished thin section [13]. Light colors denote high average atomic number (~density). Semicircular features are carbonate-rich ellipsoids, concentrated in and replacing plagioclase (P), which is now shock glass (maskelynite). Note strong compositional zoning. White grains are chromite and pyrite; most of field at top and bottom is orthopyroxene (light gray).

crystallization, and the latter probably represents a metamorphic event. ALH 84001 is composed almost entirely of the mineral orthopyroxene, with lesser quantities of chromite, augite (clinopyroxene), plagioclase (converted to maskelynite glass), the phosphate whitlockite, silica, and olivine [3,13,14]. A few percent (volume) of ALH 84001 is an assemblage of secondary alteration minerals, which preferentially replaces plagioclase. The secondary minerals include magnesite-siderite carbonates [$MgCO_3$–$(Mg,Fe)CO_3$], dolomite-ankerite carbonates [$Ca(Mg,Fe)(CO_3)_2$], pyrite (FeS_2), magnetite (Fe_3O_4), an Fe sulfate, and a Zn sulfide [3,13,15–17]. The carbonate minerals are most abundant, and occur as ellipsoids and truncated ellipsoids with concentric layering (Fig. 1). Iron-enriched carbonates at the cores give way to magnesite at the rims with thin layers of submicron magnetite grains in magnesite. This alteration assemblage is preterrestrial, i.e., martian [3,13]. Aromatic hydrocarbons have been detected [18], but it is not clear if they are martian. Despite careful searching, no hydrous silicates (clay, mica, amphibole) or Fe oxy-hydroxides (ferrihydrite, goethite) have been detected; these minerals are present in other martian pyroxenites [19,20].

ALH 84001 Alteration: The secondary mineral assemblage in ALH 84001 represents low-temperature aqueous alteration [13], presumably at or after 4.0 Ga (the Ar-Ar age). The alteration minerals suggest that the altering water was alkaline (low pH) and quite reducing (low Eh or fO_2) [15]. Further, the formation of magnesite suggests water with high carbonate alkalinity ($mHCO_3 \pm mCO_3^{2-}$) and very high Mg/(Mg + Ca) [21,22], while dissolution of plagioclase suggests water that had not recently been in contact with basalt [23]. This water may be compared to some on Earth that has reacted with dunites or serpentinites [24].

Evidence for earlier alteration must be sought in textures and compositions detained through the 4.0-Ga metamorphism. None have been observed. If ALH 84001 had been aqueously altered, one might have expected its plagioclase to be converted to micas and clays, and its orthopyroxene to be converted to serpentine, talc, or saponite clay. Textural and compositional relicts of these phases ought to be retained through metamorphism, and none have been noted.

Implications for Early Mars: ALH 84001 is a very fresh rock, and has been little altered since its formation at 4.55 Ga. There is no evidence for aqueous alteration before the 4.0-Ga Ar-Ar event (metamorphism). After 4.0 Ga, there is evidence for a single aqueous alteration, which basically dissolved plagioclase and deposited Fe-Mg carbonates. It seems likely that ALH 84001 never experienced weathering conditions like those found on Earth (even in Antarctica [25,26]), and so never experienced an episode of "warm, wet" climate. Thus, models of the early climate of Mars must permit at least some highland rocks to remain dry.

References: [1] Baker et al. (1991) *Nature, 352*, 589. [2] Squyres and Kasting (1994) *Science, 265*, 744. [3] Mittlefehldt D. (1994) *Meteoritics, 28*, 214. [4] Clayton R. (1993) *Antarc. Meteorite Newsletter, 16*, 4. [5] Romanek et al. (1994) *Nature, 372*, 655–657. [6] Swindle T. et al. (1995) *GCA, 59*, 793. [7] Miura Y. et al. (1995) *GCA, 59*, 2105. [8] Miura Y. and Sugiura N. (1995) *NIPR Symp. Antarc. Meteorites, 19*, 151. [9] Dreibus G. et al. (1994) *Meteoritics, 29*, 461. [10] Jagoutz E. et al. (1994) *Meteoritics, 29*, 478. [11] Nyquist L. et al. (1995) *LPS XXVI*, 1065. [12] Ash R. et al. (1995) *Meteoritics, 30*, 483. [13] Treiman A. (1995) *Meteoritics, 29*, 294. [14] Harvey R. and McSween H. (1994) *Meteoritics, 29*, 472. [15] Wentworth S. and Gooding J. (1995) *LPS XXVI*, 1489. [16] Romanek et al. (1995) *Meteoritics, 30*, 567. [17] Grady et al. (1995) *Meteoritics, 30*, 511. [18] Thomas K. (1995) *Meteoritics, 30*, 587. [19] Gooding J. et al. (1991) *Meteoritics, 26*, 135. [20] Treiman A. et al. (1993) *Meteoritics, 28*, 86. [21] Garrels R. and Christ C. (1965) *Solutions, Minerals and Equilibria*. [22] Nesbitt H. (1990) *Geochem. Soc. Spec. Paper 2*, 335. [23] Gíslason S. and Arnórsson S. (1993) *Chem. Geol., 105*, 117. [24] Nesbitt H. and Bricker O. (1978) *GCA, 42*, 403. [25] Claridge G. and Campbell J. (1984) *New Zealand J. Geol. Geophys., 27*, 537. [26] Allen C. and Conca J. (1991) *Proc. LPS, Vol. 21*, 711–717.

THERMAL EVOLUTION MODELS OF MARS: IMPLICATIONS FOR RELEASE OF VOLATILES. A. Weizman, D. Prialnik, and M. Podolak, Department of Geophysics and Planetary Sciences, Tel-Aviv University, Ramat Aviv 69978, Tel-Aviv, Israel.

Observational evidence indicates that there was abundant water on Mars in the past. Greeley [1] made an estimate of the amount of water released by volcanism by mapping the volcanic materials and inferring the volatile content of the lavas. No attempt has been made, however, to estimate the amount of water based on thermal evolution models.

We have developed a numerical model of the thermal evolution and internal structure of Mars, which simultaneously solves the equations for energy conservation and hydrostatic equilibrium throughout the planet. The model uses an equation of state that includes the thermal pressure computed according to the Debye theory. The composition of Mars is assumed to be characterized by two types of material: core material and mantle material. The mantle material contains silicates, mainly olivine, with varied ratios of fayalite and forsterite. Phase transitions from olivine to spinel and from solid to liquid are included. The core material contains Fe and

a light constituent assumed to be S. These components are initially mixed with the mantle material, but can descend to form the core by a process of sedimentation, which is connected to the process of whole-mantle subsolidus convection.

We have calculated several evolutionary models of Mars, choosing the initial mass fractions of different materials comprising the core and mantle to match the measured radius and moment of inertia of Mars at the present time. Constraints on the composition and internal structure of Mars were thus obtained. We found that core formation occurs almost immediately, as is generally accepted today.

The melting process of silicates can lead to release of water and other volatiles to the surface, either as a consequence of pressure release melting and mass transport, or of heat delivered from the core through plumes. These two processes may lead to volcanism, which is an obvious source of water. Using our model of thermal evolution we can estimate the total amount of volatiles released, as well as the rate of volatile release throughout martian history.

References: [1] Greeley R. (1987) *Science, 236,* 1653–1654.

HAS MARTIAN ATMOSPHERIC CO_2 BECOME DEPLETED IN ^{13}C WITH TIME? I. P. Wright[1], M. M. Grady[2], and C. T. Pillinger[1], [1]Planetary Sciences Unit, Open University, Milton Keynes, MK7 6AA, UK, [2]Cosmic Mineralogy, Natural History Museum, London, UK.

Recent work by Pepin [1] has provided much food for thought regarding the long-term evolution of the martian atmosphere. In order to constrain such a theoretical treatment, it would be highly desirable to make appropriate measurements of historical samples of the atmosphere. Clearly this may become possible within the framework of a Mars sample-return program (possibly as an extension to Surveyor [2]). However, in the meantime we should turn our attention to those martian materials already available for study on Earth: SNC meteorites [3]. What makes this proposition attractive, in regard to atmospheric evolution studies, is that we now have samples that encompass all the history of the planet, from 4.56 Ga [4] in ALH 84001 (referred to as A84), to 1.3 Ga [5] (meteorites such as Nakhla), to perhaps 0.18 Ga [6] in EET A79001 (referred to as E79). All that is required is a suite of diagnostic indicators from each chronologically distinct grouping that can themselves be dated. This might sound illusive, but consider that carbonate minerals have been reported petrographically in A84, Nakhla, and E79; these minerals have the potential to record details of atmospheric CO_2, e.g., its stable isotopic compositions. Note that, as discussed below, it is possible to provide an assessment of the ages of carbonates in A84, Nakhla, and E79; it should thus be possible to assess the evolution of carbonate minerals. In a sense this has parallels with investigations of carbonates on Earth, which have been used, among other things, to demonstrate the long-term operation of photosynthesis [8].

Before attempting to coordinate the relevant information it is necessary to consider some facts about the data that are available. First, for A84, there is universal agreement (oddly enough) that the carbonates in this sample are preterrestrial in origin, and by inference, martian. Furthermore, their C isotopic composition is well constrained at $\delta^{13}C$ = 39.5–42‰ [9] and 41‰ [10]. Slight differences in $\delta^{13}C$ are due to primary processes, reflecting changes in conditions during formation. The age of the carbonates have been assessed as 3.6 Ga, using a combination of laser extraction and the ^{39}Ar-^{40}Ar method [7]. Second, for Nakhla, preliminary measurements of the carbonates in this sample showed $\delta^{13}C$ values between 6‰ and 49‰, with the majority of the minerals in the range 12–24‰ [11]. Subsequent work [10] puts $\delta^{13}C$ at about 35‰, a conclusion supported herein by new analyses using acid dissolution and stepped combustion (which appear to give $\delta^{13}C$ of ~30‰). As alluded to above, the age of carbonates in this sample is unknown, but is presumably less than the formation age of the sample, 1.3 Ga [5]. Finally, for E79, the carbonates in this sample are unfortunately controversial. On the one hand, ^{14}C measurements appear to show a large contribution from terrestrial sources [12], although it has been argued that the ^{14}C data could have been misinterpreted [13]. On the basis of petrography [14], it would appear that at least some of the carbonates, and in particular those associated with lithology C (the shock-produced glass), are preterrestrial. Stable isotope studies of the carbonates associated with the glass fraction of E79 show $\delta^{13}C$ of 11.1‰ [15]. These carbonates could be relatively young, having been incorporated during the ejection of the sample from Mars (i.e., an age less than 0.18 Ga).

Thus, the $\delta^{13}C$ of martian carbonates appears to change from ~41‰ (3.6 Ga) to ~30‰ (≤1.3 Ga) to 11‰ (now). Some caution needs to be exercised here: The exact formation of the carbonates within their individual hosts remains a subject of intense study: Different mechanisms may involve a variety of processes, all of which could impart their own distinctive isotopic characteristics. However, ignoring these (potential) effects and taking the above results at face value, it would appear that there has been a general depletion of ^{13}C in martian carbonates with time. If we can establish the role of atmospheric CO_2 during carbonate formation, then we clearly have a means to study directly the long-term evolution of its isotopic composition.

References: [1] Pepin R. O. (1994) *Icarus, 111,* 289–304. [2] McCleese D. J. (1995) *Ann. Geophys., Part III, 13 (Suppl.),* C804. [3] McSween H. Y. (1994) *Meteoritics, 29,* 757–779. [4] Jagoutz E. et al. (1994) *Meteoritics, 29,* 478–479. [5] Papanastassiou D. A. and Wasserburg G. J. (1974) *GRL, 1,* 23–26. [6] Jones J. H. (1986) *GCA, 50,* 969–978. [7] Knott S. F. et al. (1995) *LPS XXVI,* 765–766. [8] Schidlowski M. et al. (1979) *GCA, 43,* 189–199. [9] Romanek C. S. et al. (1994) *Nature, 372,* 655–657. [10] Jull A. J. T. (1995) *Meteoritics, 30,* 311–318. [11] Carr R. H. et al. (1985) *Nature, 314,* 248–250. [12] Jull A. J. T. et al. (1992) *LPS XXIII,* 641–642. [13] Wright et al. (1995) *LPS XXVI,* 1523–1524. [14] Gooding J. L. et al. (1988) *GCA, 52,* 909–915. [15] Wright I. P. and Pillinger C. T (1994) *Philos. Trans. R. Soc. London, A349,* 309–321.

NEW ESTIMATES OF THE ADSORPTION OF H_2O ON MARTIAN SURFACE MATERIALS. A. P. Zent, SETI Institute and NASA Ames Research Center, Moffett Field CA 94035, USA.

Adsorption of H_2O onto the martian regolith creates a potential reservoir of exchangeable volatiles. Water adsorbed onto the regolith exchanges within the atmosphere-cap-regolith system. Adsorption slows the diffusion of H_2O through the regolith. In effect, the diffusion coefficient must be scaled by the slope of the adsorp-

tion isotherm in order to account for the fact that a given molecule spends considerably more time adsorbed onto the walls of the pores than in actual diffusion. Finally, H_2O adsorption retards formation of ice by segregating H_2O molecules into another phase. In climate models run without adsorption, H_2O sublimated from the north polar cap quickly condenses across much of the martian surface, forming extensive surface ice deposits.

The model of H_2O adsorption on basalt that has been used in the literature for years is based on a set of measurements made by Fanale and Cannon (1971, 1974). Measurement conditions were T = 250–300 K and P = 2–2000 Pa; they found that on the order of 10^{-3} kg of H_2O kg^{-1} were adsorbed. The data had to be numerically modeled to apply to Mars, since the conditions under which the measurements were made were different from Mars (T = 180–280 K, P = 10^{-3} to 0.1 Pa).

Several empirical representations of this data were later developed and used extensively to estimate the total abundance of H_2O adsorbed in the regolith, the diffusion scale of H_2O over a variety of depths, the behavior of H_2O in the diurnal boundary layer, and the extent and distribution of ground ice.

Zent and Quinn (1995) reported on the measurement of simultaneous H_2O and CO_2 adsorption, as well as H_2O alone, onto Mauna Kea palagonite. Subsequently, we compared the measured H_2O adsorbate density on the palagonite to the predicted adsorbate density on basalt, using an interpolation of the measured adsorption data on palagonite

$$\rho_a = A_s \delta P^{\gamma} T^{\beta} \quad (1)$$

The variables δ, γ, and β are fit via a least-squares technique to the data. We calculated that the density of H_2O adsorbate at partial pressures of 4×10^{-2} Pa, when T = 200 K, was 4.88×10^{-9} kg m^{-2}. When the Fanale and Cannon (1974) basalt isotherm was calculated for the same conditions, the predicted density of adsorbate is 1.87×10^{-7} kg m^{-2}. The difference is a factor of 38, which was considered to be unacceptable. Interestingly, when the same calculation was done for partial pressures of 50 Pa, when T = 260 K, the densities differed by only a factor of 4, which is well within the range anticipated for mineralogical differences. At the high P and T conditions, both basalt and palagonite isotherms are being used to interpolate between data points. At Mars-like conditions, the basalt isotherm is being used to extrapolate (by 1 to 2 orders of magnitude in pressure), while the palagonite isotherm is still in an interpolation domain.

Our hypothesis was that extrapolation of an unrealistic adsorption isotherm accounts for much of the apparent discrepancy between the number densities measured for the palagonite and those predicted for basalt. As a check on this, and to examine the possible importance of mineralogical variations, we collected a sample of Page Mill basalt, a Miocene basalt from the Franciscan complex of the San Francisco Peninsula, similar to the Vacaville basalt on which Fanale and Cannon acquired their adsorption data. We ground the sample, seived it to <34 μm, and measured H_2O adsorption at P = 0.34 Pa, and T = 209 K. The results indicate that 2.9×10^{-4} kg/kg adsorbed onto the basalt; we measured its specific surface area as 1.801×10^4 m^2 kg^{-1}, and the resulting adsorbate density was 1.6×10^{-8} kg m^{-2}. At very similar conditions (P = 0.47 Pa, T = 210), the average of seven separate measurements of H_2O adsorption on palagonite is 1.052×10^{-8} kg m^{-2}, a difference of approximately 50% (cf. the factor of 38 difference with which we started).

Geologic materials are composed of a variety of minerals and poorly crystalline solids. The surface of a solid of complex chemical composition contains many exposed atoms and functional groups, which interact in various ways with adsorbent molecules. Surface imperfections of molecular dimensions such as dislocations, vacancies, flaws, cracks, and chemical contaminants also may be a major source of heterogeneity (e.g., Jaronic and Madey, 1988). All realistic models of the adsorptive behavior of the martian regolith must take this heterogeneity into account.

The empirical adsorption isotherm heretofore used to estimate H_2O adsorption on basalt at Mars-like conditions implicitly assumes adsorbents are homogeneous. This can be demonstrated by using equation (1) to generate an adsorption isotherm, and then using the Clausius-Clapeyron equation to calculate the partial molar enthalpy of adsorption for a variety of coverages. The adsorption energies is found to be independent of coverage. Alternative forms of this equation also implicitly assume homogeneous adsorbents.

We have used a revised version of the basalt isotherm, which incorporates our low P and T basalt adsorption data, to assess the effective diffusion coefficient of H_2O through the martian regolith.

TABLE 1.

Hour	New Isotherm		Old Isotherm	
	D_f (m^2 s^{-1})	δ(m)	D_f (m^2 s^{-1})	δ(m)
1200 h	1.4×10^{-7}	1.5×10^{-2}	3.8×10^{-9}	2.6×10^{-2}
2400 h	6×10^{-11}	3.3×10^{-3}	9×10^{-13}	4×10^{-4}

Where we have calculated the adsorption at appropriate temperatures, where the effective length scale for diffusion is $\delta = (2tD_f)^{1/2}$ and $t = 8.874 \times 10^4$ s, Mars' rotation period. When the Ames Boundary Layer model is amended to take into account the reduced adsorption at low temperatures, ice is predicted to stablize in the uppermost few millimeters of the regolith at night, a consequence of the fact that the greatest difference between the old and current basalt isotherms is at low temperatures.